

Durham E-Theses

Electric force microscopy and plasma studies of polymer surfaces

Bradley, Thomas James

How to cite:

Bradley, Thomas James (2005) *Electric force microscopy and plasma studies of polymer surfaces*, Durham theses, Durham University. Available at Durham E-Theses Online:
<http://etheses.dur.ac.uk/2799/>

Use policy

The full-text may be used and/or reproduced, and given to third parties in any format or medium, without prior permission or charge, for personal research or study, educational, or not-for-profit purposes provided that:

- a full bibliographic reference is made to the original source
- a [link](#) is made to the metadata record in Durham E-Theses
- the full-text is not changed in any way

The full-text must not be sold in any format or medium without the formal permission of the copyright holders.

Please consult the [full Durham E-Theses policy](#) for further details.

Electric Force Microscopy and Plasma Studies of Polymer Surfaces

Ph. D. Thesis

By

Thomas James Bradley

Department of Chemistry

University of Durham

2005

The copyright of this thesis rests with the author or the university to which it was submitted. No quotation from it, or information derived from it may be published without the prior written consent of the author or university, and any information derived from it should be acknowledged.



0.9 JUN 2006

For my Parents, my Granddad and For Caroline

Statement of Copyright

The Copyright of this thesis rests with the author. No quotation from it should be published without prior written consent and information derived from it should be acknowledged.

Declaration

The work described in this thesis was carried out in the Chemistry Department at the University of Durham between October 2001 and December 2004. It is the original work of the author, except where otherwise acknowledged, and has not been submitted previously for a degree at this or any other University.

Film thickness measurements (Chapters 3, 6 and 7) were carried out by Dr Wayne Schofield (University of Durham). Pulsed plasma polymerisation of styrene, allylmercaptan, and vinylbenzylchloride (Chapter 3) and 4-vinylpyridine (Chapter 6) was carried out by Dr Wayne Schofield (University of Durham). Pulsed plasma polymerisation of 3-vinylbenzaldehyde (Chapter 3) was carried out by James McGettrick (University of Durham). Continuous wave plasma deposition of methylmethacrylate was carried out by Dr Wayne Schofield (University of Durham). Scanning XPS (Chapter 5) was carried out by Dr Ian Fletcher (ICI).

Publication

Work carried out in this thesis has been published or will be submitted for publication as follows :-

- (1) Electroless Metal Deposition onto Poly(4-Vinylpyridine) Functionalized Solid Surfaces, *in progress*.

Acknowledgements

I would like to thank my supervisor Professor J. P.S. Badyal for his help and guidance over the last four years. I would also like to thank everyone in lab 98, past and present for guidance and support.

Thanks also to George, Kelvin and Barry in the electrical workshop, Neil and Jim in the mechanical workshop and Peter and Malcolm the glassblowers for all their technical support.

Abstract

The present work studies the functionalisation, modification and analysis of polymers surfaces for use as templates for the self assembly of nano-particles from aqueous dispersions; the production of nano-scale charge patterns; the surface autocatalytic deposition of patterned metals; and the generation of superhydrophobic, antireflective coatings. The polymer surfaces were characterised by a variety of surface sensitive techniques, such as X-ray Photoelectron Spectroscopy (XPS), Atomic Force Microscopy (AFM), Fourier Transform Infra-Red (FTIR), Electric Force Microscopy (EFM) and Video Contact Angle.

The ability of an Electric Force Microscope (EFM) to create charge patterns on polymer surfaces was studied in detail. Large dc voltages were applied to a chromium coated cantilever leading to the induction of a charged region on the polymer substrate. The effects of applied voltage, tip-sample separation, scanning speed and deposition area on the resultant deposition pattern were studied. Charging thresholds for different polymer substrates were experimentally determined.

A polymer blend surface consisting of nanometer sized islets of conducting polybutadiene within an insulating polystyrene matrix was also produced. The different charge storage properties of these two polymers were exploited in order to produce a nanometer scale charge patterned substrate. Charge patterns were also used as templates for the directed deposition of gold nano-particles.

The pulsed plasma deposition of a 4-vinylpyridine monomer was studied in order to investigate the production of aromatic nitrogen surfaces. The retention of the nitrogen functionality allowed the plasma polymer to act as a seed site for the electroless deposition of both copper and nickel. Patterning was facilitated on a micrometer scale by embossing a grid into the polymer substrate.

An investigation into the plasma fluorination of a polymethylmethacrylate yielded surfaces that combined both anti-reflective and super-repellent characteristics. The magnitudes of these properties were found to depend on the fluorine content and roughness of the treated surface.

Table of Contents

Chapter 1: Introduction to Surface Functionalisation and Patterning	1
1.1 Surface Functionalisation	2
1.2 Plasma Deposition and Modification of Polymer Surfaces	6
1.2.1 Introduction	6
1.2.2 Plasma Types	6
1.2.3 Plasma Theory	7
1.3 Surface Patterning	10
1.3.1 Soft Lithography	11
1.3.2 Photolithographic	15
1.3.3 Embossing	17
1.3.4 Moulding	18
1.3.5 Laser Ablation	18
1.3.6 Scanning Probe Microscope Lithography	19
1.3.7 Multiple Tip Scanning Probe Systems	25
1.4 References	27
Chapter 2: Surface Analysis Techniques	40
2.1 X-Ray Photoelectron Spectroscopy (XPS)	41
2.1.1 Instrumentation	42
2.2 Video Contact Angle (VCA)	44
2.2.1 Contact Angle Hysteresis	48
2.3 Reflectometry	48
2.4 Fourier Transform Infrared (FT-IR) Spectroscopy	49
2.5 Scanning Probe Microscopy	51
2.5.1 Introduction	51
2.5.2 Contact Mode	52
2.5.3 NonContact Mode	52
2.5.4 Tapping Mode	53

2.5.5	Force Curves	54
2.5.6	Phase Imaging	54
2.5.7	Electric Force Microscopy	55
2.6	References	56

Chapter 3: Non-Contact Charging of a Polymer Surface using Electric Force Microscopy **58**

3.1	Introduction	59
3.2	Theory	60
3.2.1	The effect of force gradient on the phase lag of a freely oscillating cantilever	60
3.2.2	Mapping Surface Charge with Lift-Mode EFM	64
3.2.3	Surface Charging Using an EFM	69
3.3	Experimental	75
3.4	Results	78
3.4.1	Investigation into the EFM technique	78
3.4.2	Polymer structure effects on substrate charging	93
3.5	Discussion	100
3.5.1	Investigation into the EFM technique	100
3.5.2	Polymer structure effects on substrate charging	103
3.6	Conclusions	106
3.7	References	107

Chapter 4: Selective Phase Charging at the Nanoscale **110**

4.1	Introduction	111
4.2	Experimental	115
4.3	Results	117
4.4	Discussion	126
4.5	Conclusions	130
4.6	References	131

Chapter 5: Electrostatic Attachment of Gold Colloids to Polystyrene Surfaces Using EFM **134**

5.1	Introduction	135
5.2	Experimental	137
5.3	Results	139
5.4	Discussion	145
5.5	Conclusion	147
5.6	References	148

Chapter 6: Electroless Metal Deposition onto Poly(4-Vinylpyridine) Functionalised Solid Surfaces **149**

6.1	Introduction	150
6.2	Experimental	153
6.3	Results	157
6.4	Discussion	164
6.5	Conclusions	166
6.6	Reference	167

Chapter 7: Super-Repellent Anti-Reflective Surface Coatings **170**

7.1	Introduction	171
7.1.1	The Fluorination of Polymer Surfaces	171
7.1.2	Anti-Reflective Properties	173
7.2	Experimental	175
7.3	Results	177
7.4	Discussion	188
7.5	Conclusions	192
7.6	References	193

Chapter 8: Conclusions **198**

Table of Figures

Figure 2-1 Contact Angle formed by a probe liquid droplet on a surface.	45
Figure 2-2 Schematic diagram of the probe liquid spreading to equilibrium on the surface.	46
Figure 3-1 The effect of force gradients on the phase shift of a freely oscillating cantilever. (a), The phase lag of a freely vibrating cantilever at resonance, ϕ_{free} is 90° ; (b), The phase lag of a vibrating cantilever exposed to a repulsive force, $\phi_{\text{interacting}}$ is less than 90° ; (c), The phase lag of a vibrating cantilever experiencing an attractive force, $\phi_{\text{interacting}}$ is more than 90° .	63
Figure 3-2 Diagram showing lift mode operation of tapping mode AFM.	64
Figure 3-3 Schematic of the forces present between the EFM tip and a region of positively charged surface as a function of tip voltage.	67
Figure 3-4 Schematic of the forces present between the EFM tip and a region of negatively charged surface as a function of tip voltage.	68
Figure 3-5 Schematic showing (a), Contact Electrification of a surface, (b), Corona Discharge onto a Surface and (c), Dielectric Breakdown of a surface.	72
Figure 3-6 $20\ \mu\text{m} \times 20\ \mu\text{m}$ micrographs of polystyrene following charging of the central $5\ \mu\text{m} \times 5\ \mu\text{m}$ square with + 60 V, (a) Height (150 nm) and (b) Phase (180°).	79
Figure 3-7 $20\ \mu\text{m} \times 20\ \mu\text{m}$ micrographs of polystyrene recorded with + 12 V (left column) and - 12 V (right column) applied to the tip. The central square was previously exposed to (a) and (b) + 60 V lift-mode bias, (c) and (d) + 20 V lift-mode bias and (e) and (f) + 10 V lift mode bias. Z Scale 10° .	80
Figure 3-8 $20\ \mu\text{m} \times 20\ \mu\text{m}$ micrographs of polystyrene recorded with - 12 V applied to the tip. The central square was previously exposed to a + 60 V lift-mode bias (Scan speed = 1.0 Hz): (a) Lift-height during charge deposition = 15 nm; (b) Lift height during charge deposition = 30 nm; (c) Lift height during charge deposition = 45 nm and (d) Lift height during charge deposition = 60 nm. Z Scale 10° .	81
Figure 3-9 $20\ \mu\text{m} \times 20\ \mu\text{m}$ micrographs of polystyrene recorded with - 12 V applied to the tip. The central square was previously exposed to a + 80 V lift-	

mode bias: (a) Scan speed while charging = 1 Hz; (b) Scan speed while charging = 3 Hz. Z Scale 10 °.	82
Figure 3-10 20 μm × 20 μm micrographs of polystyrene following charging of the central 5 μm × 5 μm square with - 110 V, (a) Height (150 nm) and (b) Phase (180 °).	83
Figure 3-11 20 μm × 20 μm micrographs of polystyrene recorded with + 12 V (left column) and - 12 V (right column) applied to the tip. The central square was previously exposed to (a) and (b) - 110 V lift-mode bias, (c) and (d) - 60 V lift-mode bias and (e) and (f) - 55 V lift mode bias. Z Scale 10 °.	84
Figure 3-12 20 μm × 20 μm micrographs of polystyrene recorded with + 12 V applied to the tip. The central square was previously exposed to a - 110 V lift-mode bias (Scan speed = 1.0 Hz): (a) Lift-height during charge deposition = 15 nm; (b) Lift height during charge deposition = 30 nm; (c) Lift height during charge deposition = 45 nm and (d) Lift height during charge deposition = 60 nm. Z Scale 10 °.	85
Figure 3-13 20 μm × 20 μm micrographs of polystyrene recorded with - 12 V applied to the tip. The central square was previously exposed to a + 80 V lift-mode bias: (a) Scan speed while charging = 1 Hz; (b) Scan speed while charging = 3 Hz.	86
Figure 3-14 Graph showing relationship between positive charge deposition area and area of polystyrene substrate charged. Small dashed line signifies limitation due to tip geometry; large dashed line indicates a 1:1 relationship.	87
Figure 3-15 Graph showing relationship between negative charge deposition area and area of polystyrene substrate charged. Small dashed line signifies limitation due to tip geometry; large dashed line indicates a 1:1 relationship.	88
Figure 3-16 Graphs showing the EFM Phase Shift dependence on deposition voltage, imaging voltage and imaging lift-mode height. a, -110 V deposition voltage, b, -120 V deposition voltage, c, -130 V deposition voltage.	92
Figure 3-17 Graph showing polymer charging thresholds with positive and negative voltage.	95
Figure 4-1 Polystyrene Surface 20 μm +60V deposited. AFM and EFM images following charging, height (150 nm) (a), phase (180 °) (b), +12V (10 °) (c), 0V (10 °) (d) and -12V (10 °) (e).	120

Figure 4-2 Polybutadiene Surface 20 μm +60V deposited. AFM and EFM images following charging, height (150 nm) (a), phase (180 $^\circ$) (b), +12V (10 $^\circ$) (c), 0V (10 $^\circ$) (d) and -12V (10 $^\circ$) (e).	121
Figure 4-3 90% Polystyrene 10% Polybutadiene Surface 20 μm +60V deposited. AFM and EFM images following charging, height (150 nm) (a), phase (180 $^\circ$) (b), +12V (10 $^\circ$) (c), 0V (10 $^\circ$) (d) and -12V (10 $^\circ$) (e).	122
Figure 4-4 Polystyrene Surface 20 μm -110V deposited. AFM and EFM images following charging, height (150 nm) (a), phase (180 $^\circ$) (b), +12V (10 $^\circ$) (c), 0V (10 $^\circ$) (d) and -12V (10 $^\circ$) (e).	123
Figure 4-5 Polybutadiene Surface 20 μm -110V deposited. AFM and EFM images following charging, height (150 nm) (a), phase (180 $^\circ$) (b), +12V (10 $^\circ$) (c), 0V (10 $^\circ$) (d) and -12V (10 $^\circ$) (e).	124
Figure 4-6 90% Polystyrene 10% Polybutadiene Surface 20 μm -110V deposited. AFM and EFM images following charging, height (150 nm) (a), phase (180 $^\circ$) (b), +12V (10 $^\circ$) (c), 0V (10 $^\circ$) (d) and -12V (10 $^\circ$) (e).	125
Figure 5-1 Atomic force micrographs of positively charged polystyrene surface following the electrostatic attachment of gold colloids to the deposited charge. Height (500nm) (a), Phase (90 $^\circ$), EFM + 12 V (2 $^\circ$), EFM 0 V (2 $^\circ$) and EFM – 12 V (2 $^\circ$).	141
Figure 5-2 100 μm square scanning XPS micrographs of a polystyrene surface following the charging of a 15 μm square with positive voltage and the immersion of the sample in a gold colloid suspension in Fluorinert. Scans map Au 4f (a), C 1s (b), O 1s (c) and Si 2p (d). Z Scale Normalised Counts.	142
Figure 5-3 Atomic force micrographs of negatively charged polystyrene surface following the electrostatic attachment of gold colloids to the deposited charge. Height (500 nm), Phase (90 $^\circ$), EFM + 12 V (2 $^\circ$), 0 V (2 $^\circ$) and EFM – 12 V (2 $^\circ$).	143
Figure 5-4 100 μm square scanning XPS micrographs of a polystyrene surface following the charging of a 5 μm square with negative voltage and the immersion of the sample in a gold colloid suspension in Fluorinert. Scans map Au 4f (a), C 1s (b), O 1s (c) and Si 2p (d). Z Scale Normalised Counts.	144
Figure 6-1 XPS C(1s) spectrum of pulsed plasma deposited poly(4-vinylpyridine).	158

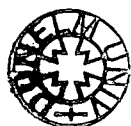
- Figure 6-2** FTIR spectra of: (a) 4-vinyl pyridine monomer; (b) spin-coated poly(4-vinylpyridine); (c) pulsed plasma deposited poly(4-vinyl pyridine); and (d) 10 W continuous wave 4-vinyl pyridine plasma polymer. (* denotes polymerisable alkene bond.) 160
- Figure 6-3** XPS wide scan of (a) 4-vinylpyridine pulsed plasma polymer; (b) 4-vinylpyridine pulsed plasma polymer reacted with Palladium chloride solution; (c) pp4VP-PdCl₂ films reacted in copper sulphate bath and (d) pp4VP-PdCl₂ films reacted in Shipley EL468 nickel bath. 162
- Figure 6-4** Optical images of arrays of: (a) 150 nm thick pulsed plasma deposited poly(4-vinylpyridine) onto PTFE; (b) Pd²⁺ functionalized (a); (c) electroless deposition of metallic copper onto (b); and (d) electroless deposition of metallic nickel onto (b). 163
- Figure 7-1** 10 min CF₄ plasma modification of a 2 µm thick polymethylmethacrylate film as a function of power: (a) XPS elemental composition; (b) H₂O contact angle; (c) AFM RMS surface roughness. 181
- Figure 7-2** AFM height images of polymethylmethacrylate as a function of CF₄ plasma power level (time = 10 min): (a) 0 W, (b) 20 W, (c) 30 W, (d) 40W, (e) 50 W and (f) 60 W. Resolution (x = y = 20 µm, z = 500 nm). 182
- Figure 7-3** 50 W CF₄ plasma modification of a 2 µm thick polymethylmethacrylate film as a function of time: (a) XPS elemental composition; (b) H₂O contact angle; (c) AFM RMS surface roughness. 183
- Figure 7-4** AFM height images of polymethylmethacrylate as a function of CF₄ plasma exposure time (power = 50 W): (a) 2 mins, (b) 4 mins, (c) 6 mins, (d) 8 mins, (e) 10 mins and (f) 20 mins. Resolution (x = y = 20 µm, z = 500 nm except f where z = 2000 nm). 184
- Figure 7-5** Comparison of transmittance as a function of plasma power following a 10 minute treatment at short (350 nm), medium (700 nm) and long (1000 nm) wavelengths (dotted line represents untreated sample). 186
- Figure 7-6** Comparison of transmittance as a function of time following a 50 W treatment at short (350 nm), medium (700 nm) and long (1000 nm) wavelengths (dotted line represents untreated sample). 187

Table of Tables

Table 1-1 Overview of Ink / Substrate Combinations for DPN.	22
Table 3-1 Effects of Force Gradient on the phase shift of a freely oscillating cantilever.	62
Table 3-2 Table showing polymer charging thresholds and related physical constants.	96
Table 6-1 Theoretical and experimental XPS elemental compositions of pulsed plasma deposited poly(4-vinylpyridine).	157
Table 7-1 Transmission Measurements for uncoated and PMMA coated BDH Glass Wafer at various wavelengths.	180
Table 7-2 Contact angle measurements for CF ₄ plasma treated 2 μm thick polymethylmethacrylate (50 W, 10 min).	185

Chapter 1

Introduction to Surface Functionalisation and Patterning



1.1 Surface Functionalisation

There are a number of key methodologies that may be used to produce a thin film on a surface. The major deposition methods for thin film creation are physical (and chemical) vapour deposition,^{1,2} electro-deposition,³ self assembled monolayer (SAM) formation,⁴ spin coating,⁵ electroless deposition of metals⁶ and plasma deposition,⁷ which offers many routes to functionalised surfaces. The functionalities these methods provide surfaces with a number of properties including scratch resistance,⁸ water resistance,⁹ corrosion resistance,¹⁰ conductivity,¹¹ anti-reflective¹² or anti-bacterial.¹³

Physical vapour deposition (PVD) and its subset, chemical vapour deposition (CVD), are primarily used for the deposition of inorganic molecules onto surfaces. Deposited surfaces include ceramics,¹⁴ metals,¹⁵ carbides¹⁶ and nitrides.¹⁷ Additionally, small organic molecules can be deposited using these techniques although under softer than standard conditions.¹⁸ In this case, due to the softer conditions used the resultant film in general is only weakly bound to the substrate. Vapour deposition experiments are carried out under vacuum; the source material for the coating is transferred into the vapour phase. In PVD this is carried out in a variety of ways: ion plating,¹⁹ sputtering²⁰ and laser surface alloying.²¹ In CVD a heated precursor is used as the reactive gas used during the deposition. The reactive gas travels to the substrate to be coated where it is adsorbed on the surface. Deposited films created in this manner are known to be highly crystalline, although they can feature grain boundaries, cracks or disclinations.²²

Electrodeposition is the process of producing metal platings on substrates by the action of an electric current.³ The substrate to be coated is

immersed in a metal salt solution where the metal ions are the required coating. A circuit is then formed in the solution, in which a negative potential is then applied to the substrate (required to be conducting) whilst a positive potential is applied to a metal anode, usually made of the metal being deposited. Positively charged metal ions from the solution are then attracted to the negatively charged substrate and form a coating. Meanwhile electron flow at the metal anode produces more positively charged metal ions which replenish the deposition solution. A thin film may be produced using this technique. However, due to the requirement to reduce to metal ions, only conducting substrates may be coated using electrodeposition.

The self assembly of molecules onto substrates provides a quick, cheap and non-corrosive route for the production of highly ordered monolayer films.⁴ There are two key types of SAM involving different molecules and substrates, Alkanethiolates on gold²³ and Alkylsiloxanes on hydroxylated surfaces.²⁴

Self assembled monolayers of alkanethiolates form via the adsorption of long chain alkanethiols from either solution or vapour phase onto a gold substrate according to the following reaction;²⁵



The surface structure of these SAM's has been well characterized with a highly ordered structure.²⁶ The sulphur atom in the thiol group coordinates with the gold atom on the surface. The trans alkyl chains orientate with a 30° tilt normal to the surface.²⁶ These surfaces are of particular versatility as the

terminal functional group of the SAM can be easily tailored prior to adsorption onto the gold through straight forward organic synthesis.²⁷

Self assembled monolayers of alkylsiloxanes are formed onto hydroxylated surfaces (usually silicon or glass). In the reaction the siloxane group condense with water and the hydroxyl groups on the surface and neighbouring siloxanes to form a crosslinked network.²⁸ The arrangement of the molecules on the surface is not as ordered as those formed by thiols on gold and is dependent upon reaction conditions. The SAM's formed in this manner are more stable than thiol SAM's, but they lack the variety of functionality that are present in the thiol system. This is mainly due to the difficulty in introducing functionality into the alky siloxane precursor.

The deposition of a thin polymer film onto a flat substrate can be accomplished using spin-coating techniques.²⁹ The desired polymer is dissolved in a suitable and volatile solvent. The resultant polymeric solution is then added drop-wise to the desired substrate, accelerated and rotated at high speed. This causes the solution to spread evenly over the surface depositing a thin, defect free film whilst the solvent evaporates. The homogeneity of the generated film will depend on the solvent, spinning speed, atmosphere and lab conditions.⁵ The attachment between the polymer film and the substrate is solely due to physisorption and therefore the film is not strongly attached and may be removed. A limit in the practical thickness of films that can be deposited in this manner is 200 μm .

Electroless deposition of metals is a popular alternative technique for the deposition of thin metal films to electrodeposition.³⁰ It is a redox solution based technique in which a catalytically activated surface is immersed in a

quasi-stable deposition bath. Metal salts are then reduced from the solution by a reducing agent and selectively form on catalytically activated regions of the substrate. Once deposition has started the newly created metal surface acts as a catalyst for further reduction, allowing thick films to quickly form.

1.2 Plasma Deposition and Modification of Polymer Surfaces

1.2.1 Introduction

A plasma, often called the fourth state of matter, is a partially or fully ionised gas consisting of electrons, positive and negative ions, neutral and metastable species as well as electromagnetic radiation.^{31,32} The reactive species found in a plasma can all initiate, participate in and undergo reactions.³³ Overall plasmas are classified as being uncharged, consisting of equal numbers of positive and negatively charged species, although local perturbations in the charge may occur.

1.2.2 Plasma Types

Plasmas are classified into three different categories determined by the method of plasma ignition and their physical properties. The first type of plasma exists in thermodynamic equilibrium. This occurs when all species within the plasma have the same temperature and such state occurs in stars. The second type of plasma occurs when all species, with the exception of the electromagnetic radiation, are in thermodynamic equilibrium and therefore at the same temperature. This state results in a very dense plasma that is considered 'hot'. As they exist at high temperatures hot plasmas find applications in situations where high temperatures are required for thermal reactions, such as metallurgy.³² The third type of plasma, commonly termed a glow discharge or 'cold', is a non-equilibrium plasma. Within the plasma the temperature that is reached by the electrons is much greater than that of the

other species within the gas (10 000 K and 300 – 500 K respectively). Glow discharges are commonly used for the modification of surfaces, through three key routes: etching,³⁴ polymerisation,³⁵ and functionalisation via chemical reactions with species within the plasma.³⁶

1.2.3 Plasma Theory

Glow discharge or cold plasmas are achieved by the running of a radio frequency oscillating electric field through copper coils around a low pressure gas or vapour. The ignition of the plasma requires energy greater than the ionisation energy of the gas molecules to be applied to the system. The randomly occurring free electrons in the gas are accelerated.³⁷ These electrons undergo inelastic collisions leading to ionisation of molecules within the gas and the production of secondary electrons.³² After plasma ignition the glow discharge may be continued with a lower applied power being applied, the initial ionisation having produced many reactive species which propagate the reaction in a cascade effect through further excitations and ionisations.

Plasma stability relies on a quasi-neutral state being maintained. This requires that the discharge volume of the plasma be greater than the Debye length, λ_D , the distance over which a perturbation on the plasma may occur due to a small change in potential,³³ Equation 1-1;

$$\lambda_D = \left(\frac{\epsilon_0 k T_e}{n_e e^2} \right)^{1/2}$$

Equation 1-1

where ϵ_0 is the permittivity of free space, k is the Boltzmann's constant, T_e is the electron temperature, n_e is the electron density per cm^3 in the plasma and e is the charge of an electron. For glow discharge plasmas T_e and n_e are typically found to be around 1 eV and 10^{10} respectively. This gives a Debye length of 74 μm . Localised charge perturbations occur with the plasma, but the range is limited by the value of λ_D . Electric fields within a plasma are minimised by movement of charged components within the plasma leading to a redistribution of charge. Electrons, as they have a significantly lower mass than ions, move quickly through the plasma. As a result of this movement Debye shielding occurs leading to a quasi-neutral system. Due to this there is a potential formed in the plasma, caused by the acceleration of electrons towards the reactor walls. This leaves a net positive charge in the plasma and a potential difference between the bulk plasma and the reactor walls.³⁸

Ionisation reactions in a plasma are essential for the continuation of the plasma discharge. In a thermal plasma the temperature of the electrons is equal to the temperature of the gas ($T_e = T_g$) and the electron energies can be fit with a Maxwellian distribution.³³ In non-equilibrium, glow discharge, plasmas the electron energy fits to a Druyvesteyan distribution,³³ in which the electron temperature is fitted as being much greater than the surrounding gas. Both distributions have high energy tails. These high energy electrons play an important part in the chemistry and physical conditions of plasmas.

Different components within the plasma treat the surfaces within it to different depths. UV and VUV components from the plasma penetrate deeply within the surface being treated leading to a modification of both the surface

and the bulk properties. Neutral species, ionic species and electrons will only effect the surface being treated and will not penetrate to the bulk.³⁹

Plasma treatment of surfaces offers a number of advantages over conventional treatment methods. It is economical as only a small quantity of gas or vapour needs to be introduced into the reaction chamber and as the plasma treatment occurs at low pressure. The treatment is shape independent as the plasma is a gaseous medium. Bulk properties are unaffected by the plasma treatment unless harsh reaction conditions are utilised. As the reactions occur within a sealed environment waste products are trapped in a cold finger allowing them to be disposed of safely. With careful selection of plasma parameters well adhered, defect free, polymer films with various functionalities can be formed on a variety of substrates. Plasma treatments are complex and many reactions occur within the plasma, this can lead to unforeseen consequences that have to be monitored.

1.3 Surface Patterning

There are a number of techniques that have developed for the production of micro and nano scale patterns on substrates, these are needed for a variety of applications including microfluidic devices,⁴⁰ micro-optics,⁴¹ molecular diagnostics,⁴² plastic electronics⁴³ and nano-electromechanical systems.⁴⁴

Two approaches have been taken for the production of patterns and devices at the nano-scale. These methodologies have been classified as the 'top down' and the 'bottom up' approach. Top down techniques have evolved out of work by the engineering and physics communities, they involve attempts to reduce the size of devices by using the most recently developed patterning techniques. Most of this research has developed out of downscaling work carried out in the microelectronics industry on lithographic techniques.

Bottom up construction of micro and nanostructures approach the problem from the opposite direction and the research and development has been carried out primarily, but not exclusively, by chemistry and biochemistry groups. In this research nanostructures are formed by the self-assembly of various small molecules, bio-molecules and polymers into structures of defined periodicity and long range order, examples of which can easily be found in nature. The order in these structures is due to non-covalent forces between the molecules such as, hydrogen bonding,⁴⁵ π - π interactions,⁴⁶ van der Waals forces,⁴⁷ metal-ligand interactions⁴⁸ and phase separation effects in polymers.⁴⁹ Bottom up patterning is interesting and can produce novel and fascinating structures. However it has some disadvantages and within the

long term goal, the production of nano-devices, it is not a practical option. This is due to the fact that the production of patterns alone is not sufficient. It is also necessary to control the size, structure, orientation and position of the nanoscale structures manufactured.

Top down lithographic techniques can be traced back to 1798, when Alois Senefelder developed a method for the replication of a pattern by image transfer from one surface to another. He discovered that ink could be adsorbed onto an image produced on limestone rock with a greasy fluid. Subsequent contact between the rock and a sheet of paper resulted in the ink image being transferred.⁵⁰ Since its inception, lithography has developed and evolved and it is currently not only used for the printing of images, although its original spirit lives on in microcontact printing,⁵¹ a soft lithographic technique developed by Whitesides in which a surface can be both printed on or chemically modified using a polydimethylsiloxane (PDMS) stamp.⁵² Other lithographic techniques that have been developed include photolithographic,⁵³ embossing,⁵⁴ injection or cast moulding,⁵⁵ laser ablation⁵⁶ and scanning probe based techniques.⁵⁷

1.3.1 Soft Lithography

Soft lithography is a collective name given to a number of lithographic techniques based on contact between an elastomeric mask or stamp and a surface.⁵⁸ The techniques that fall within this area are microcontact printing (μ CP),⁵⁹ replica moulding (REM),⁶⁰ micromoulding in capillaries (MIMIC),⁶¹ microtransfer moulding (μ TM)⁶² and solvent assisted micromoulding (SAMIM).⁶³ These techniques all utilise a patterned elastomer, usually PDMS

as the mask to create the pattern. Soft lithography has advantages over other lithographic techniques in its ability to pattern non-planar and large substrates. This is due to the flexibility of the stamps used.

The elastomeric stamps used in soft lithography are very flexible but ultimately their resolution is limited to the resolution with which a master can be prepared. Once the master has been prepared it is possible to cast a large number of stamps from it with no decrease in the quality. Elastomeric stamps are prepared using a master that has been formed using conventional lithographic techniques, such as photolithography or micromoulding, and as such, the ultimate resolution of these stamps is limited in this manner. Therefore although soft lithography represents an increase in the speed and versatility of patterning techniques they cannot improve resolution by themselves.

A key strength of soft lithography techniques is the possibility of twenty-four hour turn around between the original idea and the patterned substrate.⁶⁴ A CAD program is used to design the required pattern. This is subsequently printed onto polymer sheet in black ink using a specially prepared printer. This pattern is then transferred into a photoresist material on a silicon wafer. After development it is then possible to cast PDMS stamps from the newly created master. Then standard patterning with the stamp may occur, with a minimum feature size of 20 μm or greater.

There are some problems that are associated with the use of PDMS stamps that limits their ability to produce certain patterns. Fine features may 'pair' together; this may be due to gravity, adhesion or capillary forces.⁶⁵ If the spaces between the protruding features are too large a sagging effect may

occur, this results in parts of the mask not designed to come into contact with the surface drooping under their own weight. Other problem factors include the PDMS shrinks on curing⁶⁶ and swells on contact with certain nonpolar solvents such as toluene⁶⁷ or hexane.⁶⁸

1.3.1.1 Microcontact Printing

Microcontact printing is perhaps the most well known of the soft lithography family and is based on a remarkably simple idea.⁵² By bringing a stamp coated with the desired patterning 'ink' into contact with a surface, transfer will occur from the protruding features on the stamp to the surface. The 'ink' commonly used in this procedure is a self-assembled monolayer (SAM) solution. An example of this is an alkanethiolate on a gold or silver surface.⁶⁹

The ability of SAM's to form highly ordered monolayers after less than 1 seconds contact with the surface means that they are widely used in the formation of surface patterns.⁷⁰ The fact that SAM's are autophobic⁷¹ and therefore do not spread across the surface also helps the formation of well defined structures. After the deposition of a SAM pattern two options are commonly used to further pattern the surface. The SAM can be used as a resist in selective wet etching.⁷² It may also be used as a template for further deposition forming patterned structures of a variety of materials.⁷³

1.3.1.2 Replica Moulding

In replica moulding a rigid original or master is formed using standard lithographic techniques. An elastomeric cast of the original is then produced.⁶⁰

This stamp is then used itself for the moulding of a number of new replicas produced from organic polymers. The use of an elastomer allows for easier separation of the replica from the mould.⁷⁴ Small structures have also been found to be preserved well using this method.⁷⁵ Another advantage is the possibility of thermal or mechanical manipulation of the mould. This can result in the production of patterns smaller than those originally cast in the elastomer.⁷⁶

1.3.1.3 Microtransfer Moulding

In the micro-transfer moulding technique a pre-polymer is placed into an elastomeric mould.⁶² The excess pre-polymer is then scrapped or blown off. The mould is then placed in contact with a substrate and the polymer is cured. Following curing the mould is removed to leave a microstructure on the surface. This patterning method works on non-planar substrates.⁷⁷ It is also possible to combine patterns formed in this manner to give three-dimensional structures.⁷⁸ This requires the careful positioning of the moulds but is otherwise straight forward.

1.3.1.4 Micro-moulding in Capillaries

Micro-moulding in capillaries relies on capillary action occurring when a droplet of low viscosity liquid pre-polymer is placed at openings of the mould.⁷⁹ The mould is placed face down on a substrate and forms a network of channels between the substrate and the mould. After the filling of the channels the pre-polymer is cured and the mould removed to give the final

structure. The structures that are possible with this methodology are limited by the necessity that they all be interconnected. If they are not there will be areas that are not reachable by the pre-polymer. The pre-polymer used in this method may be a solventless species or a solution. Three dimensional structures may be built up by the repeated use of this technique.⁸⁰

1.3.1.5 Solvent Assisted Micromoulding

Solvent assisted micromoulding is a method of fabricating microstructures in polymer substrates.⁶³ A mould is wetted by a liquid that will be a solvent for the substrate being patterned. The mould is then pressed into contact with the substrate. The solvent dissolves a thin layer of the substrate. This solvent/polymer mix will conform to the shape of the mould used. The mould is maintained in contact with the substrate until the polymer has re-solidified. A pattern in the shape of the relief of the mould is then formed on the surface and the mould may be removed.

The key to this procedure is the choice of solvent. It must be able to rapidly dissolve or swell the surface of the polymer being patterned, but it should not swell the PDMS mould used. Swelling the PDMS would result in distortions in the pattern and would reduce the ability of the mould to form a good contact with the surface.

1.3.2 Photolithographic

Photolithography is the most successful and widely used technology for microfabrication in modern times.⁸¹ It has been used extensively in the

microelectronic industry since its introduction in 1959 and essentially all integrated circuits are made in this manner.⁸² At its most basic a photolithographic system consists of a monochromatic source (electromagnetic or particle) that illuminates regions of a thin film resist that has been spin coated onto a silicon wafer through lenses and a mask in order to produce a pattern on the sample surface. UV and deep UV light sources have been found to produce lines down to a resolution of 80 nm.⁵³ If a higher resolution is desired particle systems with ion⁸³ or e beam⁸⁴ sources allow a resolution of 50 nm to be reached. These systems however are more developmental than UV mask technology; they are also considerably more expensive.

The overall resolution, R, that can be reached using photolithography is limited by optical diffraction and can be determined by the Rayleigh equation,⁸⁵ Equation 2.

$$R = k_1 \lambda / NA$$

Equation 2

Where λ is the wavelength of the illuminating radiation, NA is the numerical aperture of the lens system and k_1 is a constant that depends on the photoresist used. The theoretical limit due to diffraction is approximately $\lambda/2$, although the minimum feature size that is commonly obtained is of λ size. Therefore in order to produce smaller features, light sources with increasingly smaller wavelengths have been used. However, as the wavelength of the light decreases and the feature size becomes smaller the system becomes more complex and expensive.

There are two main ways that the pattern is transferred to the surface. Firstly, a mask that has the ability to block the radiation or particles may be interposed between the surface and the source.⁸⁶ Alternatively the source may be focused into a spot and scanned across the surface.⁸⁷ These two methods have different and complementary strengths. Using a mask allows the rapid production of a number of samples with the same pattern. The pattern formed is limited by how intricate the mask can be. Scanning a focused spot across a surface can be used to produce any 2D pattern that can be visualised using a CAD package. The patterning of the surface takes longer as the beam must be raster scanned across the surface. A scanning system is also more expensive as more complicated equipment set ups are required. A mask system only requires the focusing of the beam onto the mask.

1.3.3 Embossing

Embossing is a high throughput, low cost technique used in manufacturing. Microstructures are imprinted into a thermoplastic material using a master. Recently this technique has been shrunk down and applied to silicon with the production of 25 nm features showing the potential of embossing.⁵⁴ It has also been applied to semi-crystalline polymers such as poly(tetrafluoroethylene-co-hexafluoropropylene), which was embossed with a silicon master and reproduced edge details of less than 10 nm.⁸⁸

1.3.4 Moulding

In moulding a cast, called a master is prepared that is the inverse of the desired final shape allowing original three dimensional shapes to be reproduced. The material of the final product is then introduced in a liquid form, this can be a molten metal or a liquid polymer. The material in the mould is then allowed to set, usually by cooling and the mould removed to leave a replica of the interior structure of the mould. In modern manufacturing techniques to liquid precursor is injected into the mould under high pressure at a high temperature. Micromoulding has been use for the preparation of microstructures, such as 10 μm indium wires⁵⁵ and as a part of the production of submicroporous CdS films.⁸⁹

1.3.5 Laser Ablation

The ablation of a material (inorganic or polymer) through exposure to laser light can be used in the production of nano-scale patterns. Metals and glasses exposed to lasers are vaporised due to the heat, whilst polymer surfaces may become photo-chemically changed allowing selective dissolution in a process similar to photolithography. Recent work in this field has included the formation of arrays of nano-bumps on a silicon substrate by the irradiation of polystyrene micro-spheres,⁵⁶ mask fabrication,⁹⁰ thermopile formation⁹¹ and micro-fluidic component fabrication.⁹²

1.3.6 Scanning Probe Microscope Lithography

Scanning probe microscopy techniques were originally developed as methods for the examination of surfaces on the nanoscale.⁹³ In developing this field it has also become apparent that there is the possibility of using the probe to modify the surface.⁵⁷ There have been a number of different areas studied, these include the positioning of atoms⁹⁴ and molecules⁹⁵ in specific sites on a surface, the local deformation of the surface using high contact force,⁹⁶ the local application of inks to the surface (dip-pen nanolithography)⁹⁷ and probe based oxidation of suitable surfaces.⁹⁸ These techniques can be divided into two areas, physical and oxidative. Physical techniques involve the manipulation of the surface through mechanical interactions such as indentation, scratching, particle manipulation and molecular deposition. Oxidative techniques involve the exposure of regions of the surface to electric fields in order to induce chemical modification.

1.3.6.1 Physical Probe Lithography Techniques

1.3.6.1.1 Surface Indentation and Scratching

Since its inception as a technique for the studying of surfaces research into the usage of the atomic force microscope has concentrated on methods to reduce the possibility of the tip damaging the substrate.⁹⁹ However it has been found that imaging of soft samples (for example polymer or organic) in contact mode can lead to surface damage.¹⁰⁰ Due to this it has been common to study these surfaces in either tapping or noncontact mode thus reducing tip induce surface damage. There therefore exists the possibility of controlled contact

between the tip and the surface for the purpose of patterning substrates. The limiting factor in the use of the tip to mechanically modify the sample surface is the stability of the tip which may become deformed or contaminated through excessively hard contact. To reduce the damage to the tip several groups have taken to using diamond or diamond coated tips.¹⁰¹

The mechanical patterning of surfaces has been carried out on a number of substrates including soft metals such as gold,¹⁰² copper¹⁰³ and nickel¹⁰³ along with polymer¹⁰⁴ and semiconductor materials such as GaSb, InSb,¹⁰⁵ InAs,¹⁰⁶ and GaAs.¹⁰⁷ Patterns on surfaces have been formed by atomic force microscopes operating in both tapping and contact mode. The patterns formed are made up of thin lines and pits on the surface and the resolution of these lines is dependent on the geometry of the tip and the substrate material.

Nanoscratching has been applied to SAM¹⁰⁸ and Langmuir-Blodgett¹⁰⁹ films. If the scratching is carried out in a solution containing molecules or nanoparticles attachments may form between the particles and the underlying substrate, filling the free surface area created in situ,¹¹⁰ thus forming stable, ordered, mixed monolayers on a nanometre scale. Examples of this patterning method have been carried out on a gold substrate functionalised with a 1-octadecanethiol SAM.¹⁰⁸ Following scratching in a solution of 11-sulfanyl-1-undecanol a bifunctional surface was created. Furthermore, the remaining hydroxyl groups can be further functionalised, in effect producing a negative resist surface. Gold nanoparticles have also been positioned into wells created in a SAM surface in a similar manner.¹¹⁰

1.3.6.1.2 Particle Manipulation

The atomic manipulation and positioning of particles using a probe tip as a cue to push atoms,¹¹¹ molecules¹¹² and nanoparticles¹¹³ around a surface offers intriguing possibilities. Eigler and co-workers demonstrated in 1990 the ability to write on a metallic surface by the movement of adsorbed atoms with a scanning probe under ultra-high vacuum conditions at low temperatures.⁹⁴ Since then applications of this have been further developed and the construction of logic circuits including AND and OR gates from CO adsorbed on a Cu (111) surface has been demonstrated.⁹⁵

1.3.6.1.3 Dip Pen Nanolithography

Dip pen nanolithography is a direct write technique that has been pioneered by Mirkin and co-workers.⁹⁷ It consists of a transfer of material from the AFM tip to the underlying substrate. This material can be chemicals physisorbed upon the tip or constituents of the tip itself. Upon being brought into contact with the surface capillary forces enact the transfer of the material.¹¹⁴ The range of chemicals that have been patterned in the manner is large including a variety of dyes¹¹⁵ and dendrimers¹¹⁶ onto silicon substrates. Gold substrates have been patterned with a variety of SAM's. A comprehensive list is given in Table 1-1.

The effective line width that can be generated is dependent on the writing speed and temperature utilised and can be as low as 15 nm.¹¹⁷ Early studies also suggested that the transport of materials was dependent upon a water meniscus forming between the AFM tip and the surface,⁹⁷ writing

experiments have now been carried out under zero humidity conditions indicating that surface diffusion is a transport factor.¹¹⁸

A further development of DPN has been the introduction of hollow tip systems to produce fountain pen nanolithography systems.¹¹⁹ The tip used is a nano-pipette through which it is possible for a variety of molecules to flow. These molecular inks can then interact with the substrate, either etching¹¹⁹ or depositing as appropriate. Deposition of photoresists and protein patterns have also been reported using this technique.^{120,121}

Table 1-1 Overview of Ink / Substrate Combinations for DPN.

Ink	Substrate	Reference
Alkylthiols	Au	97,122,123,124,125,126,127
Ferrocenylthiols	Au	128
Silazanes	SiO _x , GaAs	129, 130
Proteins	Au, SiO _x	131,132,133,134,135
Conjugated Polymers	SiO _x	136,137,138
DNA	Au, SiO _x	139,140
Fluorescent Dyes	SiO _x	138,141
Sols	SiO _x	142,143,144
Metal Salts	Si, Ge	145,146,147
Colloidal Particles	SiO _x	148,149,150
Alkynes	Si	151
Alkoxysilanes	SiO _x	152
ROMP materials	SiO _x	153

1.3.6.2 Probe Oxidation Techniques

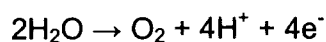
1.3.6.2.1 Scanning Tunnelling Microscope Oxidation

After the invention of the Scanning Tunnelling Microscope in 1982 researchers quickly noticed its ability to modify surfaces. Early results demonstrated the possibility of creating structures on a Pd₈₁Si₁₉ substrate.⁵⁷ This structure formation was attributed to the polymerisation of an adsorbed layer of oil originating from the vacuum oil pumps.

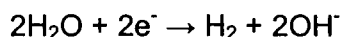
STM has been found to operate in two separate patterning modes. Firstly, electrons from the negatively biased tip oxidise the local material under the tip, this can be described as a type of low energy electron tunnelling.¹⁵⁴ Secondly, when operating in air or other humid atmospheres, the electric field from the tip causes the oxidation of the surface material via a faradic current.¹⁵⁵

The use of electron tunnelling to produce surface patterns has been reported for a number of surfaces, including organic SAM's.^{156,157} In these cases hexadecanethiol and N-biphenylthiol on gold and octadecyltrichlorosilane on silicon were used. Other surfaces that have been patterned in this manner include PMMA.¹⁵⁸

During the oxidation of surfaces through a faradic current the tip is immersed in the water layer between it and the surface, oxygen and water present are decomposed and these reaction products subsequently oxidise the substrate. The anodic reactions that take place on the surface are:



whilst the cathodic reaction occurring at the tip can be said to be:



and examples of this patterning method have been carried out on hydrogen terminated Si(100) substrates.¹⁵⁹

1.3.6.2.2 Atomic Force Microscopy Oxidation

Following the pioneering oxidative lithography experiments with STMs in the early 1990's the technique was transferred across to the STM's sister instrument, the Atomic Force Microscope (AFM). Field induced oxidation was applied to a number of metal surfaces such as Si,¹⁶⁰ Ti,¹⁶¹ Ta¹⁶² and Cr.¹⁶³ Electron induced oxidation was also applied to organic resists,¹⁶⁴ SAMs¹⁶⁵ and Langmuir-Blodgett films.¹⁶⁶

In the first set of experiments a metallic substrate was oxidised by the tip. This technique has been used to produce a number of nanodevices including thin titanium wires containing metal-oxide junctions,¹⁶⁷ metal-oxide semiconductor field-effect transistors (although parts of the structure was formed using photolithography)¹⁶⁸ and single electron transistors.¹⁶⁹

It was also found that it was possible to oxidise a silicon surface through an organic resist layer such as octadecyltrichlorosilane (OTS), causing SiO₂ to protrude through the resist layer.¹⁷⁰ These protrusions were then available for further modification such as the attachment of a second silane to the surface and the subsequent attachment of gold to the resulting terminal amine groups. The modification of the underlying layer through an organic resist has also been carried out on a gold substrate coated with octadecanethiol.¹⁷¹

The aforementioned techniques all featured the direct oxidation of the substrate or the destruction of a thin passive resist layer on an oxidizable substrate. A modification of this technique was found where instead of the oxidation of the underlying substrate, the organic layer was oxidised. This work was first demonstrated on a monolayer of 18-nonadecenytrichlorosilane on a p-doped silicon wafer.¹⁷² The terminal vinylic groups were found to be oxidised to carboxylic acid end groups. The possibility was later demonstrated to oxidise other SAMs such as OTS, providing the underlying silicon substrate is protected from oxidation by a densely packed closed monolayer.¹⁷³

1.3.7 Multiple Tip Scanning Probe Systems

One of the main disadvantages when using scanning probe techniques for the patterning of a surface is the time taken due to the serial nature of the process. In order to get round this problem a number of systems have been developed in which multiple probes are used. The two areas where this has been looked into are the thermal heating of the probe prior to indentation into a polymer surface¹⁷⁴ and for use in dip pen nanolithography.¹⁷⁵

The 'Millipede' system is a novel AFM based data storage system. In its last incarnation the system consisted of an array of 4096 tips (64 × 64) with integrated read / write capabilities using both contact force and applied heat.¹⁷⁴ The process of writing bits of data into a thin PMMA film achieved by heating selected tips to 400 °C using a current travelling through a highly doped section at the end of the cantilever. Data can subsequently be erased from the polymer storage area by heating the entire medium to 150 °C, causing the PMMA film to thermally flow, reforming a flat substrate. Reading

the data was possible by scanning a heated tip (300 °C) over the sample in order to measure the heat resistance; over a hole the cantilever comes closer to the PMMA, increasing the heat conductivity.

In dip pen nanolithography an eight tip nano-plotter has been developed by Mirkin.¹⁷⁵ This system has been used for the deposition of eight identical patterns of octadecylthiol on a gold substrate. A systems with thirty two parallel tips has been reported to provide eight identical dip pen patterns.¹⁷⁶

1.4 References

- [1] Sproul, W. D. *Surf. Coat. Technol.* **1996**, *81*, 1.
- [2] Choy, K. L. *Prog. Mater. Sci.* **2003**, *48*, 57.
- [3] Osaka, T. *Electrochim. Acta* **2000**, *45*, 3311.
- [4] Ulman, A. *Chem. Rev.* **1996**, *96*, 1533.
- [5] Bornside, D. E.; Macosko, C. W.; Scriven, L. E. *J. Appl. Phys.* **1989**, *66*, 5185.
- [6] Oskam, G.; Long, J. G.; Natarajan, A.; Searson, P. C. *J. Phys. D: Appl. Phys.* **1998**, *31*, 1927.
- [7] Chan, C. -M.; Ko, T. -M.; Hiraoka, H. *Surf. Sci. Rep.* **1996**, *24*, 1.
- [8] Barrel, Y.; Creatore, M.; Schaepkens, M.; Iacovangelo, C. D.; Miebach, T.; van de Sanden, M. C. M. *Surf. Coat. Technol.* **2004**, *180-181*, 367.
- [9] Woodward, I.; Schofield, W. C. E.; Roucoules, V.; Badyal, J. P. S. *Langmuir* **2003**, *19*, 3432.
- [10] Hubbard, K. M.; Espinoza, B. F. *Thin Solid Films* **2000**, *366*, 175.
- [11] Washiro, S.; Yoshizawa, M.; Nakajima, H.; Ohno, H. *Polymer* **2004**, *45*, 1577.
- [12] Chen, H. L.; Fan, W.; Wang, T. J.; Ko, F. H.; Zhai, R. S.; Hsu, C. K.; Chuang, T. J. *Appl. Opt.* **2004**, *43*, 2141.
- [13] Wang, J.; Huang, N.; Yang, P.; Leng, X. Y.; Sun, H.; Liu, Z.Y.; Chu, P. K. *Biomaterials* **2004**, *25*, 3163.
- [14] Soderlund, E.; Ljunggren, P. *Surf. Coat. Technol.* **1998**, *110*, 94.
- [15] Boyd, E. P.; Ketchum, D. R.; Deng, H.; Shore, S. G.; *Chem. Mater.* **1997**, *9*, 1154.

-
- [16] Sezer, A. O.; Brand, J. I. *Mater. Sci. Technol.* **2001**, *B79*, 191
- [17] Chi, E. J.; Shim, J. Y.; Baik, H. K.; Lee, S. M. *App. Phys. Lett.* **1997**, *71*, 324.
- [18] Caro, J.; Fraxedas, J.; Santiso, J.; Figueras, A.; Gorostiza, P.; Sanz, F. *Synth. Met.* **1999**, *102*, 1607.
- [19] Chen, Y. M.; Yu, G. P.; Huang, J. H. *Surf. Coat. Technol.* **2002**, *155*, 239.
- [20] Rodriguez, R. J.; Garcia, J. A.; Martinez, R.; Lerga, B.; Rico, M.; Fuentes, G.; G.; Guette, A.; Labruguere, C.; Lahaye, M. *App. Surf. Sci.* **2004**, *235*, 53.
- [21] D'Alessio, L.; Santagata, A.; Teghil, R.; Zaccagnino, M.; Zaccardo, I.; Marotta, V.; Ferro, D.; De Maria, G. *Appl. Surf. Sci.* **2000**, *168*, 284.
- [22] Suh, C. -M.; Hwang, B. -W.; Murakami, R. -I. *Mater. Sci. Eng., A* **2003**, *343*, 1.
- [23] Zhao, X. -M.; Wilbur, J. L.; Whitesides, G. M. *Langmuir*, **1996**, *12*, 3257.
- [24] Silberzan, P.; Leger, L.; Ausserre, D.; Benattar, J. J. *Langmuir* **1991**, *7*, 1647.
- [25] Thomas, R. C.; Sun, L.; Crooks, R. M.; Ricco, R. J. *Langmuir* **1991**, *7*, 620.
- [26] Himmelhaus, M.; Buck, M.; Grunze, M. *App. Phys. B.* **1999**, *68*, 595.
- [27] March, J. *Advanced Organic Chemistry*, 4th Ed., Wiley: New York, 1992.
- [28] McGovern, M. E.; Kallury, K. M. R.; Thompson, M. *Langmuir* **1994**, *10*, 3607.

-
- [29] Hall, D. B.; Underhill, P.; Torkelson, J. M. *Polym. Eng. Sci.* **1998**, *38*, 2039.
- [30] Shacham-Diamand, Y.; Dubin, V. M. *Microelectron. Eng.* **1997**, *33*, 47.
- [31] Cowburn, J. W. *IEEE Trans. Plas. Sci.* **1991**, *19*, 1048.
- [32] Von Engel, A. in *Electric Plasma: Their Nature and Uses*, Taylor and Francis, London, **1983**.
- [33] Grill, A. in *Cold Plasma in Materials Technology* IEEE press, Piscataway, New Jersey, **1994**.
- [34] Flamm, D. L.; Donnelly, V. M.; Ibbotson, D. E. *J. Vac. Sci Technol., B*, **1983**, *1*, 23.
- [35] Biederman, H.; Osada, Y. *Adv. Polym. Sci.*, **1990**, *95*, 57.
- [36] Hopkins, J.; Badyal, J. P. S. *J. Phys. Chem.*, **1995**, *99*, 4261.
- [37] Penning, F. M. in *Electrical Discharges in Gasses*, Phillips Technical Library, **1957**.
- [38] Chapman, B. in *Glow Discharge Processes*, John Wiley and Sons, USA, **1980**.
- [39] Clark, D. T.; Dilks, A. *J. Polym. Sci., Chem. Ed.*, **1977**, *15*, 2321.
- [40] Paegel, B. M.; Blazej, R. G.; Mathies, R. A. *Curr. Opin. Biotechnol.*, **2003**, *14*, 42.
- [41] Stern M. B. *Microelectron. Eng.*, **1997**, *34*, 299.
- [42] Munro, N. J.; Snow, K.; Kant, J. A.; Landers, J. P. *Clin. Chem.* **1999**, *45*, 1906.
- [43] McAlpine, M. C.; Friedman, R. S.; Lieber, C. M. *Nano Lett.*, **2003**, *3*, 443.
- [44] Craighead H. G. *Science*, **2000**, *290*, 1532.

-
- [45] Jiang, X. -P.; Clark, S. L.; Hammond P. T. *Adv. Mater.* **2001**, *13*, 1669.
- [46] Jin, J.; Iyoda, T.; Cao, C.; Song, Y.; Jiang, L.; Li, T. J.; Zhu, D. B. *Angew. Chem. Int. Ed.* **2001**, *40*, 2135.
- [47] Lukas, S.; Witte, G.; Wöll Ch. *Phys. Rev. Lett.*, **2002**, *88*, 028301-1.
- [48] Lohmeijer, B. G. G.; Schubert, U. S. *J. Polym. Sci. Part A: Polym. Chem.*, **2003**, *41*, 1413.
- [49] Lazzari, M.; Lopez-Quintela, M. A. *Adv. Mater.*, **2003**, *15*, 1583.
- [50] Alois Senefelder, tr. J.W. Muller. *The Invention of Lithography*, The Fuchs & Lang Manufacturing Company, New York, **1911**.
- [51] Kohli, N.; Worden R. M.; Lee, I. *Chem. Commun.*, **2005**, ??, 316.
- [52] Kumar, A.; Whitesides, G. M. *Appl. Phys. Lett.*, **1993**, *63*, 2002.
- [53] Service, R. F. *Science*, **2001**, *293*, 785.
- [54] Chou, S. Y.; Krauss, P. R.; Renstrom, P. J. *Appl. Phys. Lett.* **1995**, *67*, 3114.
- [55] Huber, T. E.; Luo, L. *Appl. Phys. Lett.* **1997**, *70*, 2502.
- [56] Huang, S. M.; Sun, Z.; Luk'yanchuk, B. S.; Hong, M. H.; Shi, L. P. *Appl. Phys. Lett.* **2005**, *86*, 161911.
- [57] Ringger, M.; Hidber, H. R.; Schlogel, R.; Oelhafen, P.; Guntherodt, H. -J. *Appl. Phys. Lett.*, **1985**, *46*, 832.
- [58] Xia, Y.; Whitesides, G. M. *Angew. Chem. Int. Ed.* **1998**, *37*, 550.
- [59] Leufgen, M.; Lebib, A.; Muck, T.; Bass, U.; Wagner, V.; Borzenko, T.; Schmidt, G.; Geurts, J.; Molenkamp, L. W. *Appl. Phys. Lett.*, **2004**, *84*, 1582.

-
- [60] Xia, Y.; Kim, E.; Zhao, X. -M.; Rogers, J. A.; Prentiss, M.; Whitesides, G. M.; *Science* **1996**, *273*, 347.
- [61] Kim, E.; Xia, Y.; Whitesides, G. M.; *Nature* **1995**, *376*, 581.
- [62] Zhao, X. -M.; Xia, Y.; Whitesides, G. M. *Adv. Mater.* **1996**, *8*, 837.
- [63] Kim, E.; Xia, Y.; Zhao, X. -M.; Whitesides, G. M. *Adv. Mater.* **1997**, *9*, 651.
- [64] Qin, D.; Xia, Y.; Whitesides G. M. *Adv. Mater.* **1996**, *8*, 917.
- [65] Tanaka, T.; Morigami, M.; Atoda, N.; *Jpn. J. Appl. Phys.* **1993**, *32*, 6059.
- [66] Kunnavakkam, M. V.; Houlihan, F. M.; Schlax, M.; Liddle, J. A.; Kolodner, P.; Nalamasu, O.; Rogers, J. A. *Appl. Phys. Lett.* **2003**, *82*, 1152.
- [67] Künzler, J. F.; *Trends Polym. Sci.* **1996**, *4*, 52.
- [68] DeBolt, L. C.; Mark, J. E. *Macromolecules* **1987**, *20*, 2369.
- [69] Kumar, A.; Biebuyck, H.; Whitesides, G. M. *Langmuir*, **1994**, *10*, 1498.
- [70] Larson, N. B.; Biebuyck, H.; Delamarche, E.; Michel, B. *J. Am. Chem. Soc.* **1997**, *119*, 3017.
- [71] Biebuyck, H. A.; Whitesides, G. M. *Langmuir* **1994**, *10*, 4581.
- [72] Xia, Y.; Zhao, X. -M.; Kim, E.; Whitesides, G. M. *Chem. Mater.* **1995**, *7*, 2332.
- [73] Jeon, N. L.; Clem, P. G.; Payne, A. A.; Nuzzo, R. G. *Langmuir*, **1996**, *12*, 5350.
- [74] Whitesides, G. M.; Xia, Y. *Photonics Spectra* **1997**, *31*, 90.
- [75] Parashar, V. K.; Sayah, A.; Pfeffer, M.; Schoch, F.; Gobrecht, J.; Gijs, M. A. M. *Microelec. Eng.* **2003**, *67-68*, 710.

-
- [76] Xia, Y.; McClelland, J. J.; Gupta, R.; Qin, D.; Zhao, X. -M.; Sohn, L. L.; Celotta, R. J.; Whitesides, G. M. *Adv. Mater.* **1997**, *9*, 147.
- [77] Wolfe, D. B.; Ashcom, J. B.; Hwang, J. C.; Schaffer, C. B.; Mazur, E.; Whitesides, G. M.; *Adv. Mater.* **2003**, *15*, 62.
- [78] Tang, M. D.; Golden, A. P.; Tien, J. J. *Am. Chem. Soc.* **2003**, *125*, 12988.
- [79] Kim, E.; Xia, Y.; Whiteside, G. M. *Nature* **1995**, *376*, 581.
- [80] Xia, Y.; Kim, E.; Whitesides, G. M.; *Chem. Mater.* **1996**, *8*, 1558.
- [81] Campbell, S. A. *The Science and Engineering of Microelectronic Fabrication*, Oxford Univ. Press, 1996.
- [82] Kilby, J. S. U. S. Patent 3,138,743 1964.
- [83] Terris, B. D.; Folks, L.; Weller, D.; Baglin, J. E. E.; Kellock, A. J.; Rothuizen, H.; Vettiger, P. *Appl. Phys. Lett.* **1999**, *75*, 403.
- [84] Liu, K.; Avouris, Ph.; Bucchignano, J.; Martel, R.; Sun, S.; Michl, J.; *Appl. Phys. Lett.* **2002**, *80*, 865.
- [85] Okazaki, S. *J. Vac. Sci. Technol. B*, **1991**, *9*, 2829.
- [86] Malek, C. K.; Jackson, K. H.; Bonivert, W. D.; Hruby, J. J. *Micromech. Microeng.* **1996**, *6*, 228.
- [87] van Kan, J. A.; Sanchez, J. L.; Xu, B.; Osipowicz, T.; Watt, F. *Nucl. Instrum. Methods Phys. Res., Sect. A* **1999**, *148*, 1085.
- [88] Stutzmann, N.; Tervoort, T. A.; Bastiaansen, C. W. M.; Feldman, K.; Smith, P. *Adv. Mater.* **2000**, *12*, 557.
- [89] Hoyer, P.; Baba, N.; Masuda, H. *Appl. Phys. Lett.* **1995**, *66*, 2700.

-
- [90] Hayden, C. J.; Eijkel, J. C. T.; Dalton, C. J. *Micromech. Microeng.* **2004**, *14*, 826.
- [91] Chen, Q.; Longtin, J. P.; Tankiewicz, S.; Sampath, S.; Gambino, R. J. *J. Micromech. Microeng.* **2004**, *14*, 506.
- [92] Gomez, D.; Goenaga, I.; Lizuain, I.; Ozaita, M. *Opt. Eng.* **2005**, *44*, 051105.
- [93] Binnig, G.; Rohrer, H.; Gerber, C.; Weibel, E.; *Phys. Rev. Lett.*, **1982**, *49*, 57.
- [94] Eigler, D. M.; Schweizer, E. K.; *Nature*, **1990**, *344*, 524.
- [95] Heinrich, A. J.; Lutz, C. P.; Gupta, J. A.; Eigler, D. M. *Science*, **2002**, *298*, 1381.
- [96] Nyffenegger, R. M.; Penner, R. M. *Chem. Rev.*, **1997**, *97*, 1195.
- [97] Piner, R. D.; Zhu, J.; Xu, F.; Hong, S. H.; Mirkin, C. A. *Science*, **1999**, *283*, 661.
- [98] Dagata, J. A.; Schneir, J.; Harary, H.; Evans, C. J.; Postek, M. T.; Bennet, J.; *Appl. Phys. Lett.*, **1990**, *56*, 2001.
- [99] Fleming, B. D.; Wanless E. J. *Microsc. Microanal.* **2000**, *6*, 104.
- [100] Magonov, S. N.; Reneker, D. H. *Annu. Rev. Mater. Sci.* **1997**, *27*, 175.
- [101] Niedermann, P.; Hanni, W.; Blanc, N.; Christoph, R.; Burger, J. *J. Vac. Sci. Technol. A* **1996**, *14*, 1233-6.
- [102] Silva, L. A.; Laitenberger, P.; Palmer, R. E. *J. Vac. Sci. Technol. B* **1993**, *11*, 1992.
- [103] Sumomogi, T.; Endo, T.; Kuwahara, K.; Kaneko, R.; Miyamoto, T. *J. Vac. Sci. Technol. B* **1994**, *12*, 1876.

-
- [104] Heyde, M.; Rademann K.; Cappella, B.; Geuss, M.; Sturm H.; Spangenberg, T.; Niehus, H. *Rev. Sci. Instr.* **2001**, *72*, 136.
- [105] Magno, R.; Bennett, B. R. *Appl. Phys. Lett.* **1997**, *70*, 1855.
- [106] Cortes Rosa, J.; Wendel, M.; Lorenz, H.; Kotthaus, J. P.; Thomas, M.; Kroemer, H. *Appl. Phys. Lett.* **1998**, *73*, 2684.
- [107] Hyon, C. K.; Choi, S. C.; Hwang, S. W.; Ahn, D.; Kim, Y.; Kim, E. K. *Appl. Phys. Lett.* **1999**, *75*, 292.
- [108] Liu, J. -F.; Cruchon-Dupeyrat, S.; Garno, J. C.; Frommer, J.; Liu, G. - Y. *Nano Lett.* **2002**, *2*, 937.
- [109] Fujihira, M.; Takano, H. *J. Vac. Sci. Technol., B: Microelectron. Nanometer Struct.--Process., Meas., Phenom.* **1994**, *12*, 1860.
- [110] Garno, J. C.; Yang, Y.; Amro, N. A.; Cruchon-Dupeyrat, S.; Chen, S.; Liu, G. -Y, *Nano Lett.*, **2003**, *3*, 389
- [111] Oyabu, N.; Custance, O.; Yi, I.; Sugawara, Y.; Morita, S. *Phys. Rev. Lett.* **2003**, *90*, 176102.
- [112] Foubert, P.; Vanoppen, P.; Martin, M.; Gensch, T.; Hofkens, J.; Helser, A.; Seeger, A.; Taylor, R. M.; Rowan, A. E.; Nolte, R. J. M.; De Schryver, F. C. *Nanotechnology* **2000**, *11*, 16.
- [113] Resch, R.; Baur, C.; Bugacov, A.; Koel, B. E.; Echternach, P. M.; Madhukar, A.; Montoya, N.; Requicha, A. A. G.; Will, P. *J. Phys. Chem. B* **1999**, *103*, 3647.
- [114] Jang, J.; Schatz, G. C.; Ratner, M. A. *Phys. Rev. Lett.* **2003**, *90*, 156104.
- [115] Su, M.; Dravid, V. P. *Appl. Phys. Lett.* **2002**, *80*, 4434.

-
- [116] McKendry, R.; Huck, W. T. S.; Weeks, B.; Fiorini, M.; Abell, C.; Rayment, T.; *Nano Lett.* **2002**, *2*, 713.
- [117] Schwartz, P. V.; *Langmuir* **2002**, *18*, 4041.
- [118] Sheehan, P. E.; Whitman, L. J. *Phys. Rev. Lett.* **2002**, *88*, 1561041.
- [119] Lewis, A.; Kheifetz, Y.; Shambrodt, E.; Radko, A.; Khatchatryan, E.; Sukenik, C. *Appl. Phys. Lett.* **1999**, *75*, 2689.
- [120] Hong, M. H.; Kim, K. H.; Bae, J.; Jhe, W. *Appl. Phys. Lett.* **2000**, *77*, 2604.
- [121] Taha, H.; Marks, R. S.; Gheber, L. A.; Rousso, I.; Newman, J.; Sukenik, C.; Lewis, A. *Appl. Phys. Lett.* **2003**, *83*, 1041.
- [122] Hong, S. H.; Zhu, J.; Mirkin, C. A. *Science* **1999**, *286*, 523.
- [123] Hong, S. H.; Mirkin, C. A. *Science* **2000**, *288*, 1808.
- [124] Weinberger, D. A.; Hong, S. H.; Mirkin, C. A.; Wessels, B. W.; Higgins, T. B. *Adv. Mater.* **2000**, *12*, 1600.
- [125] Zhang, H.; Li, Z.; Mirkin, C. A. *Adv. Mater.* **2002**, *14*, 1472.
- [126] Zhang, H.; Chung, S. -W.; Mirkin, C. A. *Nano Lett.* **2003**, *3*, 43.
- [127] Ivanisevic, A.; McCumber, K. V.; Mirkin, C. A. *J. Am. Chem. Soc.* **2002**, *124*, 11997.
- [128] Ivanisevic, A.; Im, J. H.; Lee, K. B.; Park, S. J.; Demers, L. M.; Watson, K. J.; Mirkin, C. A. *J. Am. Chem. Soc.*, **2001**, *123*, 12424.
- [129] Ivanisevic, A.; Mirkin, C. A. *J. Am. Chem. Soc.*, **2001**, *123*, 7887.
- [130] Pena, D. J.; Raphael, M. P.; Byers, J. M. *Langmuir*, **2003**, *19*, 9028.
- [131] Wilson, D. L.; Martin, R.; Hong, S.; Cronin-Golomb, M.; Mirkin, C. A.; Kaplan, D. L. *Proc. Natl. Acad. Sci. USA* **2001**, *98*, 13660.

-
- [132] Wei, L.; Hong, X.; Guo, W.; Bai, Y. B.; Li, T. J. *Chem. J. Chin. Univ.* **2002**, *23*, 1386.
- [133] Lee, K. B.; Park, S. B.; Mirkin, C. A.; Smith, J. C.; Mrksich, M. *Science*, **2002**, *295*, 1702.
- [134] Lim, J. H.; Ginger, D. S.; Lee, K. B.; Heo, J.; Nam, J. M.; Mirkin, C. A. *Angew. Chem. Int. Ed.* **2003**, *42*, 2309.
- [135] Lee, K. B.; Lim, J. H.; Mirkin, C. A. *J. Am. Chem. Soc.* **2003**, *125*, 5588.
- [136] Mayor, B. W.; Filocamo, S. F.; Grinstaff, M. W.; Liu, J. *J. Am. Chem. Soc.* **2002**, *124*, 522.
- [137] Lim, J. H.; Mirkin, C. A. *Adv. Mater.* **2002**, *14*, 1474.
- [138] Noy, A.; Miller, A. E.; Klare, J. E.; Weeks, B. L.; Woods, B. W.; De Yoreo, J. J. *Nano Lett.* **2002**, *2*, 109.
- [139] Demers, L. M.; Ginger, D. S.; Park, S. J.; Li, Z.; Chung, S. W.; Mirkin, C. A. *Science*, **2002**, *296*, 1836.
- [140] Demers, L. M.; Park, S. J.; Taton, T. A.; Li, Z.; Mirkin, C. A. *Angew. Chem. Int. Ed.* **2001**, *40*, 3071.
- [141] Su, M.; Dravid, V. P.; *Appl. Phys. Lett.* **2002**, *80*, 4434.
- [142] Fu, L.; Liu, X. G.; Zhang, Y.; Dravid, V. P.; Mirkin, C. A.; *Nano Lett.* **2003**, *3*, 757.
- [143] Su, M.; Liu, X. G.; Li, S. Y.; Dravid, V. P.; Mirkin, C. A. *J. Am. Chem. Soc.* **2002**, *124*, 1560.
- [144] Su, M.; Li, S. Y.; Dravid, V. P. *J. Am. Chem. Soc.* **2003**, *125*, 9930.
- [145] Li, Y.; Maynor, B. W.; Liu, J. *J. Am. Chem. Soc.* **2001**, *123*, 2105.
- [146] Maynor, B. W.; Li, Y.; Liu, J. *Langmuir* **2001**, *17*, 2575.

-
- [147] Porter, L. A.; Choi, H. C.; Schmeltzer, J. M.; Ribbe, A. E.; Elliott, L. C. C.; Buriak, J. M. *Nano Lett.* **2002**, *2*, 1369.
- [148] Ben Ali, M.; Ondarcuhu, T.; Brust, M.; Joachim, C. *Langmuir* **2002**, *18*, 872.
- [149] Liao, J. H.; Huang, L.; Gu, N. *Chin. Phys. Lett.* **2002**, *19*, 134.
- [150] Garno, J. C.; Yang, Y. Y.; Amro, N. A.; Cruchon-Dupeyrat, S.; Chen, S. W.; Liu, G.-Y. *Nano Lett.* **2003**, *3*, 389.
- [151] Hurley, P. T.; Ribbe, A. E.; Buriak, J. M. *J. Am. Chem. Soc.* **2003**, *125*, 11334.
- [152] Jung, H.; Kulkarni, R.; Collier, C. P.; *J. Am. Chem. Soc.* **2003**, *125*, 12096.
- [153] Liu, X. G.; Liu, S. W.; Mirkin, C. A. *Angew. Chem. Int. Ed.* **2003**, *42*, 4933.
- [154] Li, N.; Yoshinobu, T.; Iwasaki, H. *Appl. Phys. Lett.* **1999**, *74*, 1621.
- [155] Said, R. A. *Nanotechnology* **2003**, *14*, 523.
- [156] Hartwich, J.; Sundermann, M.; Kleineberg, U.; Heinzmann, U. *Appl. Surf. Sci.* **1999**, *144-145*, 538.
- [157] Kleineberg, U.; Brechling, M.; Sundermann, U.; Heinzmann, U.; *Adv. Funct. Mater.* **2001**, *11*, 208.
- [158] McCord, M. A.; Pease, R. F. W. *J. Vac. Sci. Technol. B.*, **1987**, *5*, 430.
- [159] Sugimura, H.; Nakagiri, N. *Jpn. J. Appl. Phys.* **1995**, *34*, 3406.
- [160] Campbell, P. M.; Snow, E. S.; McMarr, P. J.; *Appl. Phys. Lett.* **1993**, *63*, 749.

-
- [161] Kramer, N.; Birk, H.; Jorritsma, J.; Schonenberger, C. *Appl. Phys. Lett.* **1995**, *66*, 1325.
- [162] Sugimura, H.; Uchida, T.; Kitamura, N.; Masuhara, H. *Appl. Phys. Lett.* **1993**, *63*, 1288.
- [163] Sugimura, H.; Nakagiri, N. *Jpn. J. Appl. Phys.* **1995**, *34*, 3406.
- [164] Majudmar, A.; Oden, P. I.; Carrejo, J. P.; Nagahara, L. A.; Graham, J. J.; Alexander, J. *Appl. Phys. Lett.* **1992**, *61*, 2293.
- [165] Marrian, C. R. K.; Perkins, F. K.; Brandow, S. L.; Koloski, T. S.; Dobisz, E. A.; Calvert, J. M. *Appl. Phys. Lett.* **1994**, *64*, 390.
- [166] Stockman, L.; Neuttiens, G.; van Haesendonck, C.; Bruynseraede, Y. *Appl. Phys. Lett.* **1993**, *62*, 2935.
- [167] Snow, E. S.; Campbell, P. M. *Science* **1995**, *270*, 1639.
- [168] Minne, S. C.; Soh, H. T.; Flueckiger, P.; Quate, C. F. *Appl. Phys. Lett.* **1995**, *66*, 703.
- [169] Martel, R.; Schmidt, T.; Sandstrom, R. L.; Avouris, P.; *J. Vac. Sci. Technol. A* **1999**, *17*, 1451.
- [170] Q. Li, Q.; Zheng, J.; Liu, Z.; *Langmuir* **2003**, *19*, 166.
- [171] Zhao, J.; Uosaki, K. *Langmuir* **2001**, *17*, 7784.
- [172] Maoz, R.; Frydman, E.; Cohen, S. R.; Sagiv, J. *Adv. Mater.* **2000**, *12*, 424.
- [173] Maoz, R.; Frydman, E.; Cohen, S. R.; Sagiv, J. *Adv. Mater.* **2000**, *12*, 725.
- [174] Vettiger, P.; Binnig, G. *Sci. Am.* **2003**, *Jan.*, 35.
- [175] Hong, S.; Mirkin, C. A. *Science* **2000**, *288*, 1808.

[176] Zhang, M.; Bullen, D.; S. Chung, S. W.; Hong, S.; Ryu, K. S.; Fan, Z. F.; Mirkin, C. A.; Liu, C. *Nanotechnology* **2002**, *13*, 212.

Chapter 2

Surface Analysis Techniques

2.1 X-Ray Photoelectron Spectroscopy (XPS)

X-Ray photoelectron spectroscopy is a powerful method of surface analysis.¹ Soft X-rays (200-2000 eV) bombard the surface, these penetrate and interact with the atoms present, ejecting core level electrons via photo-ejection.² Photoelectrons are ejected from the top 1 - 5 nm of the sample escape with a distinct energy from the surface,³ pass through an energy analyser and are detected. A spectrum mapping the electron intensity as a function of the electrons kinetic energy (K.E.) is produced. The kinetic energy of an escaped electron is dependent on the energy of the incident photon. It also depends on the work function of the spectrometer and the binding energy of the electrons (B.E.) as expressed in Equation 2-1,

$$KE = h\nu - BE - \phi$$

Equation 2-1

Where KE is the kinetic energy of the electron produced, $h\nu$ is the energy of the incident photon, BE is the binding energy of the released electron and ϕ is the work function of the spectrometer.

As all elements have different electron core energies, therefore XPS peaks reveal the atomic surface composition. Furthermore the intensity of the different peaks in the spectra can be related to the concentration of the different elements on the surface within the sampled region. In addition the chemical environment of an atom within a species will have an effect on the core electron's binding energy. This means that not only are we provided with information about the elemental species on the surface but also molecular information on how they are bound together.

2.1.1 Instrumentation

An XPS machine is made up of a number of different components; an X-ray source in order to excite the electrons, an electron energy analyzer to record the electron kinetic energies and an ultrahigh vacuum environment.

There are two reasons that ultrahigh vacuum environments are required for XPS, electron mean free paths and sensitivity. When an electron is released from the sample surface and must travel to the detector, during this journey the probability of a collision with a gas molecule should be as low as feasibly possible. This is normally realised by ensuring that the mean free path of electrons within the spectrometer is greater than the size of the chamber. To ensure this pressures in the order of 10^{-5} – 10^{-6} mbar are required. XPS could be run at these pressures, however much lower pressures are generally used. This is due to the sensitivity of the technique to surface contamination. The electrons from the first two atomic layers of the surface are the primary signal source; therefore any sample contamination will drastically affect results. By operating the spectrometer in pressures of 10^{-10} mbar the contamination of the surface is greatly reduced.

The X-ray source for an XPS machine is chosen by two key factors. These are the width of the line of emission and the energy of this emission. The energy of emission of the source must be high enough to emit electrons from the sample. In order to minimise the signal to noise ratio and gain the most information from the spectra low emission widths are required. The combination of these two requirements leads to the elimination of most materials. The ones that are most suitable as anode materials are Magnesium or Aluminium.

The energy or velocity of the released electrons is measured by an analyser. These are generally electrostatic in nature due to the difficulty of producing magnetic fields within ultrahigh vacuum environments. The resolution of the energy analyser is important. The main definition of resolution is the 'absolute' resolution. This is measured as the full width at half the maximum height of a predefined peak. The resolution is therefore defined as,

$$R = \Delta E / E_0$$

Equation 2-2

where R is the resolution, ΔE is the FWHM and E_0 is the chosen peak's energy.

In XPS it is necessary that the same absolute resolution is applicable over the entire spectra. This is to allow the identification of different chemical states. The resolution of the spectrometer will also depend on the source used. Mg has a line width of 0.70 eV and Al has a line width of 0.85 eV. Therefore a high relative resolution would be required. This would require an expensive analyser. In standard practice therefore the kinetic energies of the photoelectrons are retarded to a pre chosen value. This is known as the pass energy although a set ratio may be chosen instead. This retardation enables the same absolute resolution to be obtained but at a lower relative resolution. The most commonly used electron energy analyser for XPS is the concentric hemispherical analyser. It is made up of two hemispherical surfaces positioned concentrically. A potential is applied across the surfaces such that the outer surface is negatively charged and the inner surface is positively charged. Electrons that enter the analyser with the correct energy and at the right angle will follow a path through the analyser and emerge focused at the

other end. They are then counted by a channeltron and the results transmitted to a computer so the energy spectra may be plotted.

2.2 Video Contact Angle (VCA)

Contact angle, θ , is a quantitative measurement of the wettability of a substance.⁴ The technique is very surface sensitive, analyzing the upper-most 5 – 10 Angstroms.⁵ The VCA can be used to deposit a measured volume of liquid onto a surface. A CCD camera can then capture an image of the droplet in real time. A snap shot of the image is captured and markers used to define the droplet perimeter, allowing a computer algorithm to determine the tangent to the droplet and hence contact angle the droplet makes with the surface.

Liquids are defined as having a specific surface tension, this is the force that minimizes the surface energy of liquid droplets and causes them to adopt the shape with the lowest surface area to volume ratio (a sphere). When a droplet is brought into contact with a surface this spherical shape is perturbed, this leads to an increase in the surface energy necessitating that work be done against the surface tension. This work is termed the surface energy in the case of solid surfaces. Surface energy and surface tension are denoted with the symbol γ and subscripted to denote the interface, ie γ_{SL} for the solid / liquid interface. Upon deposition on a surface a liquid droplet will spread as a result of the surface energy outweighing the surface of the liquid. The energy is calculated as the difference between the surface energy of the solid / vapour and the solid / liquid interfaces.⁶

The surface energy can be evaluated from the contact angle, θ , formed at the three phase boundary between the droplet and the surface, Figure 2-1.

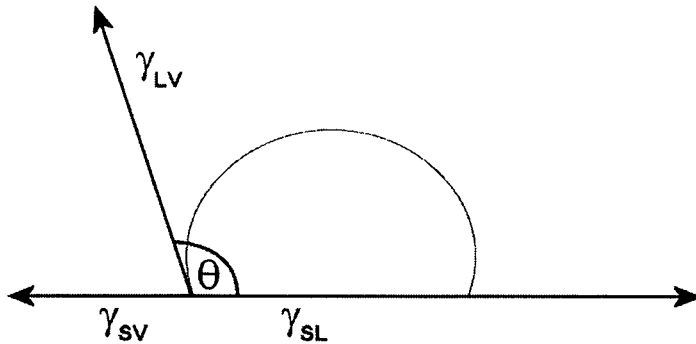


Figure 2-1 Contact Angle formed by a probe liquid droplet on a surface.

If θ is less than 90° then the liquid is said to wet the surface, above 90° and the surface is said to be non-wetting. A contact angle of 0° represents a completely wetting surface whilst a contact angle of 180° represents a completely repellent surface.

To calculate the surface energy it is necessary to establish a relationship between it and the measured contact angle. This is done through evaluation of the wetting phenomenon of a droplet placed on the surface,⁷ Figure 2-2.

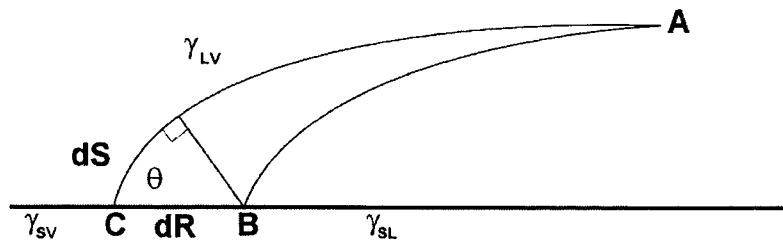


Figure 2-2 Schematic diagram of the probe liquid spreading to equilibrium on the surface.

If we consider the spreading of a drop across a surface from an initial shape, A-B, to a final equilibrium position, A-C. The change in Gibbs free energy at a constant volume may be related to the change in area, Equation 2-3 to Equation 2-8.

$$dG = 2\pi R dR \gamma_{SV} - 2\pi R dR \gamma_{SL} - 2\pi R dS \gamma_{LV}$$

Equation 2-3

And from trigonometry

$$dS = dR \cos \theta$$

Equation 2-4

So

$$dG = 2\pi R dR \gamma_{SV} - 2\pi R dR \gamma_{SL} - 2\pi R dR \cos \theta \gamma_{LV}$$

Equation 2-5

Which simplifies to

$$dG = 2\pi R dR (\gamma_{SV} - \gamma_{SL} - \cos \theta \gamma_{LV})$$

Equation 2-6

At equilibrium $dG = 0$, therefore;

$$0 = \gamma_{SV} - \gamma_{SL} - \gamma_{LV} \cos \theta$$

Equation 2-7

So

$$\gamma_{SV} = \gamma_{SL} + \gamma_{LV} \cos \theta$$

Equation 2-8

Equation 2-8 is known as Young's equation and is used to relate the contact angle to the individual surface energy components.⁸

By investigating the contact angle of the surface with a number of probe liquids of differing polar and dispersive surface energies the samples surface energy can be calculated. This can be done by utilizing the geometric mean method.⁹ The geometric mean method is derived from Young's equation and the determination that the surface energy may be split into two separate components (Polar, γ^P , and Dispersive, γ^d). Owens and Wendt⁹ have proposed that a geometrical averaging exists between the solid and liquid surface energies at the vapour interface, Equation 2-9. In combination with Young's equation the geometric mean equation can be constructed, Equation 2-10.

$$\gamma_{SL} = \gamma_{SV} + \gamma_{LV} - 2(\gamma_{SV}^d \gamma_{LV}^d)^{1/2} - 2(\gamma_{SV}^P \gamma_{LV}^P)^{1/2}$$

Equation 2-9

$$\gamma_{LV}(1 + \cos \theta) = 2(\gamma_{SV}^d \gamma_{LV}^d)^{1/2} + 2(\gamma_{SV}^P \gamma_{LV}^P)^{1/2}$$

Equation 2-10

By the measurement of contact angles for two or more fully characterized probe liquids Equation 2-10 can be solved to give the dispersive and polar surface energy components.

2.2.1 Contact Angle Hysteresis

The difference between the contact angle of a liquid advancing across a surface and the contact angle of a liquid receding across the same surface is known as contact angle hysteresis. There are two types of hysteresis possible on a surface. Kinetic hysteresis arises through modification of the sample by the probe liquid through such effects as swelling, washing or surface group orientation.¹⁰ Thermodynamic hysteresis is the second type and depends on surface roughness or surface heterogeneity.¹⁰

2.3 Reflectometry

The thickness of a thin film on a known substrate may be determined by reflectometry.¹¹ The reflectance and transmittance of a sample is measured over a range of wavelengths, usually from 190 nm to 900 nm. Light from a white light source passes through goes through a monochromator and is then focused onto the sample. The reflected and transmitted light is then detected and the intensities are conveyed to a computer for further analysis

The data collected is fitted to the Cauchy material model for dielectric materials.¹² In this model the refractive index, $n(e)$, and the absorption, $k(e)$, are said to be described by Equation 2-11.

$$n(e) = n_0 + n_1e + n_2e^2 + n_3e^3 + n_4e^4$$

$$k(e) = k_0 + k_1e + k_2e^2 + k_3e^3 + k_4e^4$$

Equation 2-11

where e is the photon energy in electron volts and n_0 - n_4 and k_0 - k_4 are the model parameters. The fitting scheme used in order to find the parameters is the Levenberg-Marquardt method. It is a solution to the fitting of non-linear curves. The thickness of the thin film is then determined from its dependence on the relationship between the reflectance, n and k of film, n and k of substrate, surface roughness and angle of incidence and the film thickness.

2.4 Fourier Transform Infrared (FT-IR) Spectroscopy

Infrared (IR) spectroscopy can be used to analyse the bulk chemical structure of polymer films by examining the various functional groups within the molecule that contain dipole moments. Many chemical groups have distinctive vibrational modes whose frequency is the equivalent of an infrared photon. Thus irradiation of a sample with IR radiation (of wavenumbers between 400 and 4000 cm^{-1}) achieves vibrational excitation as the molecule absorbs the infrared energy. A comparison of the incident IR beam with the transmitted IR beam allows the plotting of the relative transmission (T) at a given wavenumber.

$$T = \frac{I}{I_0}$$

Equation 2-12

Where I is the intensity of transmitted radiation and I_0 is the intensity of the incident radiation.

Vibrational modes are only active if there is a change in the molecular dipole moment during the vibration, therefore antisymmetric vibrations and vibrations involving polar groups are more likely to produce strong IR absorption bands.¹³

The FT-IR method has several advantages over dispersive infra-red spectroscopy.

1. The whole spectrum is scanned at once, so the time taken to acquire a spectrum with identical S/N ratio to a conventional IR spectrometer is drastically reduced.
2. There are no slits required in the optics of the spectrometer resulting in a much higher radiation throughput.
3. Resolving power in an FT-IR instrument is constant and does not vary with wavenumber.

FT-IR can be combined with the optical phenomenon of total internal reflection to study thin films. The IR beam is capable of passing through the polymer film before reflecting from the dense underlying substrate media (gold, silicon, glass).

An FT-IR spectrometer usually consists of a source of infrared radiation and a Michelson interferometer before the sample and a detector to examine the intensity of the IR beam after it has passed through the substrate.

2.5 Scanning Probe Microscopy

2.5.1 Introduction

Atomic Force Microscopy (AFM) is a powerful technique for the study of surfaces down to an Angstrom level. It was first developed by Binnig, Quate and Gerber in 1986.¹⁴ The AFM is a development of a scanning tunnelling microscope¹⁵ (STM) in which the deflection of a small cantilever as it passes over the surface is monitored.

The AFM consists of a very sharp probe tip (typical radius of curvature = 13 nm) generally made of silicon mounted at the end of a microscale cantilever.¹⁶ This is held in a fixed position above a piezoelectric scanner that is capable of lateral (X,Y) and vertical (Z) movement.

Images are generated by rastering a sample underneath the tip by using the lateral motion of the piezoelectric scanner. This rastering is controlled by the application of a slowly applied ramped voltage to one of the lateral axis (known as the slow scan axis) meanwhile a rapidly alternating voltage is applied to the other lateral axis (fast scan axis). The fast scan axis travels from limit to limit 1024 times in the time it takes for the slow scan axis to travel from one limit to the other. As the surface moves under the stationary tip surface properties can be monitored including the separation between the tip and surface that will give topographic data.

There have been a number of methods used to determine the separation distance between the cantilever and the surface. The original method was to coat the back of the AFM cantilever with a conductive material such as aluminium. This could then be tracked by a second STM above the

AFM cantilever.¹⁴ This set up was not reliable and required an STM in addition to an AFM. It has since been superseded by a beam deflection method.¹⁷ A laser beam is focused on the back of the cantilever. This is then reflected to a position sensitive photodetector. A standard photodetector is made up of four separate regions. These can be adjusted in order to get the maximum reflected signal from the reflected laser.

2.5.2 Contact Mode

Contact mode was the first mode of AFM developed. As the name suggests it involves direct contact between the cantilever tip and the surface. The tip is pushed into the surface with a force of 10^{-9} N.¹⁸ This small amount of force is not normally large enough to damage the sample being studied, but the tip can sometimes drag underneath the surface resulting in deformation of the surface and a false image.

2.5.3 NonContact Mode

A problem with contact mode AFM was damage to soft samples. This was circumvented by NonContact Mode AFM.¹⁹ In NonContact mode the cantilever is allowed to oscillate at its resonant frequency above the surface of the sample. The oscillations of the cantilever are monitored. These change when the cantilever is brought into closer contact with the surface. Therefore by maintaining a constant frequency of oscillation it is possible to map the surface. The piezoelectric crystal is used to keep the distance fixed. This

technique is not very sensitive relying as it does on Van der Waals forces between the tip and substrate.

2.5.4 Tapping Mode

Tapping mode was the next major advance in AFM techniques.²⁰ By allowing the cantilever to oscillate above the surface and come very lightly in contact with the sample it is possible to combine the features of both Contact and NonContact AFM. As the cantilever tip only makes a very soft contact with the surface damage due to lateral forces between the tip and surface is greatly reduced. It is therefore possible to image delicate samples without fear of damaging them as is likely with contact mode. The resolution is much improved over NonContact mode as we are no longer relying on only Van der Waals forces. Instead the cantilever comes into contact with the surface for a brief part of its oscillation cycle. The force with which the tip interacts or 'taps' the surface is controlled by the set point,²¹ the ratio of the free amplitude of oscillation of the cantilever to the amplitude of the cantilever during intermittent contact. Low set point values signify harder tapping of the surface whilst higher values signify softer tip surface interactions. Height artefacts can be generated in softer samples if these parameters are not correctly set.²² The tip-surface interaction is monitored by a standard laser / split photodiode system. During interaction with the surface the oscillating tip will lose energy, causing the cantilever resonance frequency to shift to a higher value and thus changing the amplitude of the peak at the frequency being monitored. A feedback loop is then used to adjust the Z position of the piezoelectric crystal so as to maintain a constant separation between the tip and surface whilst

scanning is in progress, these adjustments are recorded and used to form a topographical image.

2.5.5 Force Curves

The AFM can also provide information about the force felt by the cantilever as it scans the surface.²³ As the cantilever tip approaches the surface it begins to feel a force attracting it to the surface. At some point this force is large enough to drag the tip into contact with the surface. In contact with the surface the cantilever deflection will continue in a linear respect. If a stiff cantilever is used it is possible to indent a soft surface. Due to this effect it is possible to gain information about the elasticity of the sample from the force curve. When the cantilever is moved away from the sample surface it is possible that there is some adhesion between the tip and the surface. This can result in a continued contact between the tip and the surface. The last key point in the force curve is when the tip springs away from the surface. This gives information about the amount of force necessary to break any adhesion with the surface.

2.5.6 Phase Imaging

A key extra feature of Tapping mode AFM is the ability to generate a phase map of the surface. The phase image tracks the change in the phase of the oscillation of the cantilever with respect to its driven amplitude. As the cantilever is tracked across different surface domains the phase with which it oscillates changes. This provides us with a means of mapping different

chemical regions on a surface, as they will have different effects on the phase. The forces that influence the phase image are mechanical properties such as elasticity,²⁴ adhesion,²⁵ hydrophobicity,^{26,27} and energy dissipation.²⁸ When used in conjunction with the standard height image generated by tapping mode AFM this provides us with extra information about the sample.

2.5.7 Electric Force Microscopy

Electric Force Microscopy²⁹ (EFM) utilises the Lift Mode capacity of the AFM in which it is possible to scan a line on a surface using conventional methods, i.e. tapping mode. The same line is then rescanned at a fixed height above the surface determined from the previous height scan. Whilst on the Lift Mode scan a voltage may be applied to the cantilever tip. This voltage can be set by the Signal Access Module (SAM) or through an external source. In Lift Mode due to the separation between the tip and the sample the dominant forces are no longer due the standard forces that dominate phase images. They are instead dominated by longer-range forces such as Van der Waals or electrostatic. In the case of a charged surface the large electrostatic forces will therefore be dominant.

2.6 References

- [1] Briggs, D.; Seah, M. P. Practical Surface Analysis (second edition)
Volume 1, Wiley, 1990
- [2] Sherwood, P. M. A. in *Spectroscopy*, Straughan, B. P.; Walker, S. Eds.;
Chapman and Hall, London, **1976**.
- [3] Seah, M. P.; Deanch, W. A. *Surf. Interface Anal.* **1979**, 1, 2.
- [4] *Contact Angle, Wettability and Adhesion: Festschrift in Honor of
Professor Robert J. Good* Mittal, K. L. Eds; VSP International Science
Publishers 1993; Vol 2.
- [5] Domingue, J. *American Laboratory*, **1990**, 22, 50.
- [6] Cherry, B. W. in *Polymer Surfaces*, Cambridge University, Cambridge,
1981.
- [7] Cherry, B. W. in *Aspects of Surface Chemistry and Morphology in
Plastics, Surface and Finish*, Eds. Pinner, S. H.; Simpson, W. G.
Butterworths, London, **1971**.
- [8] Young, T. *Philos Trans. R. Soc.*, London, **1805**, 95, 65.
- [9] Owens, D. K.; Wendt, R. C. *J. Appl. Polym. Sci.*, **1969**, 13, 1741.
- [10] Andrade, J. D.; Chen, W. Y. *Surf. Int. Anal.*, **1986**, 9, 418.
- [11] Pro Optix User Manual, Version 2.0, 2000.
- [12] Tabet, M. F.; McGraham, W. A. *Thin Solid Films*, **2000**, 370, 122.
- [13] Colthup, N. B.; Daly, L. H.; Wiberley, S. E. *Introduction to Infrared and
Raman Spectroscopy 3 ed.* Academic Press, San Diego 1990.
- [14] Binnig, G.; Quate, C. F. *Phys. Rev. Lett.* **1986**, 56, 930.

-
- [15] Binnig, G.; Rohrer, H.; Gerber, C.; Weibel, E.; *Phys. Rev. Lett.*, **1982**, *49*, 57.
- [16] Ramirez-Aguilar, K. A. *Langmuir*, **1998**, *14*, 2526.
- [17] Meyer, G.; Amer, N. M. *Appl. Phys. Lett.* **1988**, *53*, 1045.
- [18] Quate, C. F. *Surf. Sci.*, **1994**, *299-300*, 980.
- [19] Martin, Y.; Abraham, D.W.; Wickramasinghe, H. K. *Appl. Phys. Lett.*, **1987**, *61*, 4723.
- [20] Zhong, Q.; Inniss, D.; Kjoller, K.; Elings, V. B. *Surf. Sci.* **1993**, *290*, L688.
- [21] Brandsch, R.; Bar, G. *Langmuir*, **1997**, *13*, 6349.
- [22] Bar, G.; Thomann, Y.; Brandsch, R.; Cantow, H. J.; Whangbo, M. -H. *Langmuir*, **1995**, *13*, 3807.
- [23] Tamayo, J.; Garcia, R. *Appl. Phys. Letts.* **1997**, *71*, 2395.
- [24] Aime, J. P.; Elkaakour, Z.; Odin, C.; Bouhacina, T.; Michel, D.; Curely, J.; Dautant, A. *J. Appl. Phys.* **1994** *76* 754-762
- [25] Noy, A.; Sanders, C. H.; Vezenov, D. V.; Wong, S. S.; Lieber, C. M. *Langmuir* **1998**, *14*, 1508.
- [26] Refier, D.; Windeit, R.; Kumpf, R. J.; Karbach, A.; Fuchs, H. *Thin Solid Films*, **1995**, *264*, 148.
- [27] Chen, X.; Davies, M. C.; Roberts, C. J.; Tendler, S. J. B.; Williams, P. M.; Davies, J.; Dawkes, A. C.; Edwards, J. C. *Ultramicroscopy*, **1998**, *75*, 171.
- [28] Tamayo, J.; Garcia, R. *Appl. Phys. Lett.* **1998**, *12*, L13.
- [29] Saurenbach, F.; Terris, B. D. *Appl. Phys. Lett.*, **1990**, *56*, 1703.

Chapter 3

Non-Contact Charging of a Polymer Surface using Electric Force Microscopy

3.1 Introduction

Surfaces that have been charged with a positive or negative voltage can find a number of uses in such areas as electrostatic filter media,¹ microphone manufacture,² microbe resistant packaging,³ optical display devices⁴ and biomedical applications.⁵ Additionally, the deposition of charge onto insulating surfaces can be used in memory storage devices,⁶ and in xerography applications.⁷ Modern laser printers and photocopiers both utilise surface charging effects in the production of printed pages.⁸

The measurement of the distribution of charge density across a surface has previously been limited to the use of electrostatic probes, with a scale in the range of mm. However, the development of Electric Force Microscopy (EFM), an off-shoot of Atomic Force Microscopy (AFM), has greatly improved the possible resolution when mapping surface charge. It has also been found to be a useful technique for the deposition of small regions of localised charge onto surfaces.⁹

There are two methods of using EFM to deposit charge: the application of high voltages through tips held static a fixed distance above the surface;⁹ and the deposition of charge onto the surface by bringing the charged tip into physical contact with the surface.¹⁰ Charge patches have also been deposited onto a homopolymer film utilising an EFM tip scanned at a fixed height above the surface.¹¹ In addition, contact between a surface and a charged tip has been found to chemically oxidise inorganic surfaces, such as silicon.¹²

3.2 Theory

3.2.1 The effect of force gradient on the phase lag of a freely oscillating cantilever

When an AFM is operating in Tapping Mode¹³ the tip is brought into intermittent contact with the sample surface. As the cantilever is driven to oscillate close to its first resonance frequency; the cantilever tip only comes briefly into contact with the surface during each oscillation. Upon approaching the surface, changes to the amplitude of frequency, resonance frequency and phase angle may be monitored.

The Phase Lag of the oscillating cantilever, ϕ , is the difference in phase between the frequency of oscillation of the cantilever and the frequency of the driving source. This value is expressed as an angle. When used in Tapping Mode AFM the phase lag is defined as being the difference in phase between the freely oscillating cantilever and the phase of the cantilever interacting with the underlying substrate: ^{14,15}

$$\Delta\phi = \phi_{\text{free}} - \phi_{\text{interacting}}$$

Equation 3-1

where ϕ_{free} is the phase of the freely oscillating cantilever and $\phi_{\text{interacting}}$ is the phase of the interacting cantilever. The value of $\Delta\phi$ across the sample may then be displayed as the AFM phase shift image. The driving frequency of the cantilever can be varied according to the experimental requirements; it is normally chosen to be close to the cantilever's resonance frequency as this

gives the maximum response. According to the theory of driven oscillators the maximum amplitude of a vibrating cantilever is equal to 90° .¹⁶ This leads to the phase of the freely vibrating cantilever, ϕ_{free} , being defined as 90° , Figure 3-1a.

Tip-substrate interactions shift the frequency at which the maximum amplitude occurs away from the driving frequency¹⁷. This results in the previously mentioned phase lag of the interacting cantilever, $\phi_{\text{interacting}}$, and produces dark (where the phase shift is lower than the background) or bright (where the phase shift is higher than the background) patches on the phase images gathered, corresponding to repulsive or attractive interactions. In a repulsive field gradient the maximum oscillation amplitude is increased. This causes the phase lag of the interacting cantilever to drop below 90° at the driving frequency. The resulting phase shift is therefore positive, Figure 3-1b, this corresponds to a brighter area in the phase image. The magnitude of the phase shift is indicative of the repulsion force experienced. The more repulsive, the brighter the resulting phase shift. In the case of an attractive force the opposite is true. The attractive force reduces the maximum oscillation amplitude frequency. The phase lag at the driving frequency rises to above 90° and so the phase shift becomes negative, Figure 3-1c, this gives a darker region on the phase image. The effect of force gradients on the cantilever phase shift is summarised in Table 3-1. These effects are discussed in more quantitative manner in an article by Garcia and Paulo.¹⁸

Table 3-1 Effects of Force Gradient on the phase shift of a freely oscillating cantilever.

Force Gradient	Resonance Frequency of Cantilever	Phase Shift, $\Delta\phi$	AFM Phase Image
Repulsive	Increases	Positive	Brighter
Attractive	Decreases	Negative	Darker

Phase Lag / Amplitude

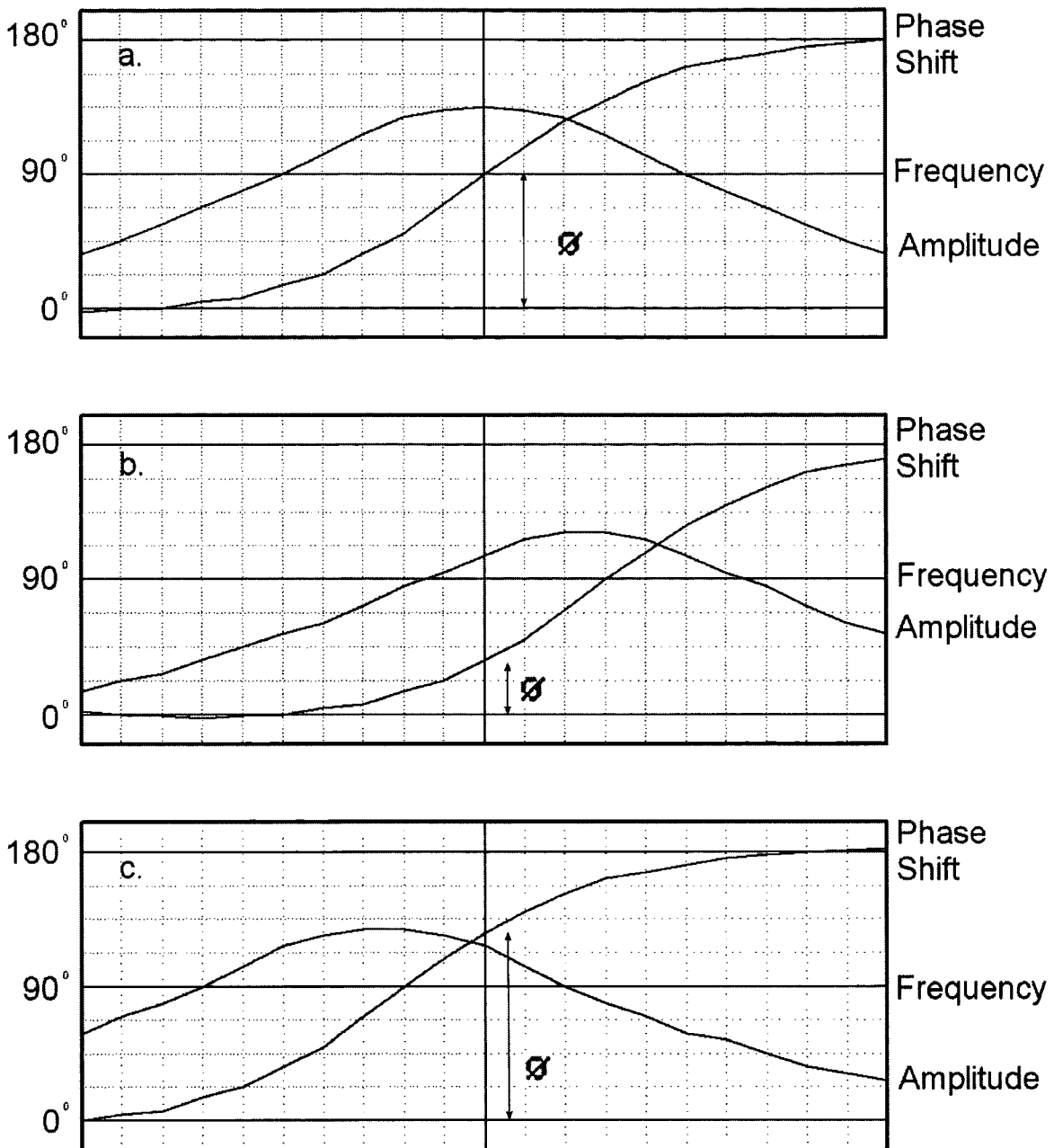


Figure 3-1 The effect of force gradients on the phase shift of a freely oscillating cantilever. (a), The phase lag of a freely vibrating cantilever at resonance, ϕ_{free} is 90° ; (b), The phase lag of a vibrating cantilever exposed to a repulsive force, $\phi_{\text{interacting}}$ is less than 90° ; (c), The phase lag of a vibrating cantilever experiencing an attractive force, $\phi_{\text{interacting}}$ is more than 90° .

3.2.2 Mapping Surface Charge with Lift-Mode EFM

In tapping mode AFM the cantilever tip comes into intermittent contact with the surface, causing the phase image to be dominated by short range forces above the sample surface. These forces provide information about the mechanical properties of the surface including elasticity,¹⁹ adhesion²⁰ and energy dissipation.²¹ In EFM studies, in order to reduce the effects of these forces, experiments are carried out in lift-mode during which the tip does not come in contact with the surface. During lift mode scanning a topographical map of the surface is determined by a preliminary scan; the scan is then repeated with the tip held at a fixed height above the surface, Figure 3-2. Any further changes in phase should therefore be due to additional long range forces. The long range forces that must be considered are Van der Waals (due to the polarisability of the surface) and electrostatic interactions. Electrostatic forces are the dominant force for charged homopolymer surfaces.⁹

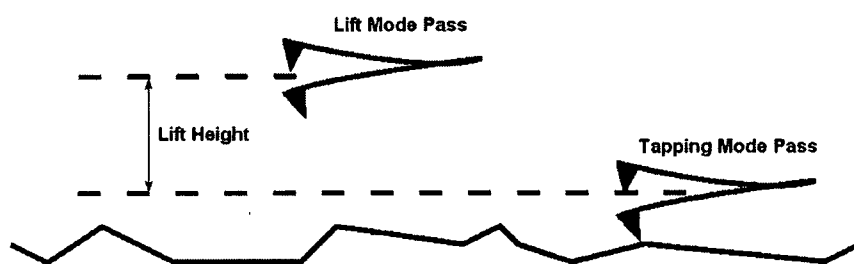


Figure 3-2 Diagram showing lift mode operation of tapping mode AFM.

The phase shift in lift-mode over a charged surface is dominated by the electrostatic interaction between the EFM tip and the surface. The surface will

have a fixed potential associated with it, V_{surface} . This voltage on the surface induces a mirror charge in the EFM tip, $-V_{\text{surface}}$. In addition to this, an external power supply may be utilised to apply a voltage to the tip, V_{applied} . The voltage experienced by the tip, V_{tip} , is therefore given by:

$$V_{\text{tip}} = V_{\text{applied}} - V_{\text{surface}}$$

Equation 3-2

The phase shift experienced by the tip whilst in lift mode will depend on both the polarity and magnitude of V_{tip} and V_{surface} . When V_{tip} and V_{surface} have the same polarity there will be a resultant repulsive force between them. This leads to a bright phase shift in the EFM image. Whereas when the charges on V_{tip} and V_{surface} are of opposite polarity an attractive force will result leading to a dark phase shift image. The magnitude of the phase shift detected depends on the product of V_{tip} and V_{surface} , therefore the intensity of the phase image gives us an indication of the magnitude of the surface voltage. When the voltage applied to the tip matches the surface voltage the induced tip voltage is zero. This results in no phase shift showing up in the EFM image.

For example, when a positive charge has been deposited on the surface, ($V_{\text{surface}} > 0$). If a negative voltage is applied to the tip, ($V_{\text{applied}} < 0$), according to the Equation 3-2, V_{tip} will be negative. As the surface charge is positive and the resultant tip charge is negative there will be an attractive force gradient between them. This leads to a dark phase shift image. The image darkens as an increasing negative voltage is applied to the tip as the attractive force between them grows. If a positive voltage is applied to the tip there are two possible results. If the positive voltage is such that $V_{\text{applied}} < V_{\text{surface}}$ the resultant value of V_{tip} will remain negative. This still leads to a dark

phase shift image. If $V_{\text{applied}} > V_{\text{surface}}$ then the value of V_{tip} will be positive. There will therefore be a repulsive force between the tip and the surface giving rise to a brighter phase patch. When $V_{\text{applied}} = V_{\text{surface}}$ there will be no phase shift attributable to the electrostatic force between the tip and the surface and there will be no variation in the phase images due to surface charge. This is summarised in Figure 3-3. The converse argument is true for a negatively charged surface, summarised in Figure 3-4.

V_{applied}	Increasing Negative Voltage		Zero Voltage	Increasing Positive Voltage				
Tip Voltage	$V_{\text{applied}} < V_{\text{surface}}$					$V_{\text{applied}} = V_{\text{surface}}$	$V_{\text{applied}} > V_{\text{surface}}$	
Force	Even More Attractive	More Attractive	Attractive	Less Attractive	Repulsive	Repulsive	More Repulsive	More Repulsive
Gradient	Even More Negative	More Negative	Negative	Less Negative	None	None	Positive	More Positive
Phase Shift	Even More Negative	More Negative	Negative	Less Negative	None	None	Positive	More Positive
	Darker Phase Image				Brighter Phase Image			

Figure 3-3 Schematic of the forces present between the EFM tip and a region of positively charged surface as a function of tip voltage.

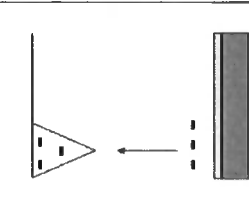
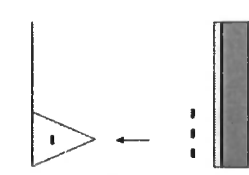
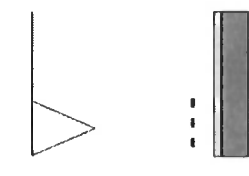
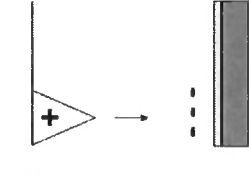
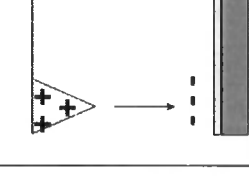
V_{applied}	Increasing Negative Voltage ←		Zero Voltage	Increasing Positive Voltage →	
Tip Voltage	$V_{\text{applied}} < V_{\text{surface}}$		$V_{\text{applied}} > V_{\text{surface}}$		
					
Force Gradient	More Repulsive	Repulsive	No Electrostatic	Attractive	More Attractive
Phase Shift	More Positive	Positive	None	Negative	Even More Negative
	Brighter Phase Image ←			Darker Phase Image →	

Figure 3-4 Schematic of the forces present between the EFM tip and a region of negatively charged surface as a function of tip voltage.

3.2.3 Surface Charging Using an EFM

There are three possible methodologies available for the charging of thin films using Electric Force Microscopy (EFM) techniques. These are contact electrification,²² corona discharge⁹ and dielectric breakdown,²³ These occur at increasing values of applied voltage and with various states of contact between the tip and surface, Figure 3-5.

In contact electrification the metallized EFM tip is brought into direct contact with the polymer surface to be charged. The tip may be under a positive or negative voltage or it may not be charged. A polymethylmethacrylate (PMMA) surface has been charged by repeated contact with a metal Atomic Force Microscope tip.^{10,24} In the reported experiments when there was no charge on the tip during polymer contact the resultant charging was found to be variable in size and polarity. This inconsistency in the polarity of the charge deposited was removed when the tip had an applied voltage during its contact with the surface.²⁵ A charge of -4 V was brought into contact with a silicon oxide layer, the surface was then imaged with ± 4 V applied to the tip in non-contact mode, at a height of 70 nm above the surface. The charge deposited was found to interact in a repulsive manner with the metal tip when scanned with a negative voltage and in an attractive manner when a positive voltage was used. The deposited charge in this case was not found to be long lasting and had decayed significantly in the 400 seconds following initial contact on scanning with positive voltage.

By increasing the electric field between a spatially separated Electric Force Microscope tip and the surface, a corona discharge may be generated,⁹

depending on the tip geometry, scanning height and surface composition.²⁶ Using this methodology 100 V pulses were applied to a metal tip that was oscillating at a height of 100 nm above a PMMA surface.²⁶ This resulted in charge being deposited onto the polymer. If a voltage lower than 100 V was used there was no evidence of charging, supporting the conclusion that a corona discharge was occurring and that there was a threshold voltage below which the corona discharge was not generated. The charge generated on the PMMA surface using this technique was found to decay over a time period of approximately 60 minutes.

Dielectric breakdown occurs when a critical value for the electric field between the surface and the charged tip is exceeded during contact.²⁷ During dielectric breakdown the field gradient between the surface and the tip is sufficient to ionise atoms within the film, turning the surface into a hot conductor. Dielectric breakdown has previously been studied by bringing the metal tip into contact with the surface and steadily increasing the voltage.²⁸ Initially there is no evidence of topographical changes and no external current is detected. However, after breaching a set voltage the surface topography becomes roughened and a current between the tip and surface is detectable.²⁹ This was defined as the dielectric breakdown of the surface. A previous investigation of this phenomenon on a silicon dioxide surface determined that breakdown was inhomogeneous. In addition, bias voltages were found to be much greater when the breakdown was induced with negative voltage compared to positive voltage. This was the opposite to the expected bulk breakdown voltage dependence as determined by measurements on conventional metal-oxide-silicon capacitors.³⁰ The cause of

this anomaly was theorised to be due to the field enhancement effect,³¹ whereby the electric field present was enhanced at the sharp end of the microscope tip. Due to this, under positive voltage, positive streamers were formed, seeming to decrease the dielectric breakdown voltage. Whereas under negative voltage the reverse happened and the dielectric breakdown voltage was increased due to negative streamers.

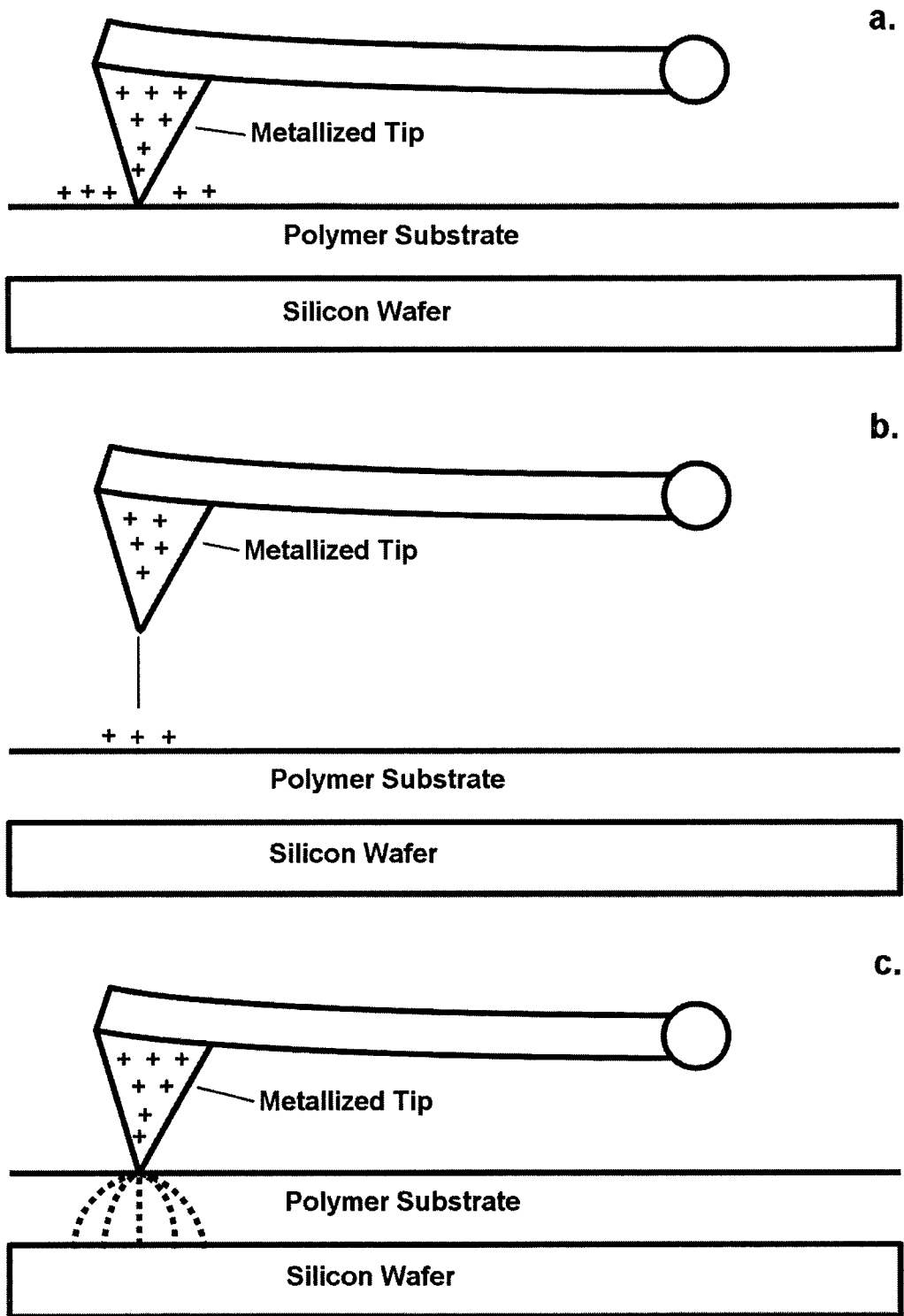


Figure 3-5 Schematic showing (a), Contact Electrification of a surface, (b), Corona Discharge onto a Surface and (c), Dielectric Breakdown of a surface.

More recently studies have looked at the deposition of charge onto organic layers using contact electrification. Care must be taken during the charging of thin organic film systems using a highly charged tip as it has been reported that the electric field can modify the surface. The modification can be of a number of different types, including polymerization,³² joule heating³³ and polymer crosslinking or breakdown.³⁴

Surface polymerization of a monomer, 3-phenyl-1-ureidonitrile, has been performed with charge pulses from a Scanning Tunnelling Microscope tip.³⁵ Once polymerized the 3-phenyl-1-ureidonitrile polymer was found to be conducting along its backbone. Scans over exposed and unexposed regions of the surface revealed significantly different I-V curves, showing that the conductance of the substrate had been changed by the polymerization.

Joule heating of polystyrene and PMMA films has been carried out by Lyuksyutov et al.³³ A tip was oscillated above the surface at a set oscillation amplitude, during this a high frequency pulse of dc voltage between -5 V and -50 V was applied. Small raised features were observed on the polymer film following voltage deposition, due to mass transport of the polymer film towards the charged tip. As the surface features were not a result of chemical modification they could be removed by annealing.

It has also been shown that scanning a PMMA surface with a charged, gold metallized tip, in contact with the surface results in modification of the polymer and the formation of a positive or negative resist.³⁴ When the scanning voltage used was -7 V the polymer chains on the surface of the substrate were broken up into chains of lower molecular weight that were

more easily dissolved in a methyl-isobutyl-ketone / isopropanol solution forming a positive resist. Upon increasing the scanning voltage to – 18 V the developed substrate was found to have raised regions corresponding to the exposed regions. This was interpreted as being due to crosslinking of the polymer surface following the exposure to the electric field. The increased molecular weight of the polymer and reduced solubility yielding negative resist behaviour on the PMMA surface.

3.3 Experimental

An Atomic Force Microscope (AFM) equipped with a Nanoscope III control module, extender electronics module and a signal access module (Digital Instruments) was employed in interleave mode to deposit charge onto polymer surfaces. A Cr sputter coated EFM probe was used with a 125 μm long silicon tip (MikroMasch NSC15/Cr, force constant ≈ 40 nN, resonance frequency ≈ 270 kHz after metallization). Tapping mode was used to capture height and phase images of the sample surface. Next, an interleave scan at a constant tip height above the surface was used in order to capture an EFM image. The interleave height was determined by the tapping mode height data.

Consistent parameters for scanning were kept constant: a set point of 2 V was used for tuning, a set point of 1.2 V was used for imaging the surface. A lift height of 30 nm was used for all depositions of charge onto the surface and a lift height of 100 nm was used for all imaging. The scan rate was maintained at 1 Hz.

Depositing charge onto the polymer surface necessitated a greater voltage than is available through the signal access module (± 12 V through 'Analogue 2'). To enable deposition of higher voltages onto the surface a custom built high voltage dc power supply (± 180 V) was hence gated through the signal access module. As this was going through the 'Analogue 2' signal the voltage was only applied during the lift mode scan.

Dilute 2% solutions of polystyrene (Aldrich, $M_w = 280,000$), polymethylmethacrylate (Aldrich, $M_w = 93,000$), polybromostyrene (Aldrich,

$M_w = 65,000$), polychlorostyrene (Aldrich, $M_w = 75,000$), polymethylstyrene (Aldrich, $M_w = 72,000$) and polymethoxystyrene (Aldrich, $M_w = 80,000$) were prepared in toluene (BDH, 99.5%). Formulated polymer solutions were deposited onto silicon wafers (Silicon Valley Microelectronics, Inc.) using a spin-coater (Cammax Precima) operating at 2000 rpm for 30 seconds. These films were left in air for 1 hour to release entrapped solvent via evaporation.

Monomers, Styrene (Aldrich, +97%), Methylmethacrylate (Aldrich, +97%), Allylmercaptan (Aldrich +97%), Vinylbenzylchloride (Aldrich, +97%) and 3-Vinylbenzaldehyde (Aldrich, +97%) were loaded into a sealable glass tube, followed by further purification using several freeze-pump-thaw cycles to remove adsorbed gases. Pulsed plasma polymerization of the precursor was undertaken in a cylindrical glass reactor (4.5 cm diameter, 460 cm³ volume, 2 x 10⁻³ mbar base pressure, leak rate 1.4 x 10⁻⁹ mol/s) surrounded by a copper coil (4 mm diameter, 10 turns, located 15 cm away from the precursor inlet) and enclosed in a Faraday cage. The chamber was evacuated using a 30 L min⁻¹ rotary pump attached to a liquid nitrogen cold trap, whilst monitoring the system pressure with a Pirani gauge. All fittings were grease-free. The output impedance of a 13.56 MHz radio frequency (RF) power supply was matched to the partially ionized gas load using an L-C network. During pulsed plasma deposition, the RF source was triggered by a signal generator and the pulse shape monitored with an oscilloscope. Prior to each deposition, the apparatus was cleaned by scrubbing with detergent, rinsing in propan-2-ol, and then oven drying. The reactor was then reassembled and evacuated to base pressure. Further cleaning entailed running a continuous wave air plasma at 0.2 mbar pressure and 40 W power lasting 30 min. Next, silicon

(100) wafers (MEMC Materials Inc) were inserted into the centre of the reactor and the system pumped back down to base pressure. At this stage, monomer vapor was introduced into the chamber at a pressure of 0.2 mbar for 5 min prior to plasma ignition. Optimum film deposition conditions for pulsed plasma deposition corresponded to 40 W continuous wave bursts lasting 100 μs (t_{on}), followed by an off-period (t_{off}) set at 4 ms. Optimum conditions for the deposition of methylmethacrylate corresponded to a 20 W continuous wave. Upon completion of deposition, the RF generator was switched off and the monomer allowed to continue flowing through the system for a further 5 min. Finally the chamber was evacuated to base pressure and vented to atmospheric pressure.

Film thickness measurements were obtained using an nkd-6000 spectrophotometer (Aquila Instruments Ltd.). Transmission-Reflectance curves (over the 350 – 1000 nm wavelength range) were fitted to a Cauchy model for dielectric materials using a modified Levenburg-Marquardt method. All films used in this study were between 100 – 150 nm in thickness.

EFM experiments consisted of two stages. Firstly, the surface was charged by applying a large voltage (5 -150 V), to the tip over a square region (typically 5 μm \times 5 μm). This was followed by characterisation of the charged region, whereby a square approximately sixteen times the area of the deposition region (or 20 μm \times 20 μm , whichever has larger,) was scanned with a voltage of \pm 12 V or 0 V applied to the tip and at a height of 100nm above the surface. The lower voltage and higher height were chosen to ensure minimal distortion of the deposited charge.

3.4 Results

Two studies have been undertaken using EFM techniques. One to probe the response characteristics and limitations of EFM itself (this was undertaken on a well-characterised single substrate (polystyrene)) and a second study undertaken with knowledge gained from the preceding study to probe the differing response of polymers to charging depending on structure and properties.

3.4.1 Investigation into the EFM technique

Charging a $5\ \mu\text{m} \times 5\ \mu\text{m}$ region upon a polystyrene surface with a high positive voltage (+ 60 V applied to the tip) resulted in no changes in the subsequent $20\ \mu\text{m} \times 20\ \mu\text{m}$ topographical or phase images, Figure 3-6. A significant contrast change (positive charge deposition) was clearly evident in the EFM lift-mode images, Figure 3-7(a-b). Scanning the polystyrene film surface (following the deposition of positive voltage with a positively charged EFM tip operating in lift-mode) a repulsive force between the surface and tip was evident as a bright patch, Figure 3-7(a). Employing a negative voltage to the tip, the surface scans reveal a dark patch (attractive force between the induced tip voltage and the charged surface), Figure 3-7(b).

The phase contrast changes observed were dependant on the magnitude of the charging voltage, Figure 3-7. Increasing the applied voltage from 10 V to 60 V resulted with a phase contrast that was initially non-evident (at 10 V), to ill-defined (at 20 V), and finally producing a more contrasted dark patch with improved definition (at 60 V).

The tip height above the sample surface was revealed as an important parameter. Decreasing the separation between tip and surface for the charge introduced greater intensity on the phase contrast image, Figure 3-8.

The deposited voltage was also found to be dependent upon the speed the tip traversed the surface during deposition. Increasing the scan speed during charge deposition whilst maintaining a constant discharge voltage (+ 80 V) and lift-height (30 nm) was found to reduce the intensity of the dark region seen afterwards in the lift-mode EFM image, Figure 3-9a-b. This indicates less charge deposition onto the surface.

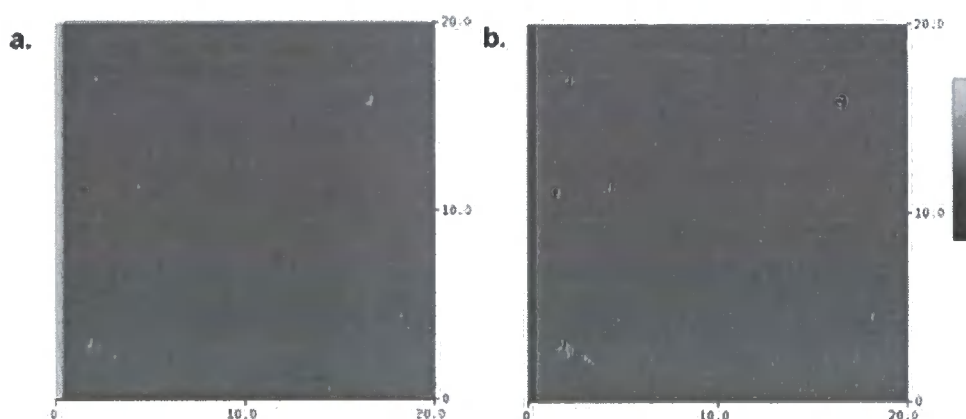


Figure 3-6 20 μm \times 20 μm micrographs of polystyrene following charging of the central 5 μm \times 5 μm square with + 60 V, (a) Height (150 nm) and (b) Phase(180 $^\circ$).

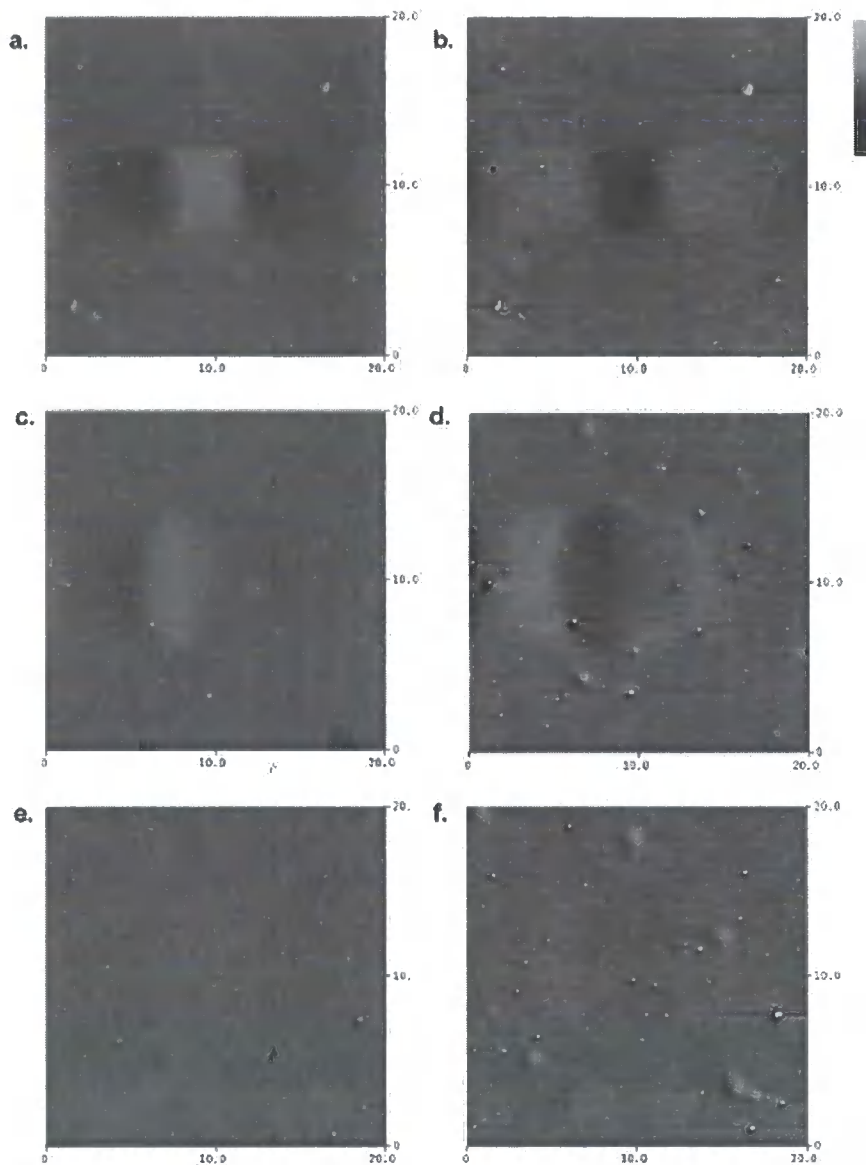


Figure 3-7 20 μm x 20 μm micrographs of polystyrene recorded with + 12 V (left column) and - 12 V (right column) applied to the tip. The central square was previously exposed to (a) and (b) + 60 V lift-mode bias, (c) and (d) + 20 V lift-mode bias and (e) and (f) + 10 V lift mode bias. Z Scale 10 $^{\circ}$.

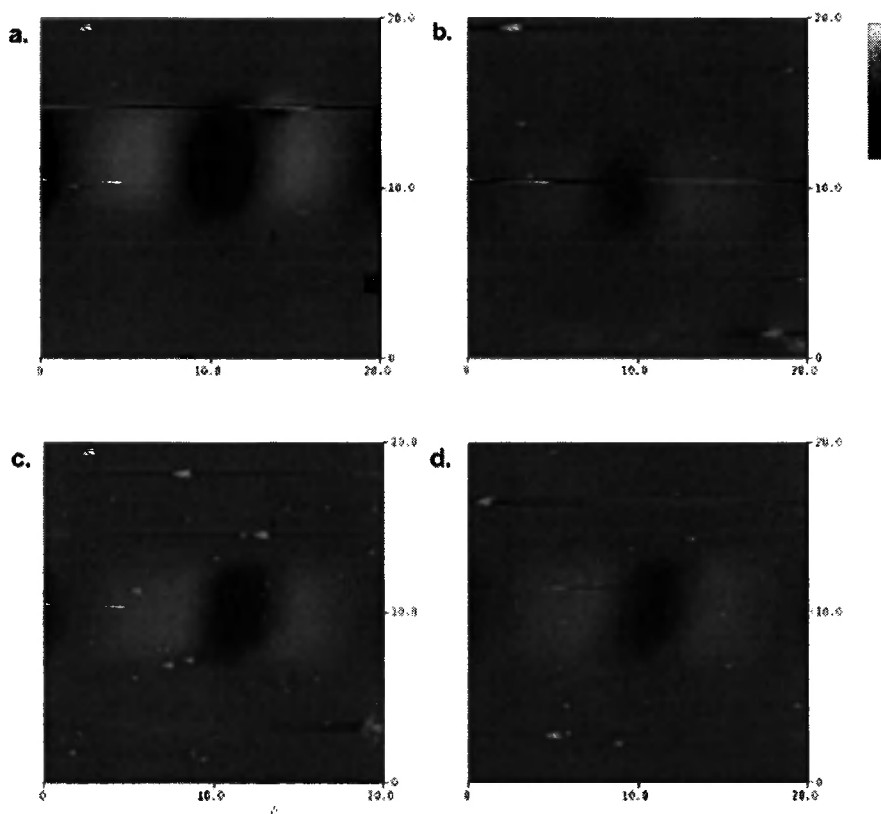


Figure 3-8 20 μm x 20 μm micrographs of polystyrene recorded with - 12 V applied to the tip. The central square was previously exposed to a + 60 V lift-mode bias (Scan speed = 1.0 Hz): (a) Lift-height during charge deposition = 15 nm; (b) Lift height during charge deposition = 30 nm; (c) Lift height during charge deposition = 45 nm and (d) Lift height during charge deposition = 60 nm. Z Scale 10°.

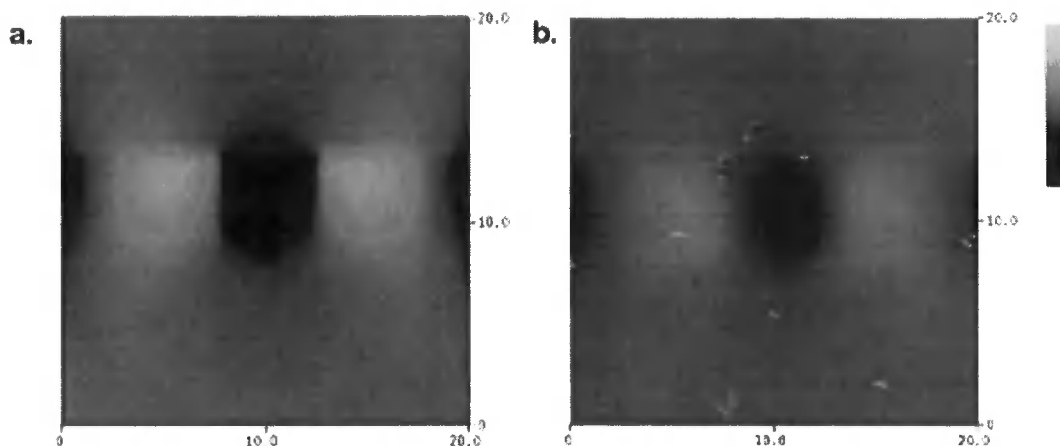


Figure 3-9 20 μm x 20 μm micrographs of polystyrene recorded with - 12 V applied to the tip. The central square was previously exposed to a + 80 V lift-mode bias: (a) Scan speed while charging = 1 Hz; (b) Scan speed while charging = 3 Hz. Z Scale 10 $^{\circ}$.

As with positive voltages, it was also possible to charge polystyrene surfaces with negative voltages using a metallized AFM tip. The threshold voltage required to ensure charging was higher (- 60 V) with negative voltage than with positive voltage (+ 20 V). The deposition of a high negative voltage (- 110 V) gave no evidence of contrast changes in the subsequent AFM topographical or phase images, Figure 3-10, hence there was no chemical modification of the surface. However, negative charge deposition was clearly evident in EFM lift-mode images, Figure 3-11(a-b).

Charge deposition voltage was found to have an effect on the resultant EFM phase contrast. No localised EFM phase contrast was visible in the lift-mode image during a scan with \pm 12 V following a tip deposition voltage of - 55 V being applied to the surface, Figure 3-11(e-f). When the deposition voltage was increased to - 60 V a phase contrast was evident upon scanning

the surface with ± 12 V, although ill-defined, Figure 3-11(c-d). Increasing the discharge voltage to - 110 V generated a well defined region of dark phase contrast, Figure 3-11(a-b). The magnitude and resolution of the EFM phase shift images were increased when scanning an area that had been exposed to a higher tip deposition voltage.

The lift-height and scan speed were found to have similar effects on the EFM phase contrast following the deposition of negative voltage onto the surface as with positive voltage, Figure 3-12 and Figure 3-13. The greater the lift height during deposition, the smaller the phase shift detected on scanning the surface and the greater the scan speed, the smaller the scanning phase shift.

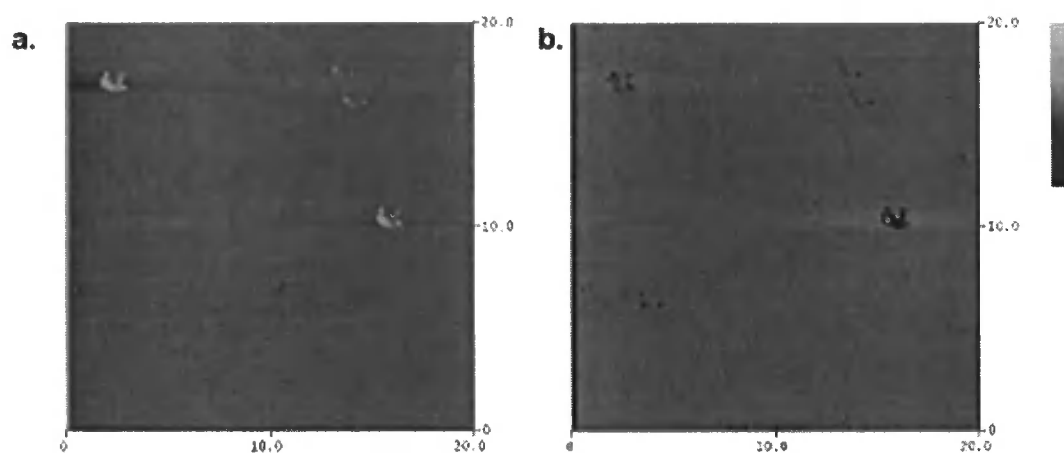


Figure 3-10 20 $\mu\text{m} \times 20 \mu\text{m}$ micrographs of polystyrene following charging of the central 5 $\mu\text{m} \times 5 \mu\text{m}$ square with - 110 V, (a) Height (150 nm) and (b) Phase (180 $^\circ$).

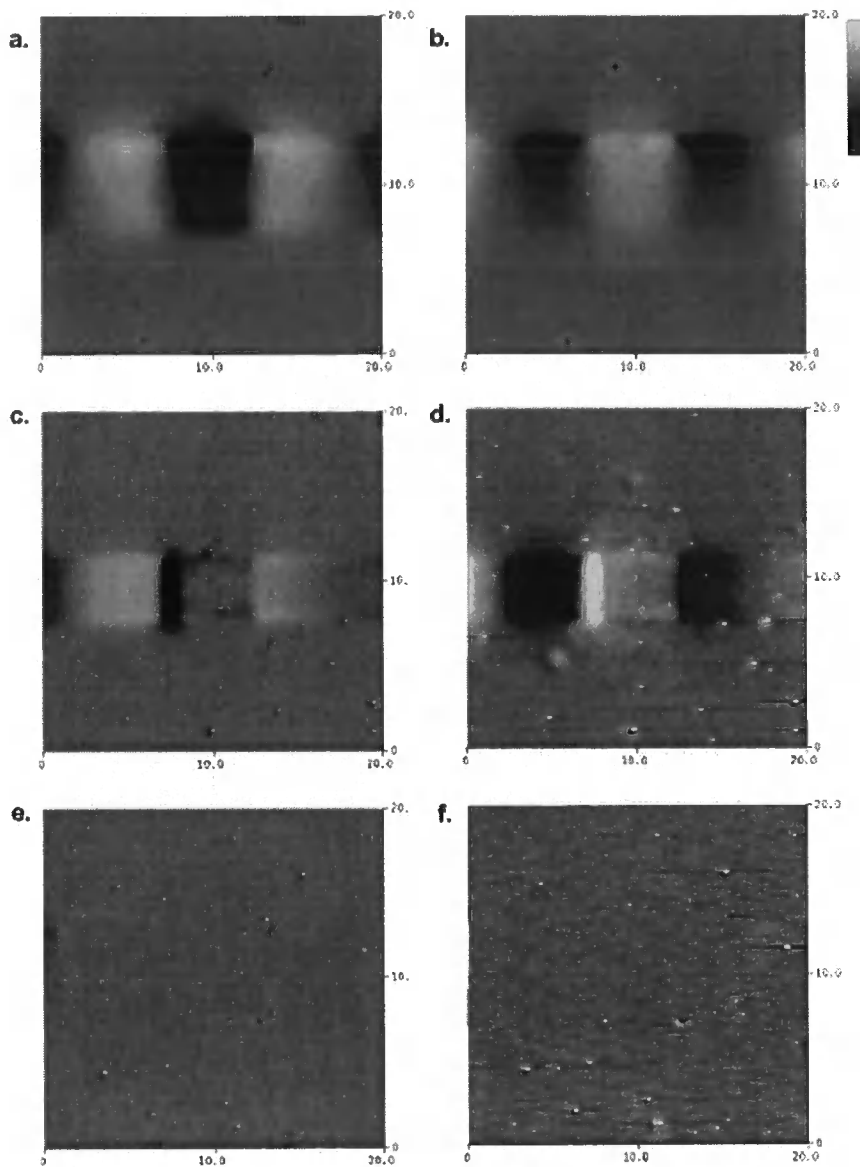


Figure 3-11 20 μm x 20 μm micrographs of polystyrene recorded with + 12 V (left column) and - 12 V (right column) applied to the tip. The central square was previously exposed to (a) and (b) - 110 V lift-mode bias, (c) and (d) - 60 V lift-mode bias and (e) and (f) - 55 V lift mode bias. Z Scale 10 $^{\circ}$.

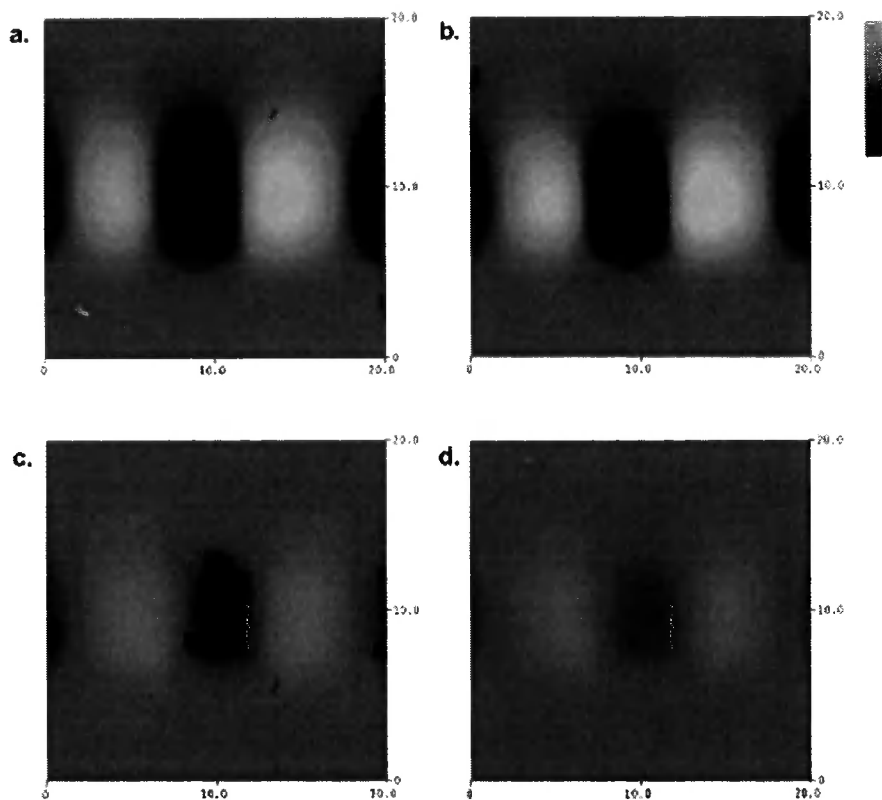


Figure 3-12 20 μm x 20 μm micrographs of polystyrene recorded with + 12 V applied to the tip. The central square was previously exposed to a - 110 V lift-mode bias (Scan speed = 1.0 Hz): (a) Lift-height during charge deposition = 15 nm; (b) Lift height during charge deposition = 30 nm; (c) Lift height during charge deposition = 45 nm and (d) Lift height during charge deposition = 60 nm. Z Scale 10 $^\circ$.

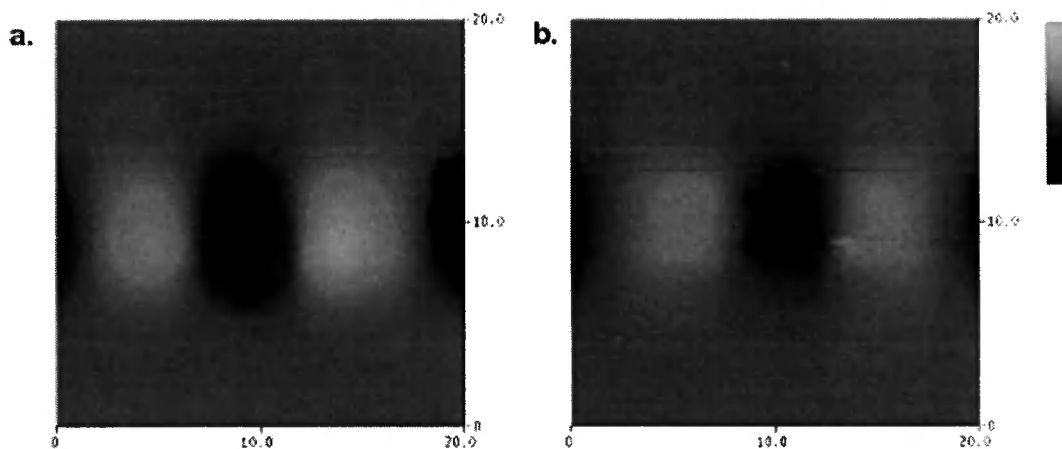


Figure 3-13 20 μm \times 20 μm micrographs of polystyrene recorded with - 12 V applied to the tip. The central square was previously exposed to a + 80 V lift-mode bias: (a) Scan speed while charging = 1 Hz; (b) Scan speed while charging = 3 Hz.

The deposited charge area (the actual size of the charged patch detected by EFM) was compared to the deposition area (the size of the area the EFM tip scanned during charge deposition) after the application of positive and negative tip voltages, Figure 3-14 and Figure 3-15. Both polarities were found to result in a minimum deposited charged area of $2.5 \times 2.5 \mu\text{m}$ square whilst the deposition area was less than $2 \times 2 \mu\text{m}$. Upon increasing the deposition area above $2 \times 2 \mu\text{m}$ it was found that the deposited charge area on the surface increased in a linear fashion, maintaining a $+ 0.5 \times 0.5 \mu\text{m}$ size greater than the depositing square. The minimum area of charge that could be deposited was therefore not limited by the minimum area that it was possible to scan during charge deposition.

Deposition Size as a Factor of Area Charged for Positive Voltage

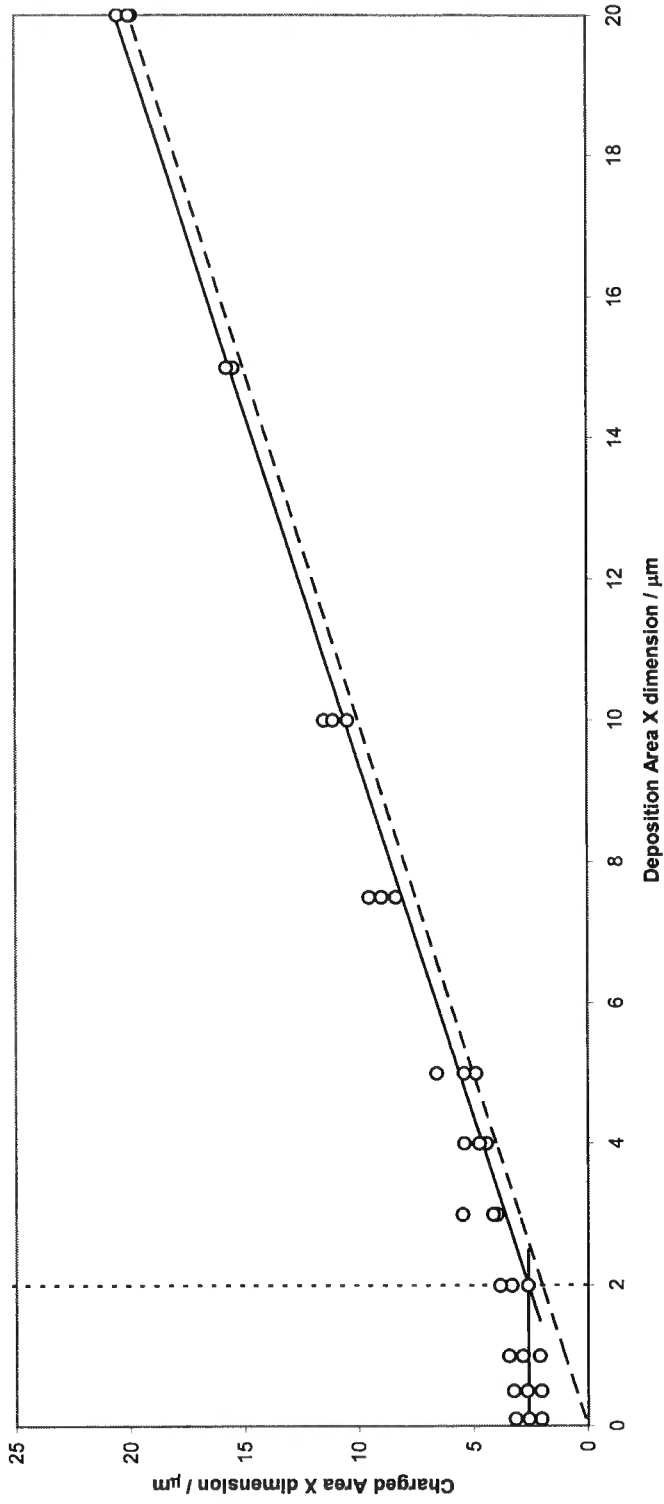


Figure 3-14 Graph showing relationship between positive charge deposition area and area of polystyrene substrate charged. Small dashed line signifies limitation due to tip geometry; large dashed line indicates a 1:1 relationship.

Deposition Size as a Factor of Area Charged for Negative Voltage

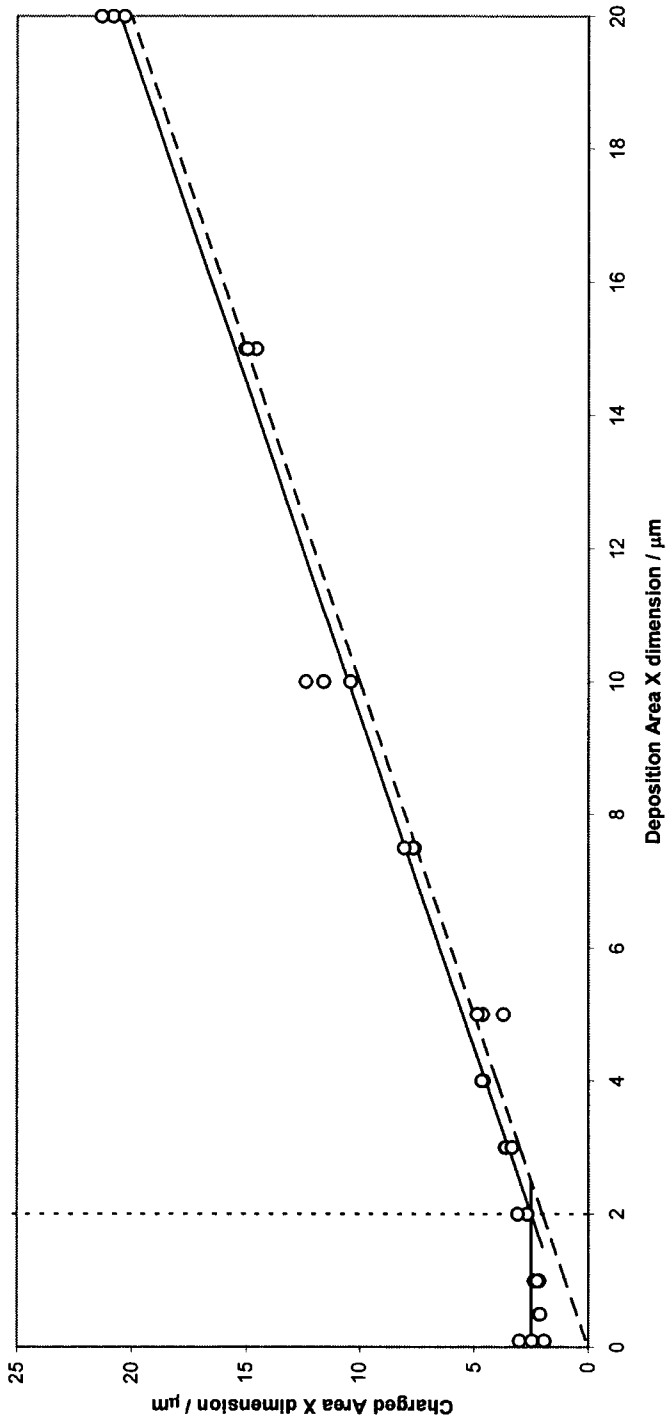
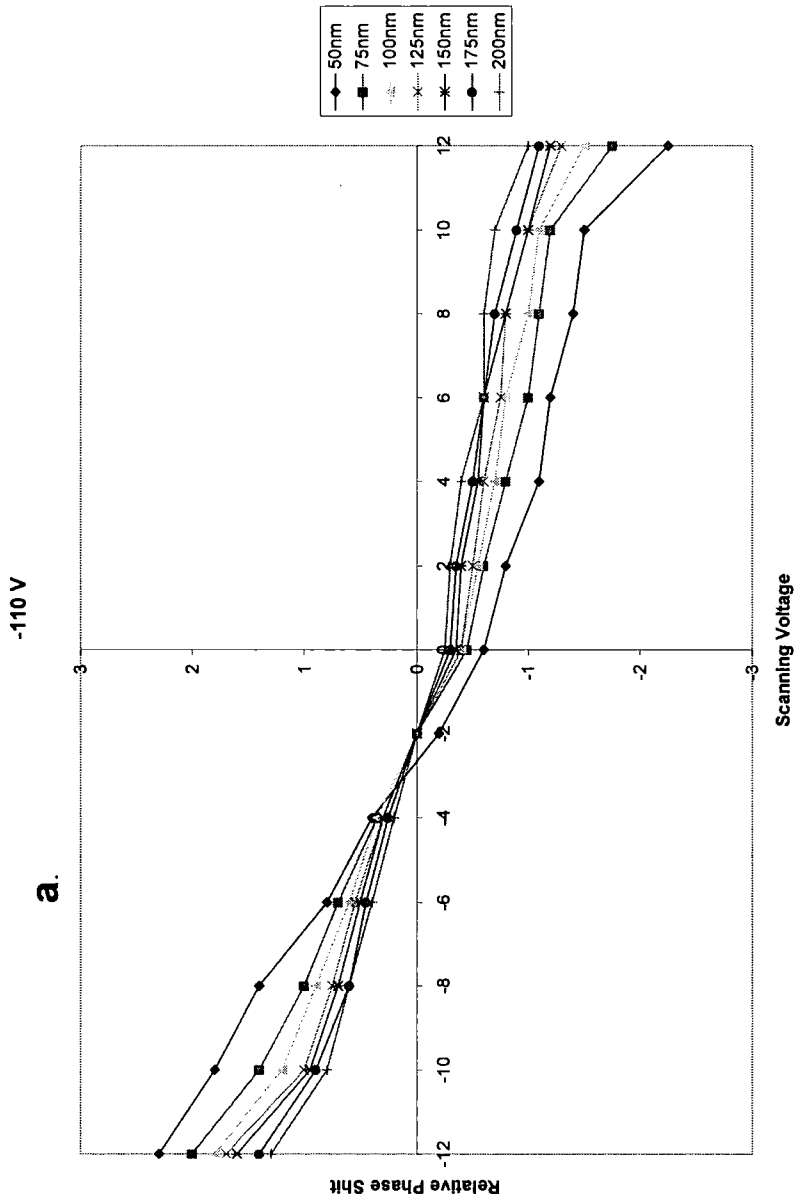
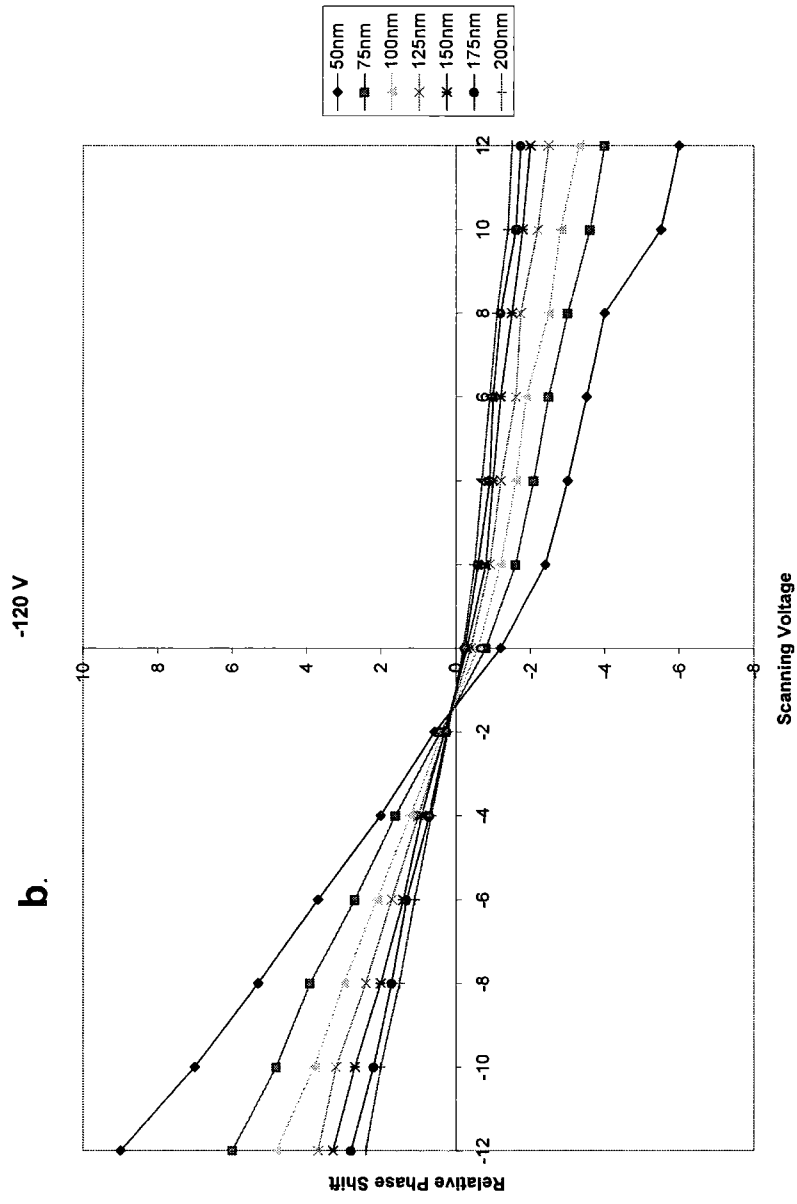


Figure 3-15 Graph showing relationship between negative charge deposition area and area of polystyrene substrate charged. Small dashed line signifies limitation due to tip geometry; large dashed line indicates a 1:1 relationship.

A negative discharge voltage was used to probe the phase shift response relative to the EFM lift-mode tip voltage and the EFM lift-mode tip height above the surface, Figure 3-16. The phase was found to be positively influenced by three factors: an increase in deposited voltage, a decrease in scanning height and an increase in the magnitude of the scanning voltage. Firstly, after increasing the magnitude of the negative voltage (-110 to -130 V) used during charge deposition it was possible to monitor the associated increase in phase change. This presented itself as an increase in measured phase shift from 2° to 10° when the surface was scanned at 50 nm and -12 V. Secondly, increasing the tip scanning height above the surface from 50 nm to 200 nm led to a decrease in the measured phase shift from 10° to 2° on scanning the -130 V surface with a tip voltage of -12 V. Thirdly, varying the scanning voltage of the tip from -12 V to $+12$ V resulted in a linear decrease in the value of the phase shift from $+10^\circ$ to -10° .



b.



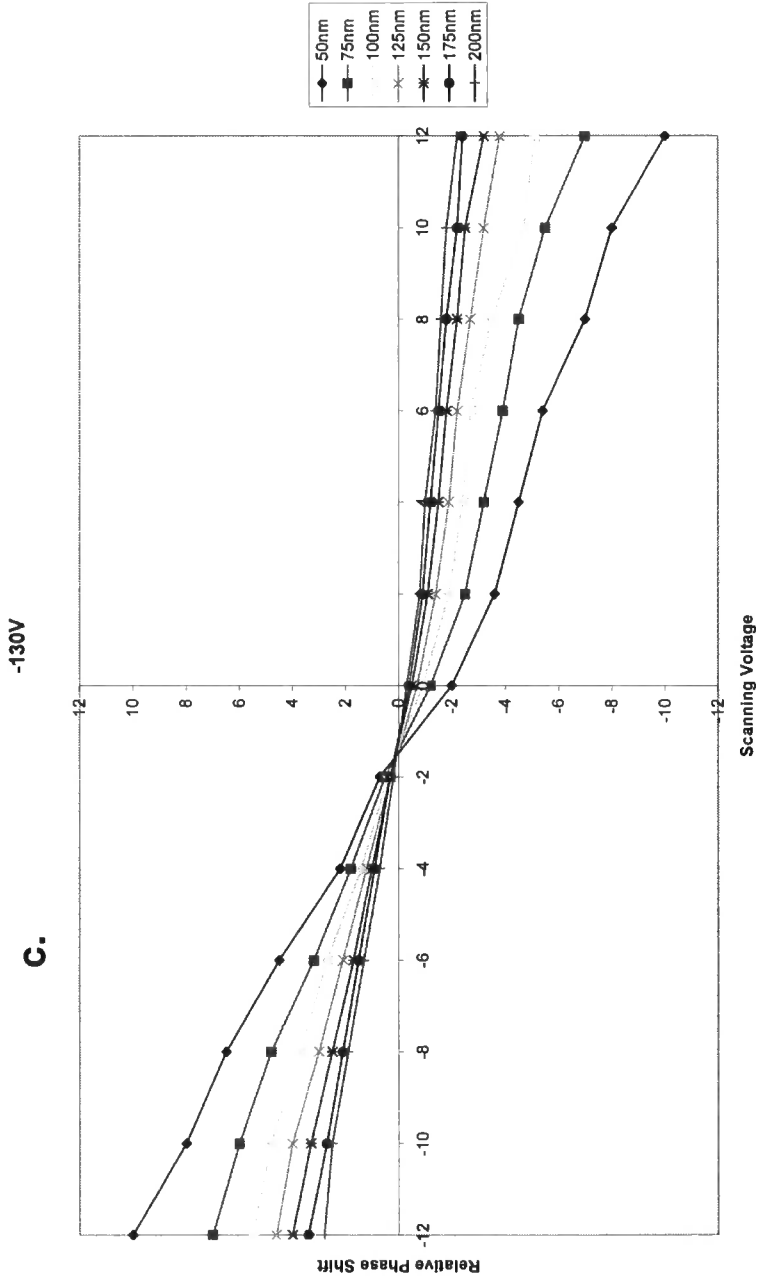


Figure 3-16 Graphs showing the EFM Phase Shift dependence on deposition voltage, imaging voltage and imaging lift-mode height. a, -110 V deposition voltage, b, -120 V deposition voltage, c, -130 V deposition voltage.

3.4.2 Polymer structure effects on substrate charging

The charging threshold of a polymer is defined as the minimum voltage that must be applied to the EFM tip to ensure charging of the surface. Below the charging threshold there is no evidence of the EFM tip having had any effect on the surface. The polymers examined in this study all had positive charging thresholds between + 20 V and + 60 V and negative charging thresholds between - 5 V and - 80 V Figure 3-17.

There are a number of factors that may explain this data. These include: tip polarity (positive or negative), deposition method (spin-coated or plasma deposited) and substituent group effects (halogen, methyl or methoxy) a summary is given in Table 3-2. The range of charging thresholds with negative voltage (75 V) was found to be larger than that of positive voltage (40 V). The minimum charging threshold with negative voltage was also lower than the minimum positive charging threshold. However, in general it was found that the surfaces studied had a lower threshold with positive voltage. Two exceptions were polybromostyrene and polymethoxystyrene that had significantly lower thresholds with negative voltage.

Interestingly, plasma deposited polymer surfaces exhibited larger charging thresholds than their commercially available, spin-coated counterparts. This is highlighted by comparison of the two polystyrene surfaces and the polymethylmethacrylate surfaces.

When examining charging thresholds with positive voltages on polystyrene and its derivatives, it can be noted that the addition of substituent groups to the para position resulted in an increase in the charging threshold.

Whereas when charged with negative voltage, the addition of a functional group to the para position resulted in a decrease in the charging threshold. However the order of effect of the functional groups on the charging threshold is not consistent between positive and negative voltage implying the lack of a direct relationship and multiple effects being responsible.

The relationship between the functional groups in the pulsed plasma and the charging threshold was studied. Styrene (S) and allylmercaptan (AM) monomers were found to have identical charging thresholds to each other with either positive or negative voltage. Vinylbenzylchloride (VBC) meanwhile was found to have a lower charging threshold with positive voltage than S or AM, however it was found to have a higher negative charging threshold than the aforementioned monomers. Vinylbenzaldehyde (VBA) was found to have the reverse charging thresholds to VBC, with a lower charging threshold with negative voltage and a higher threshold with positive voltage. Therefore the ease of charging with positive voltage followed the following series $VBC < S = AM < VBA$, whilst with negative voltage the series was found to be $VBA < S = AM < VBC$. This could be due to the different charge transport mechanisms or the stability of the polystyrene substrate to different charge polarities.

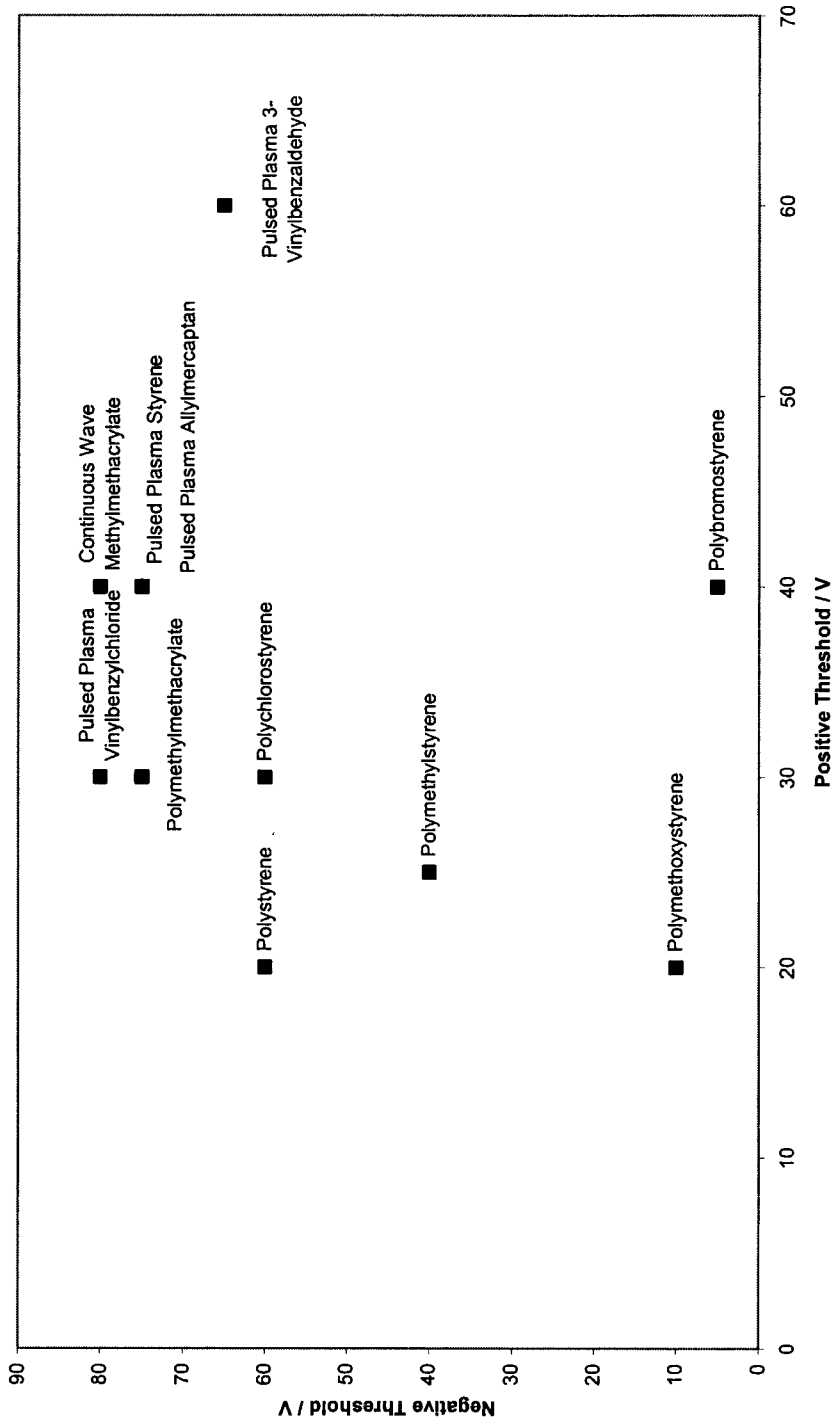
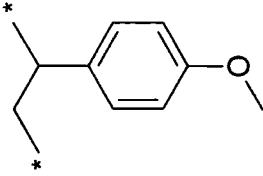
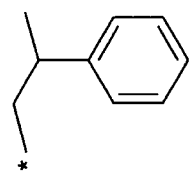
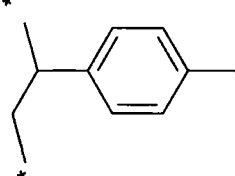
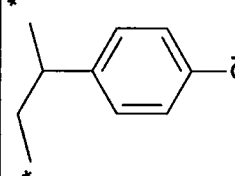
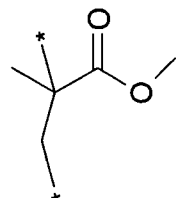
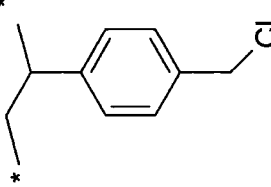
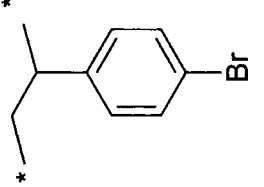
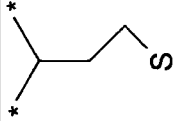


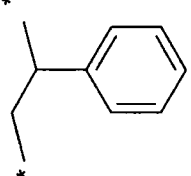
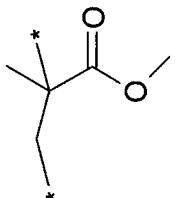
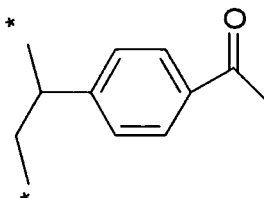
Figure 3-17 Graph showing polymer charging thresholds with positive and negative voltage.

Table 3-2 Table showing polymer charging thresholds and related physical constants.

Polymer	Positive Threshold / V	Negative Threshold / V	Ionisation Energy / eV	Electron Affinity / eV	Pauling Electronegativity
 <p>Poly(Methoxystyrene)</p>	20(=1)	10(2)	13.6181 (O)	-1.4613(O)	3.44(O)
 <p>Poly(Styrene)</p>	20(=1)	60(=4)	13.5984(H)	-0.7566(H)	2.20(H)

<p>* </p> <p>Poly(Methylstyrene)</p>	25(3)	40(3)	11.2603(C)	-1.2644(C)	2.55(C)
<p>* </p> <p>Poly(Chlorostyrene)</p>	30(=4)	60(=4)	12.9676(Cl)	-3.6710(Cl)	3.16(Cl)
<p>* </p> <p>Poly(Methylmethacrylate)</p>	30(=4)	75(=7)	13.6181 (O) 11.2603(C)	-1.4613(O) -1.2644(C)	3.44(O) 2.55(C)

<p>*  Pulsed Plasma Vinylbenzylchloride</p>	30(=4)	80(=10)	11.2603(C) 12.9676(Cl)	-1.2644(C) -3.6710(Cl)	2.55(C) 3.16(Cl)
<p>*  Poly(Bromostyrene)</p>	40(=6)	5(1)	11.8138(Br)	-3.3683(Br)	2.96(Br)
<p>*  Pulsed Plasma Allylmercaptan</p>	40(=6)	75(=7)	10.3600(S)	-2.0728(S)	2.58(S)

<p>* </p> <p>Pulsed Plasma Styrene</p>	40(=6)	75(=7)	13.5984(H)	-0.7566(H)	2.20(H)
<p>* </p> <p>Methylmethacrylate</p> <p>Continuous Wave</p>	40(=6)	80(10)	13.6181 (O) 11.2603(C)	-1.4613(O) -1.2644(C)	3.44(O) 2.55(C)
<p>* </p> <p>Vinylbenzaldehyde</p> <p>Pulsed Plasma</p>	40(=6)	65(6)	13.6181 (O) 11.2603(C)	-1.4613(O) -1.2644(C)	3.44(O) 2.55(C)

3.5 Discussion

3.5.1 Investigation into the EFM technique

Deposition of positive charge onto polymer surfaces using an EFM tip has been attributed to a positive corona discharge being formed around the microscope tip.³⁶ Although the voltage applied to the tip is much smaller than the voltages associated with macroscopic corona discharges (a few kV³⁶), the extreme radius of curvature at the tip (~ 13 nm³⁷) produces sufficient field strengths to ionise the surrounding air.²⁶ Accumulation of positive charge at the surface stems from positive ions (mainly hydrated H⁺) drifting from the ionised region towards the polymer surface across the potential difference between the tip and insulating polymer surface.³⁶

Large scale corona discharge onto polymer surfaces has been known to cause oxidation of the films along with topographical modification.³⁸ In the EFM charge deposition experiments detailed here there was no evidence of topographical changes in the AFM height image, Figure 3-6(a), or of chemical changes in the AFM phase image, Figure 3-6(b).

Corona discharges are well known to exhibit a threshold voltage, determined by the availability of free electrons to cause ionisation.³⁶ It is apparent that the deposition of positive voltage onto the polystyrene surface requires that a threshold value be reached (between +10 V and +20 V), Figure 3-7(c-f). As the tip voltage increased above this threshold, the EFM lift-mode phase shift indicated a higher degree of charging, Figure 3-7(a-d). The

definition of the charged square also improved with the use of a higher voltage.

When the separation distance between the tip and the surface during charging was reduced the amount of charge deposited on the polymer surface was increased, Figure 3-8. This corresponds to the corona discharge being more intense closer to the tip where it is originating from and therefore charging the surface more efficiently. This is consistent with the threshold voltage for corona discharge dropping at shorter tip-sample distances.³⁹

When scanning the polystyrene film surface following the deposition of positive voltage with a positively charged EFM tip in lift-mode a repulsive force between the surface and tip is evident. This is shown by the bright contrast in the EFM image, Figure 3-7(a). Upon using a negative voltage to scan the surface the EFM image reveals an attractive force between the induced tip voltage and the charged surface.

On increasing the speed of the tip traversing the surface during charging the amount of charge deposited on the polymer surface was reduced, Figure 3-9. This corresponds to each region of the polymer being exposed to the corona discharge for a shorter amount of time and therefore undergoing less charging.

The arguments outlined above for the positive discharge are also applicable to the negative discharge experiments. Varying the EFM imaging lift-mode voltage produced an opposite trend in the corresponding images, Figure 3-7(a-b) and Figure 3-11(a-b). This is consistent with negative charge deposition. In this case, charge transfer mainly results from CO_3^- ions produced in the discharge drifting across the electric field towards the



surface.²⁶ This potential has a similar magnitude to that resulting from positive discharge. As the deposition voltage is increased the charged patch better corresponds with the deposition area.

The size of the deposited charge patch on the surface was found to vary with the area that the tip was scanning over during the deposition of the voltage, Figure 3-14 and Figure 3-15. The minimum area of charge deposited was $2.5 \times 2.5 \mu\text{m}$ with both positive and negative deposition. After the deposition area had increased over this threshold the deposited charge area increased in a linear fashion. This implies that the charge deposition on the surface is not limited to the area scanned by the EFM tip during deposition, but by the area under the EFM tip.

It has been shown that the EFM lift-mode phase shift can be related to three key factors: the intensity of charge on the surface as determined by the deposition voltage, the value of the charge applied to the EFM tip during lift-mode scanning, and the separation distance between the tip and the surface during EFM scanning. The amount charge applied to the EFM tip during the charging of a polymer surface has an effect on the degree of relative phase shift that we see in the EFM lift-mode scan. The greater the voltage applied during charging the greater the recorded phase shift upon imaging the charge. However the increase in voltage used during charge deposition has not resulted in a change in the intersect point with the x-axis, which, from the theory discussed earlier, is known to represent the point where the charge applied to the EFM tip is equal to the voltage deposited on the surface. This implies that the surface is being charged up to the same voltage independent of the applied voltage during charge deposition, but that on increasing the

voltage the number of charged sites on the surface increase thus creating a larger density of charge without changing the surface voltage induced. The charge applied to the EFM tip during lift-mode scanning of a polymer surface following the injection of charge via an EFM scan at high voltage produces a linear relationship between the relative phase shift and the scanning voltage. The separation distance between the EFM tip in lift-mode and the surface during scanning has a dependence on the relative phase shift detected. This is in agreement with a $1/r^2$ relationship that would be predicted due to electrostatic interactions between charged surface and a point charge scanning above it.⁴⁰

3.5.2 Polymer structure effects on substrate charging

The thresholds for positive and negative charging of the polystyrene surface are significantly different and this is attributed to the electronic structure of the aromatic ring.⁴¹ Polystyrene consists of an aromatic ring attached to a saturated polymer backbone. The ease of charging with positive voltage compared to charging with negative voltage suggests that the aromatic structure is more susceptible to electron removal than electron addition.

There are two factors that influence the charging of the polymer surfaces, the ease of removing or adding electrons to the system (ionisation energy and electron affinity respectively) and the polarity and stability (including the ability to stabilise charge through resonance structures) of the bonds present in the polymer summarised in Table 3-2.

A combination of ionisation energies and bond polarities can be used to explain the positive charging threshold order. Ionisation energy represents the

amount of energy required to remove an electron from a gas phase atom in its ground state in order to produce a positively charged ion.⁴² The polarity of covalent bonds can be determined using Pauling electronegativity values.⁴³ When present in a polarised bond the ionisation energy of the atom will be reduced or increased depending on the bond polarisation, for example, hydrogen is more easily ionised in an O-H bond than it is in an H-H or C-H bond. Hydrogen attached directly to an aromatic carbon ring is slightly positively charged. Adding a CH₃ group does not affect the charge on the H atoms. However, as they are a step further removed from the aromatic ring, the stability of the charged system is reduced due to greater separation distance. The addition of an O atom between the methyl group and the ring serves to lower the positive charging threshold due to the high electronegativity of the oxygen reducing the relative ionisation energy of the terminal hydrogen atoms. The presence of a halogen hetroatom on the aromatic ring can also have an effect on the adjacent hydrogen atoms. The more polarised the carbon – halogen bond, the more positively charged the adjacent hydrogen atoms around the aromatic ring will be. This is shown by the positive charging threshold of polychlorostyrene being lower than polybromostyrene.

The electron affinity of an atom represents the amount of energy released when an electron is added to a gaseous atom in its ground state to form an ion.⁴² As adding electrons to an atom will result in a negative ion the electron affinity can be seen as being related to the ease with which a functionalised surface can be charged with negative voltage. The higher the electron affinity, the easier it is to add electrons to the system and therefore

the easier it is to charge with negative voltage. This is shown by comparing the order of increasing electron affinity and charging threshold with negative voltage. The order of electron affinity is $\text{Cl} < \text{Br} < \text{O} < \text{C} < \text{H}$, whilst the negative charging threshold order is $\text{Br} < \text{O} < \text{C} \equiv \text{Cl} < \text{H}$. As can be seen, the order matches up with the exception of Cl.

The presence of an excess of negative charge already present on the Cl atom is enough to influence the charging process and increase the charging threshold of polychlorostyrene relative to its position in the electron affinity series.

3.6 Conclusions

Scanning an Atomic Force Microscope tip at high voltage above polymer surfaces results in localised charge deposition. The polarity of the deposited charge corresponds to the sign of the applied voltage, whilst scan parameters govern the amount of charge deposited. Closer tip sample proximity, slower scanning speed and higher deposition voltage all yield a greater deposited charge. The minimum charged area was found to vary with deposition area above a threshold area. No accompanying morphological changes were detected in the AFM Tapping Mode height and phase images. The charging threshold was found to vary according to the polymer substrate and this was tentatively linked to the polymers electrical properties.

3.7 References

- [1] Yamazaki, K.; Shingagawa, T.; Watanabe, T.; Takahira, T. *Jpn. Kokai Tokkyo Koho* 19881110, **1988**.
- [2] Koderu. Y.; Kitamura, T.; Sawaguchi, E. U.S. *Patent* 19720104, **1972**.
- [3] Ando, K.; Ogawa, K.; li, Y.; Okumura, Y. *Jpn. Kokai Tokkyo Koho* 19900312, **1990**.
- [4] Bruneel, J. L.; Micheron, F. *Congr. Int. Electrost.* **1977**, Paper No. 38
- [5] Gottenbos, B.; Grimpma, D. W.; van der Mei, H. C.; Feijen, J.; Busscher, H. J. *J. Antimicrob. Chemother.* **2001**, 48, 7.
- [6] Barrett, R. C.; Quate, C. F. *J. Appl. Phys.* **1991**, 70, 2725.
- [7] Neugebauer H. E. *J. Appl. Optic.* **1964**, 3, 385.
- [8] Strohhriegl, P.; Grazulevicius, J. V. *Adv. Mater.* **2002**, 14, 1439.
- [9] Stern, J. E.; Terris, B. D.; Mamin H. J.; Rugar D. *Appl. Phys. Lett.* **1988**, 53, 2717.
- [10] Terris, B. D.; Stern, J. E.; Rugar D.; Mamin H. J. *Phys. Rev. Lett.* **1989**, 63, 2669.
- [11] Ebbens, S. J. Ph.D. Thesis University of Durham, 2001.
- [12] Snow E. S.; Campbell P. M. *Appl. Phys. Lett.* **1994**, 64, 1932.
- [13] Zhong, Q.; Inniss, D.; Kjoller, K.; Elings, V. B. *Surf. Sci.* **1993**, 290, L688.
- [14] Magonov, S. N.; Elings, V. B.; Whangbo, M. H. *Surf. Sci.* **1997**, 375, L385.
- [15] Whangbo, M.-H.; Bar, G.; Brandsch, R. *Surf. Sci.* **1998**, 411, L749.

-
- [16] Whelan, P. M.; Hodgson, M. J. *Essential Principles of Physics*; John Murray: London, **1978**.
- [17] Martin, Y.; Williams, C. C.; Wickramasinghe, H. K. *J. Appl. Phys.* **1987**, *61*, 4423.
- [18] Garcia, R.; Paulo, A. S. *Phys. Rev. B.* **1999**, *60*, 4961.
- [19] Tamayo, J.; Garcia, R. *Appl. Phys. Letts.* **1997**, *71*, 2395.
- [20] Noy, A.; Sanders, C. H.; Vezenov, D. V.; Wong, S. S.; Lieber, C. M. *Langmuir* **1998**, *14*, 1508.
- [21] Tamayo, J.; Garcia, R. *Appl. Phys. Letts.* **1998**, *73*, 2926.
- [22] Schonenberger C.; Alvarado A. F. *Phys. Rev. B.* **1992**, *45*, 3861.
- [23] Fukano, Y.; Sugawara, Y.; Yamanishi, T.; Oasa, T.; Morita, S. *Jpn. J. Appl. Phys.* **1993**, *32*, 290.
- [24] Schönenberger, C. *Phys. Rev. B* **1992**, *45*, 3861.
- [25] Fukano, Y.; Uchihashi, T.; Okusako, T.; Chayahara, A.; Sugawara, Y.; Yamanishi, Y.; Oasa T.; Morita, S. *Jpn. J. Appl. Phys.* **1994**, *33*, 379.
- [26] Tipler, P. A. *Physics for Scientists and Engineers*; Worth:, 1991, New York.
- [27] Wiesmann, H. J.; Zeller, H. R. *J. Appl. Phys.* **1986**, *60*, 1770.
- [28] Morita, S.; Sugawara, Y.; Fukano, Y. *Jpn. J. Appl. Phys.* **1993**, *32*, 2983.
- [29] Fukano, Y.; Sugawara, Y.; Yamanishi, T.; Oasa, T.; Morita, S. *Jpn. J. Appl. Phys.* **1993**, *32*, 290.
- [30] Harari, E. *J. Appl. Phys.* **1978**, *49*, 2478.
- [31] Torres, J. –M.; Dhariwal, R. S.; *Nanotechnology*, **1999**, *10*, 102.

-
- [32] Morariu, M. D.; Voicu, N. E.; Schaffer, E.; Lin, Z.; Russell T. P.; Steiner U. *Nat. Mater.* **2003**, *2*, 48.
- [33] Lyuksyutov, S. F.; Paramonov, P. B.; Juhl S.; Vaia, R. A. *Appl. Phys. Lett.* **2003**, *83*, 4405.
- [34] Majumdar, A.; Oden, P. I.; Carrejo, J. P. Nagahara, L. A.; Graham J. J.; Alexander, J. *Appl. Phys. Lett.* **1992**, *61*, 2293.
- [35] Ma, L. P.; Yang, W. J.; Xie S. S.; Pang S. J. *Appl. Phys. Lett.* **1998**, *73*, 3303.
- [36] Giacometti, J. A.; Oliveria Jr., O. O. *IEEE Transactions on Electrical Insulation* **1992**, *27*, 924.
- [37] Ramirez-Aguilar, K. A.; Rowlen, K. L. *Langmuir* **1998**, *14*, 2562.
- [38] Overney, R. M.; Guntherodt, H. -J.; Hild, S. *J. Appl. Phys.* **1993**, *75*, 1401.
- [39] Schönenberger, C. *Phys. Rev. B* **1992**, *45*, 45.
- [40] Lin, T.Y.; Su, W.S.; Su, W. S.; Chen, Y. F. *Solid State Communications* **2004**, *130*, 49.
- [41] Gibson, H. W. *J. Am. Chem. Soc.* **1975**, *97*, 3832.
- [42] Atkins, P; de Paulo, J. In Atkins' Physical Chemistry, 7th Ed. De Paulo, J.; Ed.; Publisher: Oxford University Press. 2004.
- [43] McMurray, J., Organic Chemistry 5th Ed. Publisher: Brooks-Cole. 2000

Chapter 4

Selective Phase Charging at the Nanoscale

4.1 Introduction

Electronic Force Microscopy (EFM) can be used to deposit positive and negative charge onto homopolymer polystyrene films; not all polymer surfaces may be charged in this fashion. This is due to the electrical properties of the polymer, such as conductivity¹ and the ability of polymers to retain charge.² The selective charging of particular morphological regions within a phase separated polymer blend could be a simple route to nanoscale charge patterning.

The properties of these polymer blend films have potential applications in areas such as optics, microelectronics and for microelectronic patterning.³ Systems such as paints, lubricants and adhesives are examples of typical polymer blends of which the phase segregation of these systems has therefore been extensively studied both in the bulk and at surfaces in the form of thin films.⁴

Spin casting of polymeric solutions onto flat substrates is commonly used for the production of thin polymer films, inherent is the ability to control resultant film thickness by adjusting polymer concentration and spin rotational speed.^{5,6} In the spin casting of polymer blend solutions, in which the components have chemically different functional groups, the phase separation of the component polymers is effected by solvent evaporation.⁷ For thin films of polymer blends the phase separation is highly constrained, due to the fact that the film thickness can be orders of magnitude smaller than the micron-scale phase separation dimensions observed in the bulk. The resultant surface morphology produced by the spin casting of an immiscible blend depends on the relative solubility of the two polymers and their ability to wet

the substrate.⁸ The immiscibility of two polymers can be predicted in terms of enthalpy and entropy according to the Flory-Huggins theory, Equation 4-1;

$$\Delta G^M = kT[(N_A \ln \phi_A + N_B \ln \phi_B) + (N_A \phi_B \chi_{AB})]$$

Equation 4-1

Where ϕ represents the volume fraction and N represents the statistical chain length. The term in the first parenthesis represents the entropy of mixing, this is small in the case of large polymer molecules and therefore we may consider only the enthalpy term in the second parenthesis. The Flory-Huggins parameter, χ_{AB} , can be evaluated using solubility parameters, Equation 4-2;

$$\chi_{AB} = \frac{V_R}{RT} (\delta_A - \delta_B)^2$$

Equation 4-2

Where δ represents the solubility parameter. The more positive the value the more immiscible the polymers, although not all interactions are taken into account in this theory, notably hydrogen bonding. Values for $\Delta\delta$ are given in the Polymer Handbook,⁹ according to the predicted polymer / polymer interaction for a given system. With apolar polymers a value of $\Delta\delta$ greater than 1.0 is predicted to result in miscible polymers.

A simple model for the spin-coating procedure¹⁰ suggests that for the homopolymer blends of two polymers the domains formed stretch from the surface interface to the air interface. This is known as two-dimensional spinodal decomposition. A solvent that has a greater affinity for one polymer

over the other may therefore be used to selectively dissolve and remove one polymer in order to form holes or columns on a substrate.

Spin casting of the polymer blend solution onto the substrate results in different morphologies forming in segregated multi-polymer films,¹¹ due to demixing. The final morphology is influenced by the film thickness (itself dependent on the polymer solution concentration) the ratio of polymers in the blend and the casting solvent.

Tapping mode AFM is a useful technique for the study and analysis of polymer blend films of differing physical character. This is due in part to the development of phase imaging which allows the mapping of heterogeneous surface properties. Contrast changes in phase images can be attributed to a number of factors including elasticity,¹² hydrophobicity,¹³ adhesion¹⁴ and energy dissipation.¹⁵ This allows imaging to differentiate between regions of physically different materials as found in phase segregated polymer films. The degree of phase shift is also dependant on the set point to free amplitude ratio used, indicating variance and even reversal according to the ratio used. The dependence of the phase shift upon the set point value is understood by correlating the phase difference curves of the individual polymers on the surface. Similarly, amplitude distance curves are correlated in order to understand height artefacts introduced by tapping parameters. Such artefacts in height images typically only alter the overall height of soft materials by 10 nm or less.

The aim of this work is to use EFM techniques to selectively charge the polystyrene phase of a phase separated polystyrene / polybutadiene blend

surface to produce micron and nanometre charged regions as a template for particle assembly.

4.2 Experimental

Solutions of polybutadiene (Aldrich, $M_w = 420,000$, 36% cis, 55% trans 1,4 addition, 9% 1,2 addition), polystyrene (Aldrich, $M_w = 280,000$) and blends of the two were dissolved in toluene (BDH, 99.5%). Polymer blend solutions were deposited onto silicon wafers (Silicon Valley Microelectronics, Inc.) using a spin-coater (Cammex Precima) operating at 2000 rpm for 30 seconds. Resultant films were then left in air for 1 hour to allow entrapped solvent to evaporate.

An Atomic Force Microscope equipped with a Nanoscope III control module, extender electronics module and a signal access module (Digital Instruments) was employed in interleave mode to deposit charge onto polymer surfaces. A Cr sputter coated EFM probe was used with a 125 μm long silicon tip (MikroMasch NSC15/Cr, force constant ≈ 40 nN, resonance frequency ≈ 270 kHz after metallisation). Following charge deposition tapping mode was used to capture height and phase images of the sample surface. An interleave scan at a constant tip height above the surface was employed concurrently to capture an EFM image.

To ensure consistent data the parameters of the scanning were kept constant. A set point of 2 V was used for tuning and a set point of 1.2 V was used for imaging the surface. A lift height of 30 nm was used for all depositions of charge onto the surface, a lift height of 100 nm was used for all imaging and the scan rate was maintained at 1 Hz.

To deposit charge onto a polymer surface, it was necessary to use a greater voltage than is available through the signal access module ($\pm 12\text{V}$

through 'Analogue 2'). This voltage is also only applied during the lift mode of the scans. To facilitate the deposition of higher voltages onto the surface, a custom built high voltage D.C. power supply ($\pm 180\text{V}$) was gated through the signal access module.

EFM experiments consisted of two stages, firstly the surface was charged over a $5\ \mu\text{m} \times 5\ \mu\text{m}$ square region with a high voltage applied to the tip. Consequently a characterisation of the charged region, a $20\ \mu\text{m} \times 20\ \mu\text{m}$ was scanned with a lower voltage applied to the tip and at an increased height above the surface (100 nm), chosen to ensure minimal distortion of the deposited charge image.

Film thickness measurements were carried out using a nkd-6000 spectrophotometer (Aquila Instruments Ltd.). Transmittance – reflectance curves (over the 350 – 1000 nm wavelength range) were fitted to a Cauchy model for dielectric materials using a modified Levenburg-Marquardt method.

4.3 Results

Electric force microscopy (EFM) images of a polystyrene surface following a deposition of +60 V charge shows a ($5\mu\text{m} \times 5\mu\text{m}$) square of the same dimensions and location as the charged region. In contrast, the corresponding height and phase images show no evidence of the charged patch, Figure 4-1(a-b). Scanning the charged square with opposing applied voltages gave different phase contrasts. When scanned with a tip potential of +12 V, Figure 4-1(c), a bright phase patch is visible, representing a repulsive interaction between the tip and surface. Upon scanning with 0 V and -12 V the intensity on the phase contrast is increased, Figure 4-1(d) and Figure 4-1(e). In contrast EFM images of a polybutadiene surface following deposition of +60 V charge gave no evidence of charging or modification of the polymer surface, Figure 4-2.

Polymer blend surfaces were created from a solution of 90 % polystyrene and 10 % polybutadiene. These polymers separated out to form two separate domains present on the polymer surface, with polystyrene forming the majority matrix, as shown by AFM phase images, Figure 4-3(b). Similar surfaces have been generated where the percentages of polystyrene and polybutadiene were varied and it was found that the polymer domain size depended on the concentrations of polymers within the spin-coating solution. Where the concentration of polystyrene present is greater than that of the concentration of polybutadiene, the polystyrene made up the matrix, whilst the polybutadiene occupied islands within it.

A charged square on the surface polymer blend surface was observed on deposition of + 60 V, Figure 4-3. Height and Phase images of the surface

show no evidence of physical or chemical changes to either of the polymer domains on the surface, Figure 4-3(a) and Figure 4-3(b). Additionally, contained within the charged square, were nano-scale non-charged regions within the charged background at a scanning voltage set to 0 V. When the surface was imaged with ± 12 V the contrast between the charged and uncharged regions was reduced. The phase contrast of the image shows a repulsive force between the tip and charged surface matrix, represented by a lighter phase patch when scanned with +12 V, Figure 4-3(c). Alternatively the force between tip and charged surface matrix is attractive, represented by a darker phase patch, when the surface is scanned with 0 V, Figure 4-3(d), and -12 V, Figure 4-3(e). Uncharged islands generated using this technique were found have a cross section of 500 nm.

EFM scans of the uncharged regions of the polymer blend surface with ± 12 V revealed areas of phase contrast, Figure 4-3. The areas of phase contrast in the EFM scans correspond to areas of phase shift revealed in the AFM phase shift images.

Application of -110 V charge to a spin coated polystyrene surface produced no changes in the height or phase, images of the surface, Figure 4-4(a-b). A marked visible contrast was evident in the EFM lift mode images, Figure 4-4(c-e). Upon scanning the surface with +12 V a well defined dark square was perceived, Figure 4-4(c). Decreasing the voltage being used to scan the surface to 0V resulted in a reduced contrast between the dark square and the background, Figure 4-4(d). Further reducing the scanning voltage to -12 V gave a switch in the phase contrast too a bright patch, the square was still well defined, Figure 4-4(e).

Application of the same -110 V to a spin coated polybutadiene surface whilst leaving the tapping mode height and phase images unchanged also showed no contrast difference in the EFM scans, Figure 4-5.

EFM deposition onto a polymer blend surface of 90 % polystyrene and 10 % polybutadiene gave a well defined region of phase contrast visible on EFM scans of the surface, Figure 4-6. There was no evidence of charging upon the height or phase images of the blend surface Figure 4-6(a-b). Scanning the surface with 0 V gave rise to a square with darker contrast than the background. Within this darker region were visible nanometer diameter holes of different contrast, Figure 4-6(d). Scanning with ± 12 V yielded a the patterned region of phase contrast of lesser distinction, Figure 4-6(c) and Figure 4-6(e).

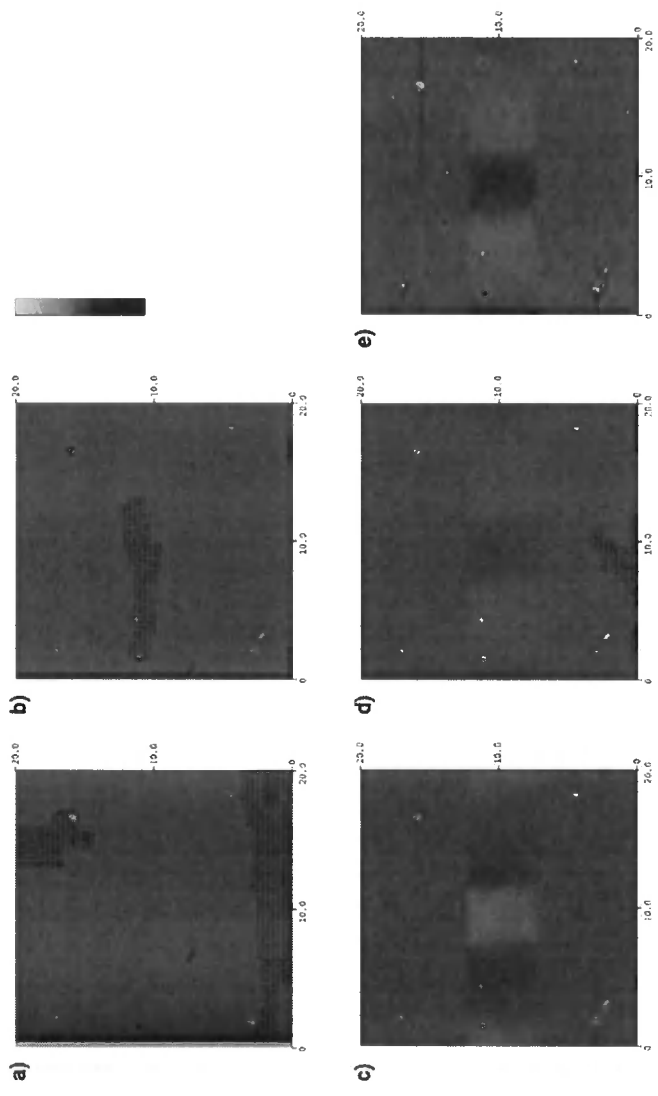


Figure 4-1 Polystyrene Surface 20 μm +60V deposited. AFM and EFM images following charging, height (150 nm) (a), phase (180 $^\circ$) (b), +12V (10 $^\circ$) (c), 0V (10 $^\circ$) (d) and -12V (10 $^\circ$) (e).

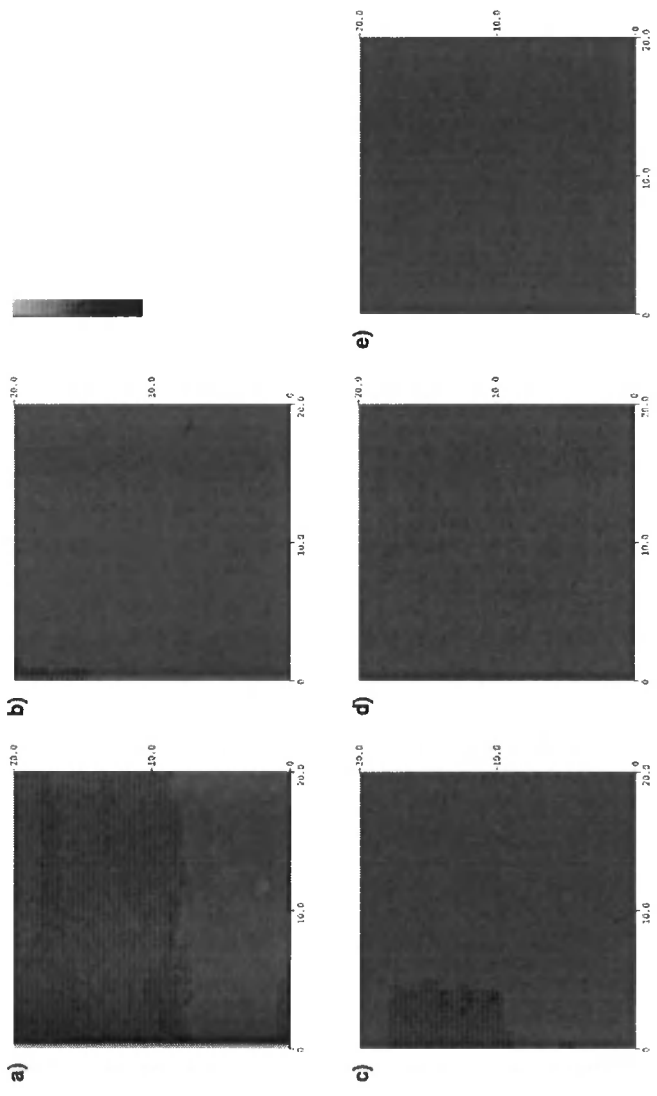


Figure 4-2 Polybutadiene Surface 20 μm +60V deposited. AFM and EFM images following charging, height (150 nm) (a), phase (180 $^\circ$) (b), +12V (10 $^\circ$) (c), 0V (10 $^\circ$) (d) and -12V (10 $^\circ$) (e).

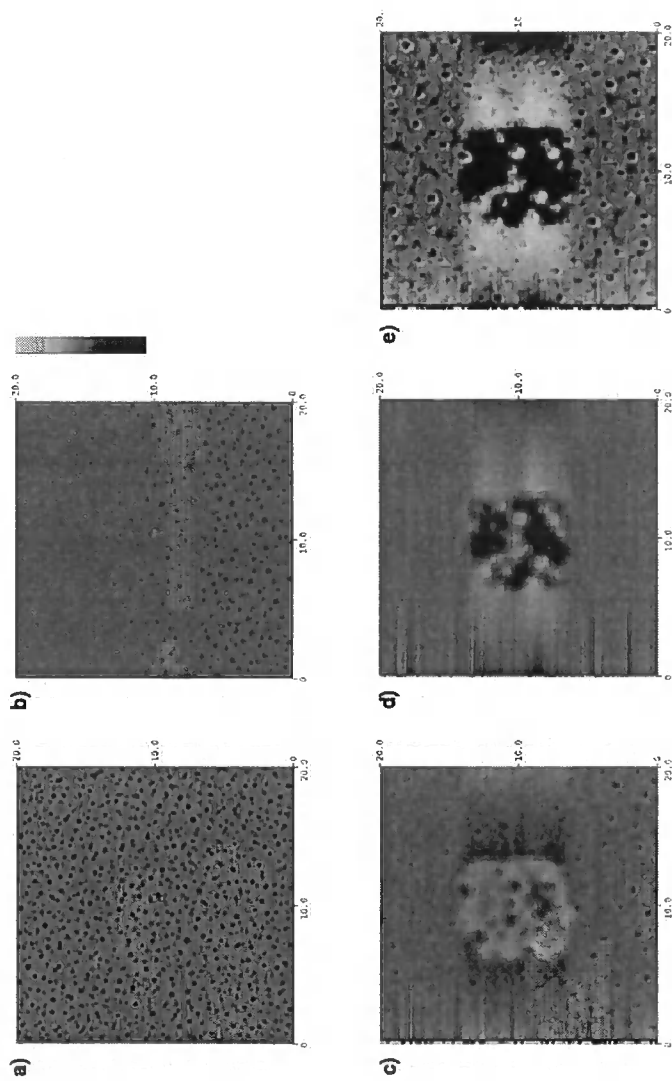


Figure 4-3 90% Polystyrene 10% Polybutadiene Surface 20 μm +60V deposited. AFM and EFM images following charging, height (150 nm) (a), phase (180 $^\circ$) (b), +12V (10 $^\circ$) (c), 0V (10 $^\circ$) (d) and -12V (10 $^\circ$) (e).

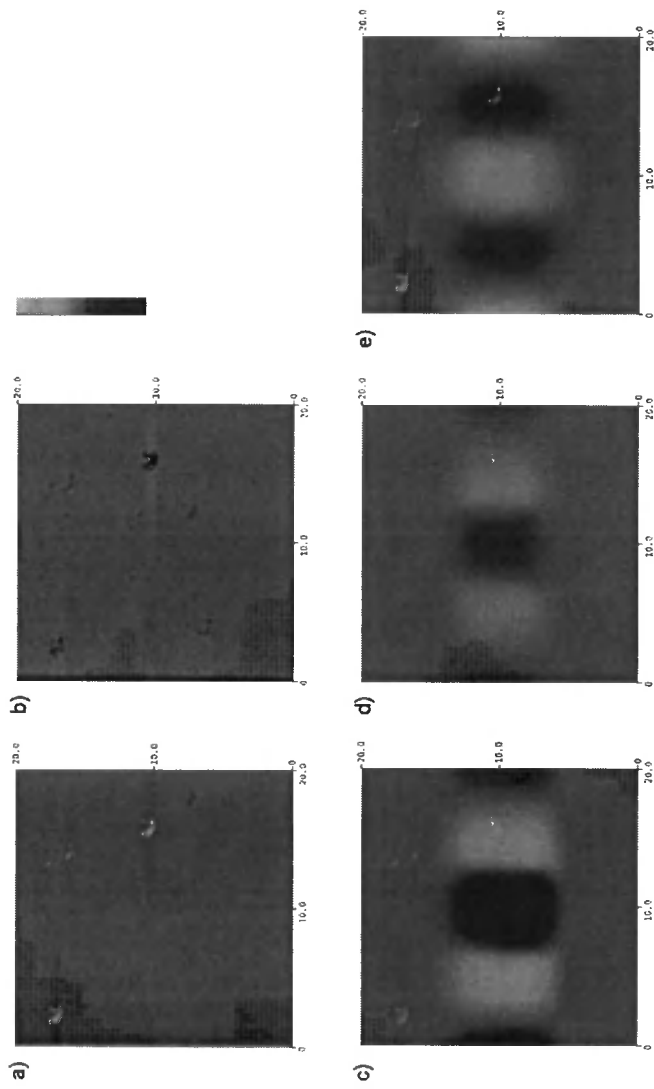


Figure 4-4 Polystyrene Surface 20 μm -110V deposited. AFM and EFM images following charging, height (150 nm) (a), phase (180 $^\circ$) (b), +12V (10 $^\circ$) (c), 0V (10 $^\circ$) (d) and -12V (10 $^\circ$) (e).

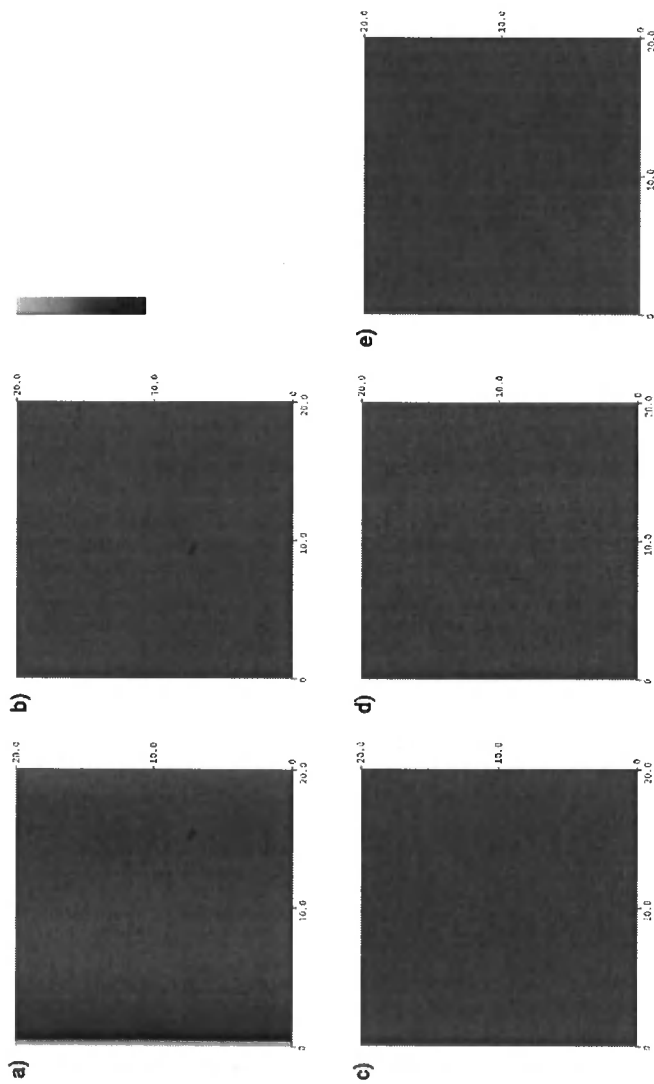


Figure 4-5 Polybutadiene Surface 20 μm -110V deposited. AFM and EFM images following charging, height (150 nm) (a), phase (180°) (b), +12V (10°) (c), 0V (10°) (d) and -12V (10°) (e).

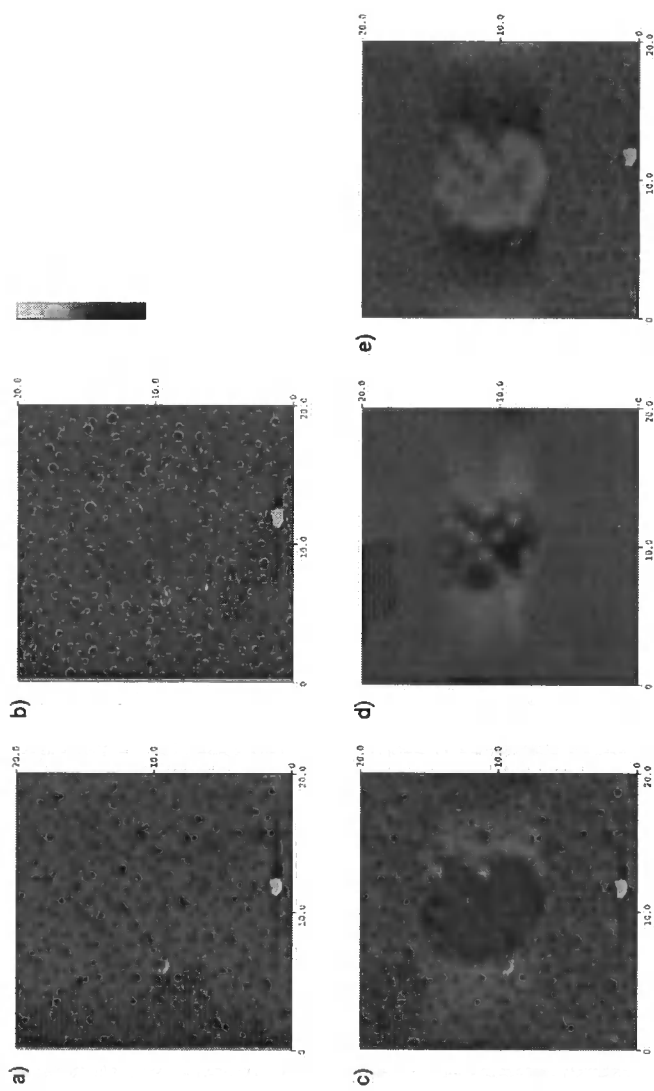


Figure 4-6 90% Polystyrene 10% Polybutadiene Surface 20 μm -110V deposited. AFM and EFM images following charging, height (150 nm) (a), phase (180 $^\circ$) (b), +12V (10 $^\circ$) (c), 0V (10 $^\circ$) (d) and -12V (10 $^\circ$) (e).

4.4 Discussion

In this study, the generation of patterned regions of charge has been accomplished by combining a number of scientific phenomenon, i.e. phase separation and selective charge retention. The solubility parameter of polystyrene has been reported to be 14-17 Mpa^{1/2}, whilst the solubility parameter of polybutadiene is reported to be 17.5-19 Mpa^{1/2}. When these values are used in Equation 4-2 in order to determine a value for the Flory-Huggins parameter, χ_{AB} , a positive value is found, therefore the polymers are immiscible leading to the formation of phase separated polymer thin films.

The spin-coated polymer blend surface reveals height differences between the two polymer domains. This has been said to be due to the spin-coating process and the affinity of the polymers to the casting solvent.¹⁶ During solvent evaporation the polymer with the least affinity for the solvent loses solvent first and therefore forms a lower surface region. The second polymer, with the greater affinity for the polymer, becomes swollen with the solvent that is left, forming raised regions. Once solvent evaporation is complete the polymer with the greater affinity collapses and drops below the level of the other polymer. In the polymer films studied it is notable that there are smaller lowered regions within the overall matrix, this implies that the lower polymer has the greater affinity for the solvent (toluene).

The induction of positive charge onto the polymer surface using the EFM tip corresponds to a positive corona discharge forming around the microscope tip.¹⁷ The voltage applied to the tip during deposition is much smaller than that associated with a macroscopic corona discharge (a few kV), due to the curvature of a sharp EFM tip (less than 35nm) a field of sufficient

strength to ionise the surrounding air should be produced. Positive charge is then accumulated at the surface from the drifting of positive ions, mainly hydrated H^+ , across the potential difference between the tip and polymer surface, whereas negative charge deposition will mainly result from drifting CO_3^- ions.

The charging of a polystyrene surface using a corona discharge treatment as been reported to cause oxidation.^{18,19} The morphology of large scale corona treated polymer films is also reported to be changed.²⁰ In the experiments presented here there was no evidence found of topographical changes in the Tapping Mode height image, Figure 4-1(a), also absent were any chemical differences highlighted in the associated phase image, Figure 4-1(b) following the EFM charging.

Following positive EFM discharge onto polystyrene surfaces, the contrast reversal between +12 V and 0 V indicates that the voltage of the charge deposited onto the polystyrene surface is between these values and that it has a positive polarity. Alternatively positive discharge onto polybutadiene surfaces yielded no evidence of any charging, chemical or topographical changes, Figure 4-2.

The lack of any recordable charge deposition on the polybutadiene surface can be attributed to the differences in electrical properties between polystyrene and polybutadiene. Polystyrene is known to undergo charging when exposed to a corona discharges,²¹ it is also known to have excellent insulating properties (i.e. low dissipation constant).²² However, polybutadiene has been reported to exhibit a low level of conductance.²³ The method of conductance in polybutadiene is not fully understood: it has been postulated

that delocalized electrons in the polymer chain may be involved, additionally there may be some ionic conductance occurring due to contaminants present during initial polymer formation. Therefore polybutadiene will not be able to hold a charge due to its conductive properties.

Thin films produced by the spin coating of polymer blends consisting of two or more polymers have been shown to form domain structures of the individual polymers.²⁴ Following charge deposition with a positively biased tip a square region of charge was evident, Figure 4-3. When the surface was scanned there was evidence of nano-scale regions where no charging had occurred, Figure 4-3(c-d) and Figure 4-6(c-d). These regions correspond with the polybutadiene domains of the polymer blend as determined from the height and phase images of the surface. This shows the selective charging with a positive voltage of the polystyrene fraction of the polymer surface.

EFM has previously been shown to be able to determine dopant profiles in semiconductors,^{25,26,27} monitor corrosion in metals,²⁸ map surface composition of Langmuir-Blodgett films^{29,30,31} and self assembled monolayers.³² It has even been shown to be able to map the terminal groups of self assembled monolayers that have been buried under a thick polymer layer.³³ Therefore the detected phase change has been attributed to regions of different polymer on the surface.

The arguments presented above for the deposition of positive charge onto polymer surfaces are also applicable to the negative discharge experiments. The polystyrene surfaces studied revealed a square, negatively charged region. Again in the case of polybutadiene there was no evidence of charge deposition supporting the low conductance theory. Finally, when

depositing negative charge onto a blend of polystyrene and polybutadiene surface the selective negative charging of the polystyrene matrix was evident, the polybutadiene islets remaining uncharged.

4.5 Conclusions

Selective localised charging of a polymer blend is possible when using a scanning Atomic Force Microscope in EFM lift-mode with a high voltage applied to the tip. Uncharged islets of 100 – 200 nm diameter of were generated within a 5 μm^2 region on the polymer matrix surface. No morphological changes were detectable in the AFM Tapping Mode height and phase images.

4.6 References

- [1] MacDiarmid, A. G. *Rev. Mod. Phys.* **2001**, 73, 701.
- [2] *Electrets*, Sessler, G. Eds. Springer-Verlag, Berlin, 1987.
- [3] Krausch, G. *Materials Science and Engineering R* **1995**, 14, 1.
- [4] Karim, A.; Slaweki, T. M.; Kumar, S. K.; Douglas, J. F.; Satija, S. K.; Han, C. C.; Russell, T. P.; Liu, Y.; Overney, R.; Sokolov, J.; Rafailovich, M. H. *Macromolecules* **1998**, 31, 857.
- [5] Hall, D. B.; Underhill, P.; Torkelson, J. M. *Polym. Eng. Sci.* 1998, 38, 2039.
- [6] Schubert, D. W.; Dunkel, T. *Mater. Res. Innovations* **2003**, 7, 314.
- [7] Walheim, S.; Böltau, M.; Mlynek, J.; Krausch, G.; Steiner, U. *Macromolecules* **1997**, 30, 4995.
- [8] Tanaka, K.; Takahara, A.; Kajiyama, T. *Macromolecules* **1996**, 29, 3232.
- [9] Brady, R. F. Jr. *Encyclopedia of Polymer Science and Technology*, Mark, H.; Bikaler, N. M.; Overberger, C. G.; Menges, G. Eds.; John Wiley & Sons: Chichester, **1984**.
- [10] Walheim, S.; Schäffer, E.; Mlynek, J.; Steiner, U. *Science* **1999**, 283, 520.
- [11] Raghavan, D.; Gu, X.; Nguyen, T.; VanLandingham, M.; Karim, A. *Macromol.* **2000**, 33, 2573.
- [12] Aime, J. P.; Elkaakour, Z.; Odin, C.; Bouhacina, T.; Michel, D.; Curely, J.; Dautant, A. *J. Appl. Phys.* **1994** 76 754-762
- [13] Refier, D.; Windeit, R.; Kumpf, R. J.; Karbach, A.; Fuchs, H. *Thin Solid Films*, **1995**, 264, 148.

-
- [14] Noy, A.; Sanders, C. H.; Vezenov, D. V.; Wong, S. S.; Lieber, C. M. *Langmuir* **1998**, *14*, 1508.
- [15] Chen, X.; Davies, M. C.; Roberts, C. J.; Tendler, S. J. B.; Williams, P. M.; Davies, J.; Dawkes, A. C.; Edwards, J. C. *Ultramicroscopy*, **1998**, *75*, 171.
- [16] Walheim, S.; Bolltau, M.; Mlynek, J.; Krausch, G.; Steiner, U. *Macromol.* **1997**, *30*, 4995.
- [17] Giacometti, J. A.; Oliveria Jr., O. O. *IEEE Transactions on Electrical Insulation* **1992**, *27*, 924.
- [18] Onyiriuka, E. C.; Hersh, L. S.; Hertl, W. *J. Colloid Interface Sci.* **1991**, *144*, 98.
- [19] Onyiriuka, E. C. *J. Appl. Poly. Sci.* **1993**, *47*, 2187.
- [20] O'Hare, L. -A; Leadley, S.; Parbhoo, B. *Surf. Interface Anal.* **2002**, *33*, 335.
- [21] Watson, P. K. *J. Phys. D: Appl. Phys.* **1990**, *23*, 1479.
- [22] Bahri, R. *J. Phys. D: Appl. Phys.*, **1982**, *15*, 677.
- [23] Tkaczyk, S. W.; Swiatek, J. *Synthetic Metals* **2000**, *109*, 255.
- [24] Wang, P.; Koberstein, J. T. *Macromol.* **2004**, *37*, 5671.
- [25] Henning, A. K.; Hochwitz, T.; Slinkman, J.; Never, J.; Hoffmann, S.; Kaszuba, P.; Daghljan, C. *J. Appl. Phys.* **1995**, *77*, 1888.
- [26] Leng, Y.; Williams, C. C.; Su, L. C.; Stringfellow, G. B. *Appl. Phys. Lett.* **1995**, *66*, 1264.
- [27] Kikukawa, A.; Hosaka, S.; Imura, R. *Appl. Phys. Lett.* **1995**, *66*, 3510.
- [28] Schmutz, P.; Frankel, G. S. *J. Electrochem. Soc.* **1998**, *145*, 2295.

-
- [29] Fujihira, M. *Annu. Rev. Mater. Sci.* **1999**, 29, 353.
- [30] Chi, L. F.; Jacobi, S.; Fuchs, S. J. *Thin Solid Films* **1996**, 284-285, 403.
- [31] Inoue, T.; Yokoyama, H. *Thin Solid Films* **1994**, 243, 399-402.
- [32] Lu, J.; Delamarche, E.; Eng, L.; Bennewitz, R.; Meyer, E.; Guntherodt, H.-J. *Langmuir* **1999**, 15, 8184.
- [33] Takano, H.; Wong, S, -S.; Harnisch, J. A.; Porter, M. D. *Langmuir* **2000**, 16, 5231.

Chapter 5

Electrostatic Attachment of Gold Colloids to Polystyrene Surfaces Using EFM

5.1 Introduction

Interactions between nano-particles and charged surfaces is of technological interest due to its importance in processes such as xerography,¹ electrostatic aerosol filtration² and membrane filtration.³ AFM is a useful tool for the study and characterization of these systems. Examples of this include experiments involving individual particles attached to the AFM cantilever probing the electrostatic interaction between colloids and membrane pores.⁴

The modern requirements of the electronics and micro-array technology calls for methods to manipulate and assemble nano-scale particles on surfaces.⁵ Once tethered to the surface, particles can be used for docking sites in molecular sensors⁶ or as the basic building blocks for new structures.⁷ Classical self-assembly methodologies do not offer the ability to position particles in predetermined places on a surface; directed assembly is being investigated as an advanced method of controlling deposition.⁸

Surface electrostatic fields can be used as a method for the guidance of particles to specific sites, known as micro- or nano-xerography and has been developed from photographers and laser printers.⁹ In xerography, a charge pattern on an appropriate carrier (electret) is used to capture small pigment particles forming an image with a resolution of about 100 μm .¹⁰

Particles may be trapped from a variety of mediums; powder,¹¹ gas phase (aerosol),¹² or liquid phase (suspension).¹³ Powder deposition involves dipping the charged substrate into an excess of the dry nano-particles. The pattern is then developed by blowing away the loosely held particles with a stream of dry nitrogen. Aerosol deposition involves exposing the charge pattern to a cloud of nano-particles. This cloud can be formed by excitation in

a sealed cylinder using a fan to mix the nano-particles with the surrounding gas (air or nitrogen). It can also be formed using a nebuliser to transfer the nano-particles from a liquid phase to a gas phase. The third form involves trapping the particles in a aqueous suspension within a fluorinert (3M) solvent.

This chapter investigates the attachment of gold nano-particles to a charged polymer surface from a fluorocarbon suspension. The localized EFM charging method described in Chapter 2 is used to achieve spatially controlled particle deposition. This approach allows high spatial deposition to be achieved without requiring the vacuum apparatus necessary for the deposition of localised charge using electron beams.¹⁴

5.2 Experimental

A spin coater (Cammax Precima) was used to form thin polymer films on a silicon wafer substrate (Silicon Valley Microelectronics, Inc.). Spin coating conditions were 30 seconds rotation at 2000 RPM; the casting solution was 2% polystyrene (Aldrich, $M_w = 280,000$) in toluene (BDH, 99.5%). For charge writing and pattern imaging of the surface an Atomic Force Microscope equipped with a Nanoscope III control module, extender electronics module and a signal access module (Digital Instruments) was employed. A Cr sputter coated EFM probe was used with a 125 μm long silicon tip (MikroMasch NSC15/Cr, force constant ≈ 40 nN, resonance frequency ≈ 270 kHz after metallisation). Charging was carried out by gating an applied voltage of + 80 V or - 110 V through the tip during interleave scanning at a height of 30 nm above the sample surface. EFM imaging was carried out with an applied voltage of 0 V or ± 12 V at a lift height of 100 nm above the surface.

Following charge patterning, samples were developed in a water in oil emulsion consisting of a fluorocarbon liquid (Fluorinert FC-77, 3M Company, St. Paul, MN, USA.) as a continuous phase and a gold colloid (Aldrich 20 nm) loaded disperse aqueous phase. The emulsion consisted of 20 μl of gold colloid solution in 2 ml of Fluorinert. Mixing of the emulsion was achieved using ultrasonification for 5 minutes; (Fluorinert was chosen due to its very high resistivity and low dielectric constant, preventing charge dissipation from samples immersed within it during deposition. Furthermore, if an ionic solution had been used, the relatively short Debye lengths would result in screening of

any remaining surface charge.) Immersion time of the charged samples was 10 minutes, followed by drying in air.

XPS analysis was then performed using a multi-technique ultra-high vacuum imaging XPS system (Thermo VG Scientific ESCALab 250) equipped with a hemispherical analyzer (of 150 mm mean radius) and a monochromatic Al K_{α} (1486.60 eV) X-ray source. The high sensitivity of this instrument obtained at a routine instrumental energy resolution of 0.5 eV fwhm at 20 eV pass energy allowed the characterization of binding envelopes for C 1s, O 1s, Si 2p and Au 4f. The resulting chemical mapping were created by subtraction of a 'background' image from the images of the binding envelopes. Background images were obtained at a 5 eV separation from the characteristic envelopes. This allows a reduction in the influence of roughness on the images.

5.3 Results

A $5\ \mu\text{m} \times 5\ \mu\text{m}$ positive charge square was deposited onto a thin film spin-coated polystyrene surface using a highly biased positive tip voltage(+80 V). Following charging using the EFM probe, it was possible to distinguish a well defined square of bright phase contrast upon imaging the surface with a positively biased tip (+12 V). Immersion of the charged surfaces in an aqueous solution yielded a deposited charge neutralised within five minutes. Conversely, charged substrate immersed in a Fluorinert solution for thirty minutes provide an unaffected charged patch.

Tapping mode AFM was used to monitor the exposure of the positively charged polystyrene surface to the gold colloid suspension. Particles of gold were observed to agglomerate selectively on the charged region, Figure 5-1(a). Height images revealed aggregations of particles in the charged square, clumping together to form a raised area surrounded by smaller individual particles. Additionally, the phase images generated revealed a phase shift in the oscillation of the cantilever, revealing that both chemical and physical differences in the surface were present. Lift-mode electric force microscope images show that that the particles on the surface exert a long range force on the cantilever, Figure 5-1(c-e). Phase shift contrast changes in the EFM images were bright indicating that repulsive forces were generated between tip and surface.

Area scanning X-ray photoelectron spectroscopy was used to monitor the exposure of the polymer surface to the gold colloid suspension. XPS gold 4f mapping identified a bright region of greater intensity gold peaks

corresponding with the deposited charge. In the same region there was no reduction in the intensity of the carbon, oxygen or silicon peaks, Figure 5-2.

Negatively charged polystyrene was also found to be able to act as a site for the electrostatic attachment of gold colloids from a suspension. The colloids are found to agglomerate around the region of negative charge. Forming a greater density towards the centre of the charged square and reducing towards the edges, Figure 5-3. The colloids were found to be attached to the surface strongly enough that repeated tapping mode scans of the region were found to have no effect, in contrast with results for the deposition of polystyrene spheres onto a polypropylene surface where the beads were found to be disturbed and shifted from the original charged area following tapping mode scans.¹⁵

XPS micrographs of the negatively charged region following immersion in the gold colloid suspension were found to reveal an area of gold deposition. Scans of carbon, oxygen and silicon in the same area revealed no change in the peak intensity over the region of gold deposition, Figure 5-4.

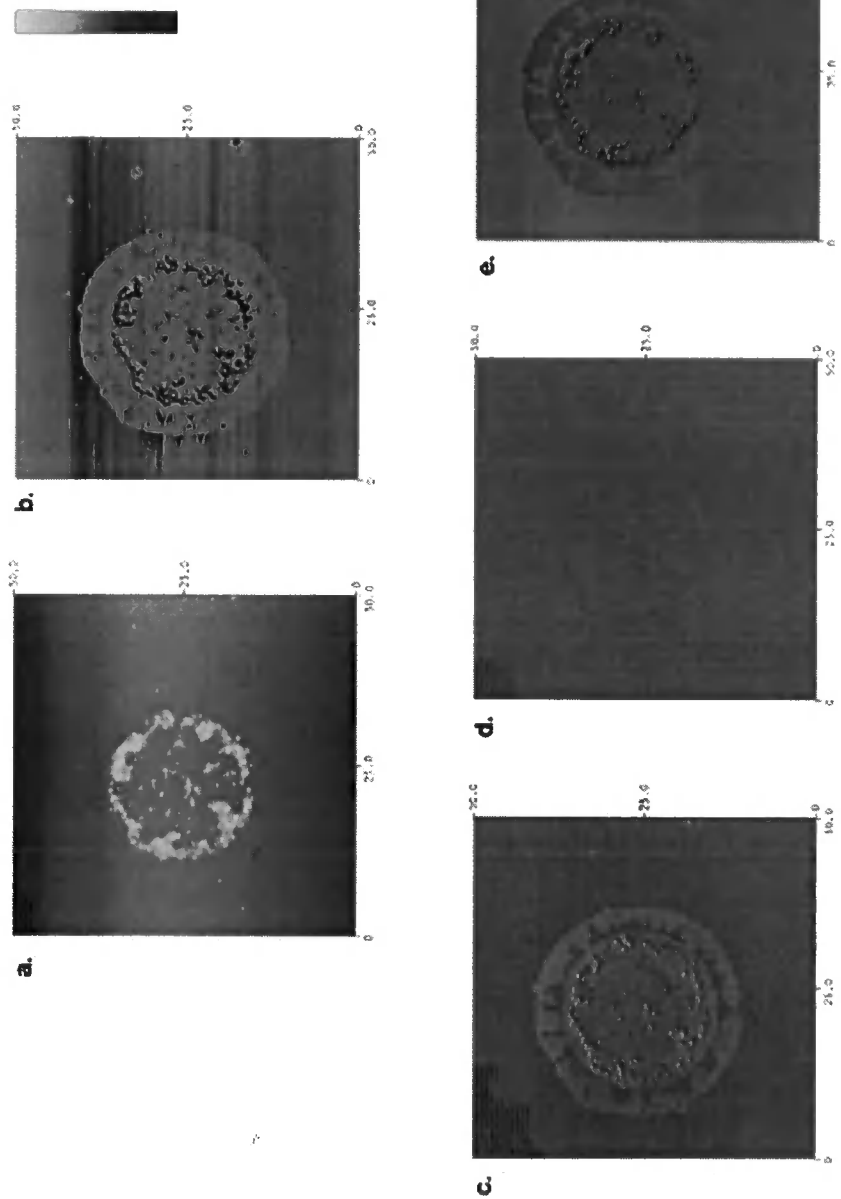


Figure 5-1 Atomic force micrographs of positively charged polystyrene surface following the electrostatic attachment of gold colloids to the deposited charge. Height (500nm) (a), Phase (90 °), EFM + 12 V (2 °), EFM 0 V (2°) and EFM – 12 V (2°).

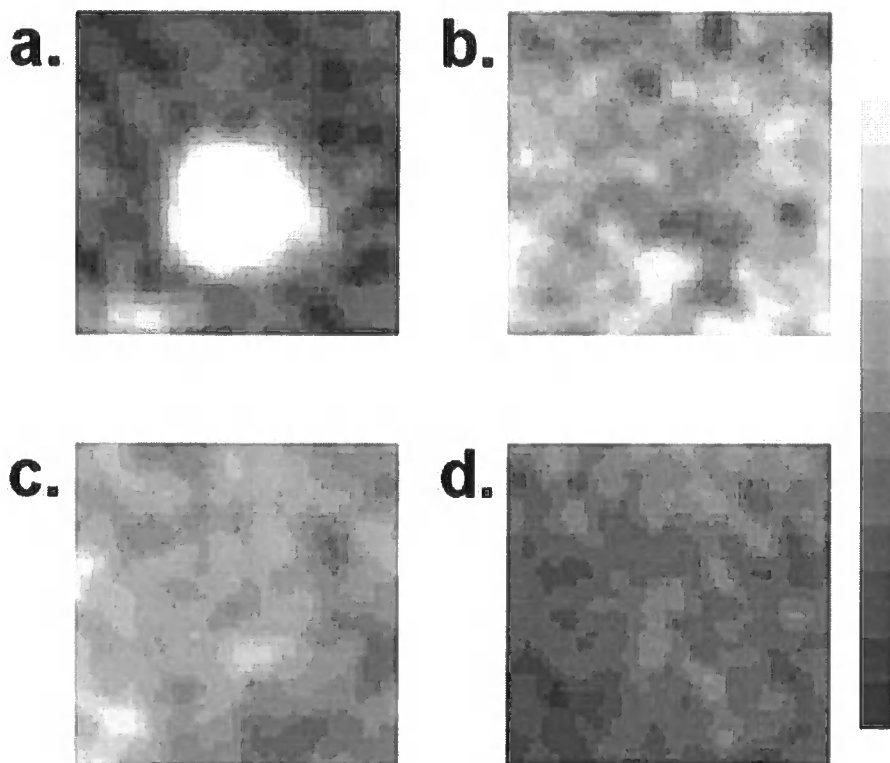


Figure 5-2 100 μm square scanning XPS micrographs of a polystyrene surface following the charging of a 15 μm square with positive voltage and the immersion of the sample in a gold colloid suspension in Fluorinert. Scans map Au 4f (a), C 1s (b), O 1s (c) and Si 2p (d). Z Scale Normalised Counts.

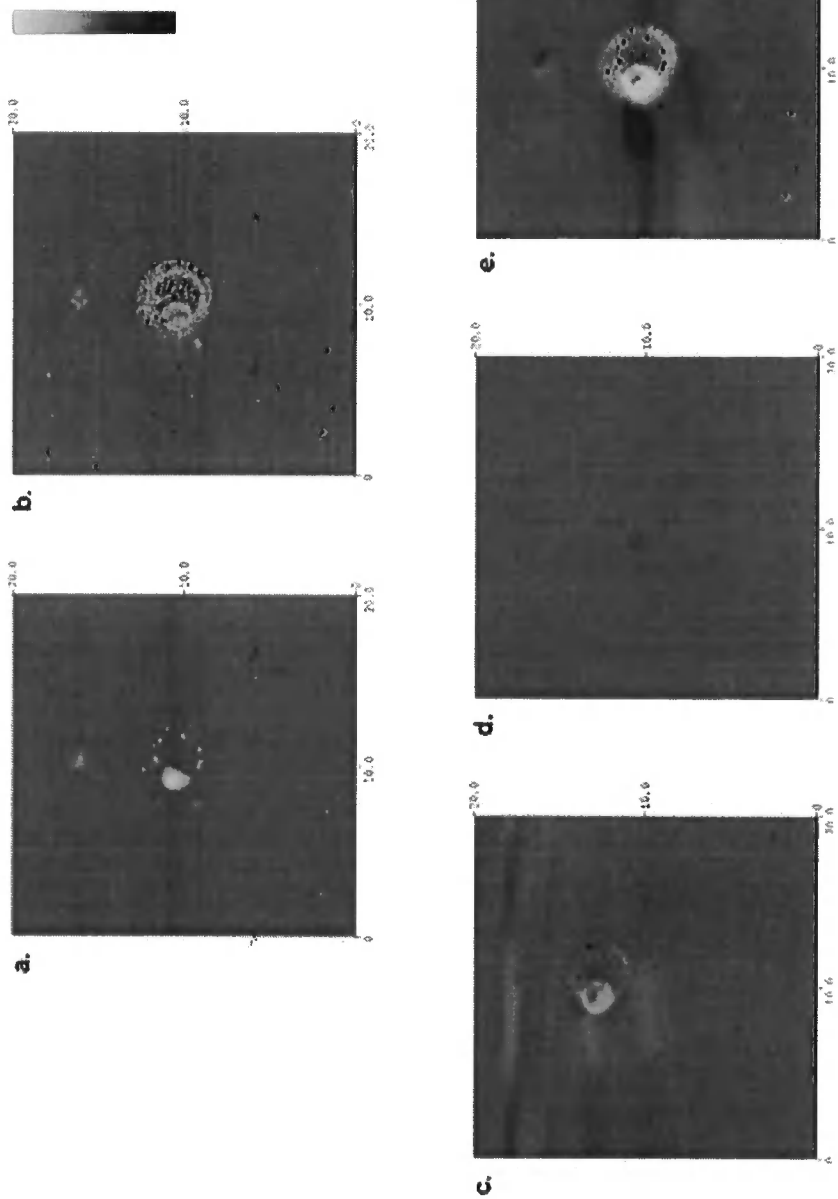


Figure 5-3 Atomic force micrographs of negatively charged polystyrene surface following the electrostatic attachment of gold colloids to the deposited charge. Height (500 nm), Phase (90 °), EFM + 12 V (2 °), 0 V (2 °) and EFM – 12 V (2 °).

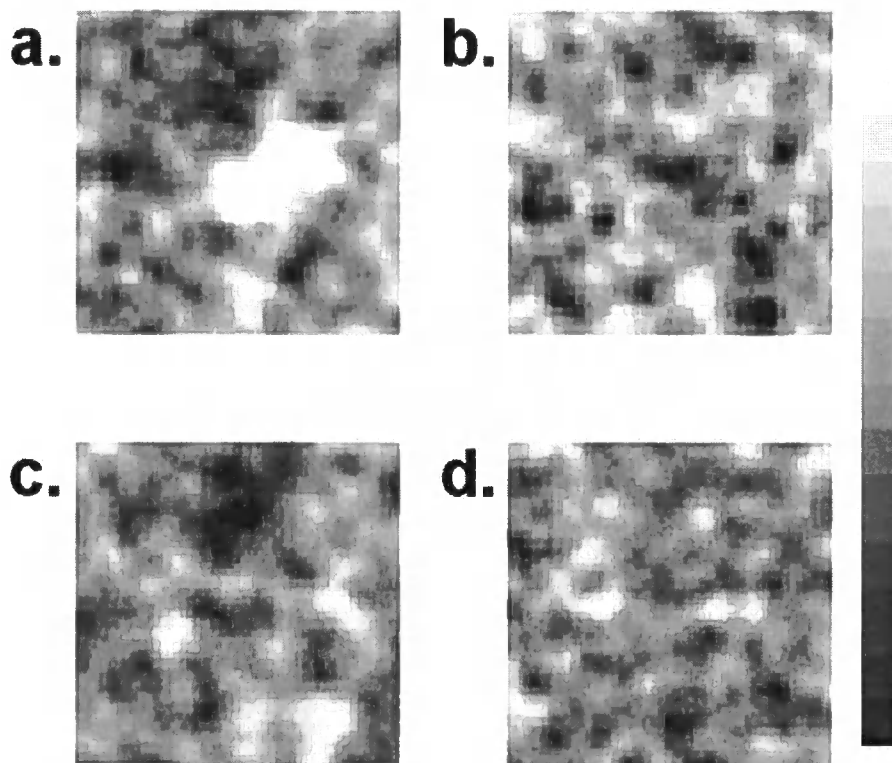


Figure 5-4 100 μm square scanning XPS micrographs of a polystyrene surface following the charging of a 5 μm square with negative voltage and the immersion of the sample in a gold colloid suspension in Fluorinert. Scans map Au 4f (a), C 1s (b), O 1s (c) and Si 2p (d). Z Scale Normalised Counts.

5.4 Discussion

Charged surfaces are capable of capturing sub-micron sized particles, both air borne particulate matter⁴ and solution based colloids.¹⁶ It has been demonstrated here the practicality that colloidal gold nano-particles preferentially accumulate onto both positively and negatively charged patches, in comparison to the uncharged surroundings on a polystyrene substrate. It has been demonstrated that for a positively charged surface the accumulation of gold particles occurs over a larger region than the initial charge deposition, with the particles showing a preference for accumulation around the edges. Conversely, with negatively charged patches deposited onto a surface the particles tend to accumulate towards the centre.

Charged particles interact with surface charge distributions via columbic forces, whereas uncharged particles are acted on by induction forces. Gold nano-particles are uncharged, whereas emulsions of water droplets in fluorocarbon solvents are known to have net positive charge. This can be attributed to the phenomenological rule of Cohen and Raydt¹⁷ that states: 'Materials with higher dielectric constants usually charge up positively when brought into contact with materials of lower dielectric constant.' In this system, Fluorinert has a low dielectric value ($\epsilon = 1.89$), whereas the water droplets emulsified within it have a higher dielectric value ($\epsilon = 80$). Coehn and Raydt's rule is based on observations for solid / liquid interfaces however, the charging mechanism in this system has not been fully characterized and friction charging may also be present.

The observation of a preference of the gold nano-particles to form in the centre of the negatively charged region on the polystyrene substrate is

due to the inherent positive charge in the water droplets in the emulsion. This serves to allow columbic effects to dominate, leading to central deposition.

With deposition of the particles onto regions of positive charge, induction effects dominate. The observed accumulation of particles at the peripheries of charged positive squares is an example of an edge effect, a phenomenon well known in xerography.¹⁸ Edge effects are generally attributed to large electric field gradient effect at the boundary between charged and uncharged regions. It has previously been demonstrated that the region directly exposed to a corona discharge loses charge more rapidly than the indirectly charged surrounding areas, charged due to excitation by UV photons.¹⁸ Therefore, it seems likely that the observed distribution of particles onto the edge of positively charged substrate results from the greater field gradient at the edge of the charge patch.¹⁸

5.5 Conclusion

The controlled deposition of gold nano-particles onto a polystyrene substrate using electrostatic attraction has been successfully demonstrated. Localised charge deposition using a scanning EFM tip provides the charged template. Subsequent exposure to a suspension of colloidal gold nano-particles then results in the production of micrometer scale gold patterns. Negative charge patches were found to produce more localised particle deposition whilst positively charged patches resulted in particle deposition around the edge of the charged region. AFM, EFM and scanning XPS were used to detect the induced charge on the surface, as well as the topographic and chemical changes in the patterned substrate.

5.6 References

- [1] Hays, D. A. *J. Adhesion* **1995**, *51*, 41.
- [2] Hilczner, B.; Malecki, J. *Electrets*, Elsevier: New York, 1986; p341.
- [3] Mizes, H.; Ott, M.; Eklund, E.; Hays, D. *Colloids Surf., A* **2000**, *165*, 11.
- [4] Van Turnhout, J. *Proc. Int. Symposium on Electrets and Dielectrics*, Academia Brasileira de Ciencias: Rio de Janeiro, 1975, 85.
- [5] Junno, T.; Magnusson, M. H.; Carlsson, S. –B.; Deppert, K.; Malm, J. – O.; Montelius, L.; Samuelson, L. *Microelec. Eng.* **1999**, *47*, 179.
- [6] Kong, J.; Franklin, N. R.; Zhou, C.; Chapline, M. G.; Peng, S.; Cho, K.; Dai, H. *Science* **2000**, *287*, 622.
- [7] Deng, Z.; Mao, C. *Agnew Chem. Int. Ed.* **2004**, *43*, 4068.
- [8] Wright, W. D. M.; Chetwynd, D. G. *Nanotechnology* **1998**, *9*, 133.
- [9] Jacobs, H. O.; Campbell, S. A.; Steward, M. G. *Adv. Mater.* **2002**, *14*, 1553.
- [10] Pai, D. M.; Springett, B. E. *Rev. Mod. Phys.* **1993**, *65*, 163.
- [11] Jacobs, H.; Whitesides, G. M.; *Science* **2001**, *291*, 1763.
- [12] Krinke, T. J.; Fissan, H.; Deppert, K.; Magnusson, M. H.; Samuelson, L. *Appl. Phys. Lett.* **2001**, *78*, 3708.
- [13] Fudouzi, H.; Kobayashi, M.; Shinya, N. *Langmuir* **2002**, *18*, 7648.
- [14] Sessler, G. M.; West, J. E.; *Phot. Sci. Eng.* **1974**, *18*, 162.
- [15] Ebbens, S. J. Ph.D. Thesis University of Durham, 2001.
- [16] Naujoks, N.; Stemmer, A. *Microelec. Eng.* **2005**, *78-79*, 331.
- [17] Coehn, A.; Raydt, U. *Ann. Phys. IV Folge.* **1909**, *30*, 777.
- [18] Neugebauer, H. E. *J. Appl. Opt.* **1964**, *3*, 385.

Chapter 6

Electroless Metal Deposition onto Poly(4-Vinylpyridine) Functionalised Solid Surfaces

6.1 Introduction

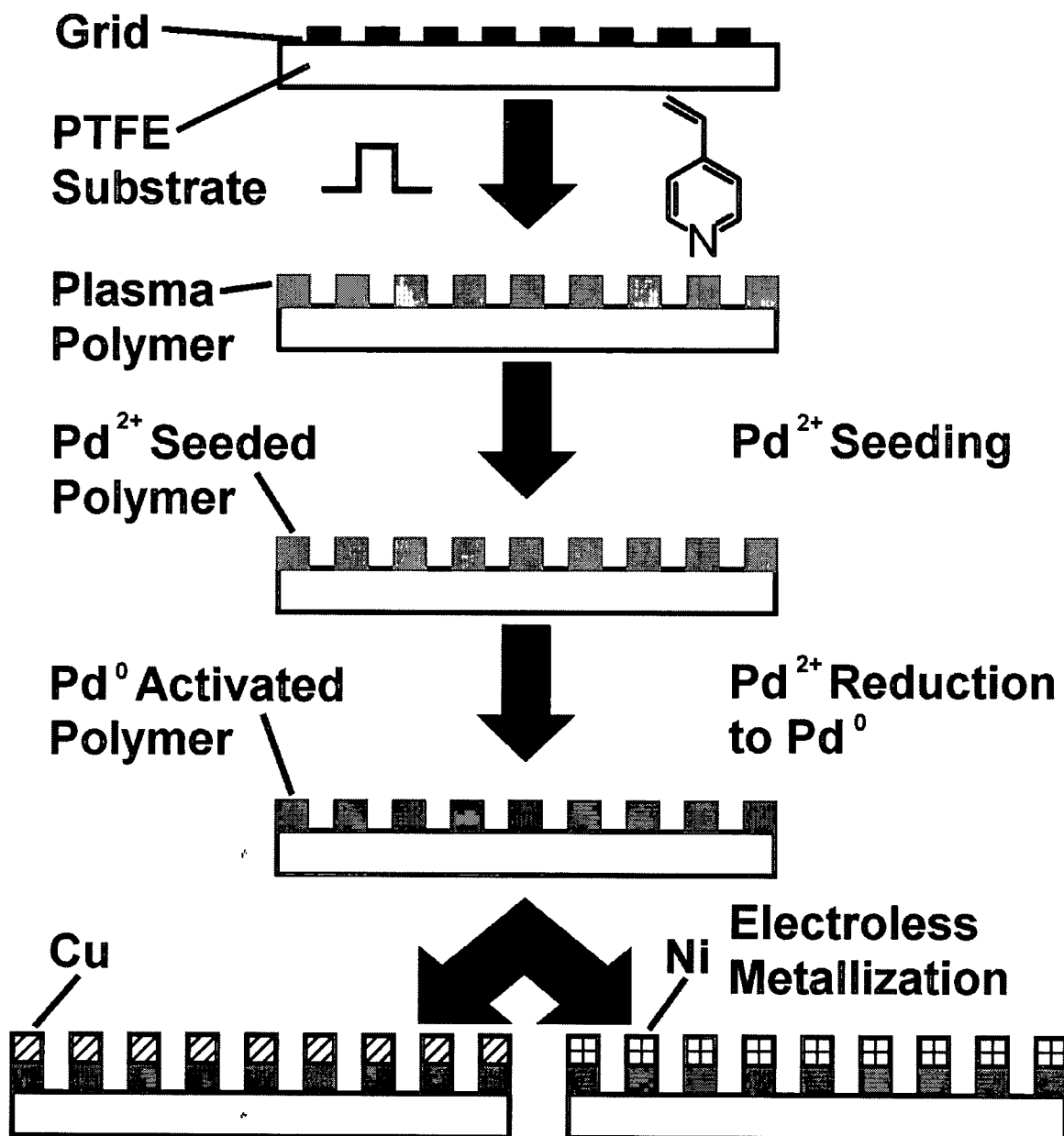
Progress in the microelectronics industry has led to an increasing demand for the replacement of aluminum by transition metals such as copper and nickel. This is due in part to the properties of these metals. Compared to aluminum, they both benefit from a lower susceptibility to electromigration, and a smaller resistance-capacitance delay¹. Other merits include the fact that both copper and nickel can be easily deposited by electroless deposition (which does not require a conductive substrate)².

In the electroless process, an aqueous chemical reducing agent (such as formaldehyde) serves as the source of electrons needed to heterogeneously reduce metal ions to their ground state at the substrate surface^{3,4}. Electroless plating solutions usually contain a metal salt of the desired metal, a suitable reducing agent, a complexing agent to solubilize the metal salt, and a base to adjust the pH to favor reduction. Such plating solutions tend to be stable until they come into contact with a catalytically active surface, at which point the thermodynamically favourable reduction of metal ions to metal occurs. For example, electroless metal deposition mechanism can be seeded by the use of palladium as the catalytic initiator⁵ (other noble metals including gold⁶ and silver⁷ are also known to work). The reaction then proceeds on the newly deposited metal layer in an autocatalytic fashion to yield a thick metallic film. Thin metal films grown in this fashion tend to trace the topography of the underlying substrate surface.

Since palladium cannot chemisorb directly onto inert substrates, additional pre-treatment steps are often required. In these cases, the substrate is sensitised using a binder molecule.^{8,9,10,11,12,13} For instance,

palladium is renowned for forming stable complexes with electron lone pair donating nitrogen groups¹⁴. Therefore, the production of surfaces containing nitrogen functionality (in particular, pyridine centres¹⁵) facilitates electroless metal deposition onto a variety of surfaces. Past work has also included the continuous wave plasma polymerisation of 4-vinylpyridine in an argon carrier gas to give functionalised surfaces.¹⁶

In this chapter we describe the use of pulsed plasmachemical functionalisation to produce a pyridine functionalized surface with a high degree of structural retention, Scheme 6-1. A Pd(II) catalyst is then complexed to these surface-nitrogen groups, permitting its subsequent reduction to Pd(0) state followed by the electroless deposition of copper and nickel. It is shown that microscopic metallic arrays can also be fabricated by masking the substrate (e.g. with a grid) prior to the plasmachemical deposition step, Scheme 6-1.



Scheme 6-1 Electroless metallisation onto pulsed plasma deposited poly(4-vinylpyridine).

6.2 Experimental

4-vinylpyridine monomer (Aldrich, +97%) was loaded into a sealable glass tube, followed by further purification using several freeze-pump-thaw cycles to remove adsorbed gases. Pulsed plasma polymerization of the precursor was undertaken in a cylindrical glass reactor (4.5 cm diameter, 460 cm³ volume, 2 x 10⁻³ mbar base pressure, leak rate 1.4 x 10⁻⁹ mol/s) surrounded by a copper coil (4 mm diameter, 10 turns, located 15 cm away from the precursor inlet) and enclosed in a Faraday cage. The chamber was evacuated using a 30 L min⁻¹ rotary pump attached to a liquid nitrogen cold trap, whilst monitoring the system pressure with a Pirani gauge. All fittings were grease-free. The output impedance of a 13.56 MHz radio frequency (RF) power supply was matched to the partially ionized gas load using an L-C network. During pulsed plasma deposition, the RF source was triggered by a signal generator and the pulse shape monitored with an oscilloscope. Prior to each deposition, the apparatus was cleaned by scrubbing with detergent, rinsing in propan-2-ol, and then oven drying. The reactor was then reassembled and evacuated to base pressure. Further cleaning entailed running a continuous wave air plasma at 0.2 mbar pressure and 40 W power lasting 30 min. Next, silicon (100) wafers (MEMC Materials Inc) or polytetrafluoroethylene strips (Goodfellows) were inserted into the centre of the reactor and the system pumped back down to base pressure. At this stage, 4-vinylpyridine vapor was introduced into the chamber at a pressure of 0.2 mbar for 5 min prior to plasma ignition. Optimum film deposition conditions corresponded to 40 W continuous wave bursts lasting 100 μ s (t_{on}), followed by an off-period (t_{off}) set at 4 ms, which yielded a film growth rate of 15 nm min⁻¹. Upon completion of

deposition, the RF generator was switched off and the monomer allowed to continue flowing through the system for a further 5 min. Finally the chamber was evacuated to base pressure and vented to atmospheric pressure.

Pulsed plasma poly(4-vinylpyridine) coated surfaces were subsequently submerged into an aqueous catalyst solution containing palladium(II) chloride (99%, Aldrich), 3.0 M sodium chloride (99.9%, Sigma), and 0.5 M sodium citrate dehydrate (99%, Aldrich) (which had been pH adjusted to 4.5 with citric acid monohydrate (99%, Aldrich)) for 12 h, and then washed in deionized water. A palladium chloride concentration of at least 1 mM was utilized to ensure that the surface was fully loaded with Pd²⁺ ions.

Electroless copper deposition onto these palladium complexed surfaces was then carried out for 60 min in an aqueous solution containing 1.5 wt% copper sulphate pentahydrate (98%, Fluka), 7 wt% potassium sodium tartrate (98%, Aldrich), 1 wt % sodium hydroxide (98%, Fluka), and 50 wt% formaldehyde (supplied as 37 wt% in water, Aldrich).

Electroless deposition of nickel was carried out in a commercially-available bath, EL468 (Shipley). The bath contained nickel sulphate, dimethylaminoborane, and other components to maintain a suitable pH. The palladium-activated 4-vinylpyridine plasma polymer films were immersed in the solution for 30 min to allow the deposition of nickel.

Plasma polymer film thickness measurements were carried out using an nkd-6000 spectrophotometer (Aquila Instruments Ltd). Transmission-reflectance curves (over the 350 – 1000 nm wavelength ranges) were fitted to a Cauchy model for dielectric materials using a modified Levenburg-Marquardt method¹⁷.

A VG Escalab spectrometer equipped with an unmonochromated Mg K α X-ray source (1253.6 eV) and a concentric hemispherical analyzer was employed for X-ray photoelectron spectroscopy (XPS) analysis of the coated surfaces. Elemental compositions were calculated using sensitivity (multiplication) factors derived from chemical standards, O(1s): C(1s): N(1s): Pd(3d) = 0.36: 1.00: 0.57: 0.05. All binding energies were referenced to the C(1s) hydrocarbon peak at 285.0 eV. A Marquardt minimization computer program was used to fit core level envelopes with fixed width at half maximum (fwhm) Gaussian peak shapes¹⁸.

Fourier transform infrared (FTIR) analysis of the plasma polymerised films at each stage of reaction was carried out using a infrared spectrometer (Perkin Elmer Spectrum One) equipped with a liquid nitrogen cooled MCT detector. Reflection-absorption (RAIRS) measurements were performed using a variable angle accessory (Specac) set at 66° with a KRS-5 polarizer fitted to remove the s-polarised component. All spectra were averaged over 256 scans at a resolution of 4 cm⁻¹.

Simple patterning was exemplified by embossing a brass grid (500 μ m holes with a centre-to-centre separation of 1 mm) using a pressure of 64 MPa onto a PTFE substrate, Scheme 6-1. This was followed by plasma polymerization of 4-vinylpyridine onto the substrate as previously described, to yield approximately 150 nm thick pixels. The grid was subsequently removed, and the pulsed plasma poly(4-vinylpyridine) patterned substrate treated in the palladium catalyst solution, followed by immersion in the electroless deposition bath for 60 min and 30 min for copper and nickel coating respectively. The metallic arrays were imaged with a multi-step optical

microscope (Spectrum One, Perkin Elmer) fitted with a x20 magnification lens and scanning at 100 μm step resolution.

6.3 Results

XPS analysis of the pulsed plasma deposited poly(4-vinylpyridine) film showed that there was only carbon, nitrogen, and a trace amount of oxygen present on the surface (the absence of a Si(2p) peak indicates complete coverage of the silicon substrate), Table 6-1. The good agreement between the pulsed plasma deposited film and the theoretical atomic percentages of poly(4-vinylpyridine) film indicates that polymerisation occurs selectively at the alkene bond, and the aromatic pyridine rings remain intact during the electrical discharge process. The C(1s) envelope can be fitted to three types of carbon environment¹⁹: hydrocarbon (285.0 eV, α), carbon within an aromatic ring (285.5 eV, β), and carbon next to a N atom within an aromatic ring (286.0 eV, γ), Figure 6-1. In addition, the π - π^* shake-up satellite at 292.3 eV is clearly indicative of the retained aromatic ring structure²⁰. The N(1s) binding energy for pulsed plasma deposited poly(4-vinylpyridine) was 399.4 eV, which compares favorably with a value of 399.4 eV measured for conventional spin-coated poly(4-vinylpyridine) as well as previous literature values¹⁹.

Table 6-1 Theoretical and experimental XPS elemental compositions of pulsed plasma deposited poly(4-vinylpyridine).

Surface	% C	% N	% O
Theoretical	87.5	12.5	0
Pulsed Plasma Polymer	87.9 \pm 0.5	11.3 \pm 0.5	0.8 \pm 0.5

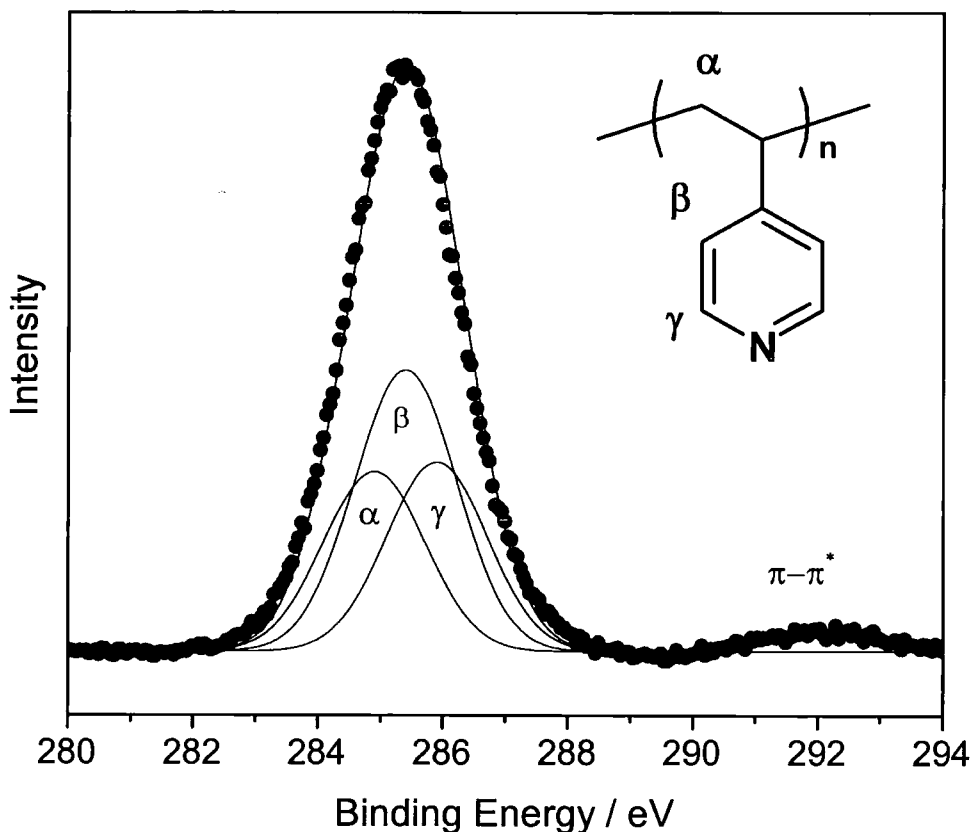


Figure 6-1 XPS C(1s) spectrum of pulsed plasma deposited poly(4-vinylpyridine).

Infrared spectroscopy provided further evidence for functional retention in the pulsed plasma deposited coatings, Figure 6-2. For 4-vinylpyridine monomer, the following fingerprint band assignments can be made²¹: vinyl C=C stretching (1634 cm^{-1}), aromatic quadrant C=C stretching (1597 cm^{-1} and 1548 cm^{-1}), aromatic semicircle C=C and C=N stretching (1495 cm^{-1} and 1409 cm^{-1} respectively), and =CH₂ wag (927 cm^{-1}). Pulsed plasma deposited poly(4-vinylpyridine) displays similar features to those associated with the monomer, except for the absence of the vinyl C=C band and =CH₂ wag

indicative of polymerization. However, a new band due to CH₂ deformation (1454 cm⁻¹) is evident, caused by the growth of the polymer backbone. The presence of intense pyridine ring stretching bands confirms minimal structural disruption during pulsed plasma polymerization. In fact, the infrared spectra of commercially-available spin-coated poly(4-vinylpyridine) and pulsed plasma deposited poly(4-vinylpyridine) are very similar; whereas continuous wave plasma polymerization of 4-vinylpyridine destroys the aromatic structure.

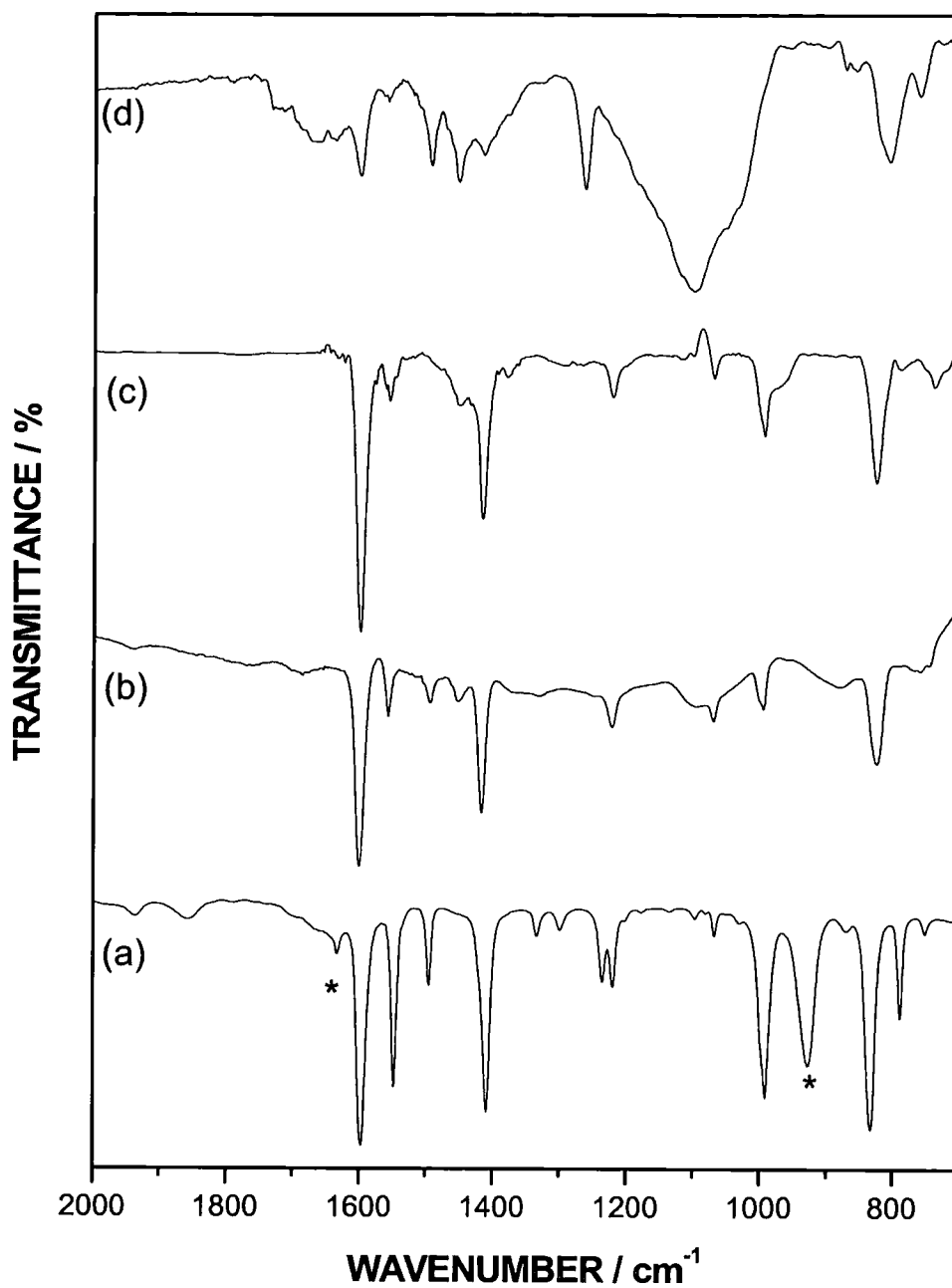


Figure 6-2 FTIR spectra of: (a) 4-vinyl pyridine monomer; (b) spin-coated poly(4-vinylpyridine); (c) pulsed plasma deposited poly(4-vinyl pyridine); and (d) 10 W continuous wave 4-vinyl pyridine plasma polymer. (* denotes polymerisable alkene bond.)

Palladium cation complexation to the plasma polymer surface was found to depend upon the solution concentration. A maximum level of 1.5 ± 0.2 at % palladium (as determined by XPS) was achieved following exposure to a $2.5 \mu\text{M}$ solution for 10 h. The N(1s) binding energy also increased from 399.4 eV to 402.8 eV, which can be taken as being evidence for the coordination of the pyridine group nitrogen lone pair electrons to the Pd^{2+} ions.

The deposition of copper/nickel onto the palladium activated plasma polymer surface following immersion into the respective electroless deposition bath was visible to the naked eye. XPS wide-scan analysis of the deposited metal films confirmed this, with binding energy peaks for Cu(2p) at 955 and 975 eV, and Ni(2p) at 873 and 893 eV, Figure 6-3. Control experiments, in the absence of palladium immobilisation, revealed no metallisation at the surface, verifying that the palladium catalyst is a necessary prerequisite for the electroless deposition of metals to occur.

Metal array structures were patterned onto a PTFE substrate by the selective deposition of pulsed plasma polymer film through an embossed metal grid. The subsequent electroless deposition was discernible with the naked eye (Figure 6-4).

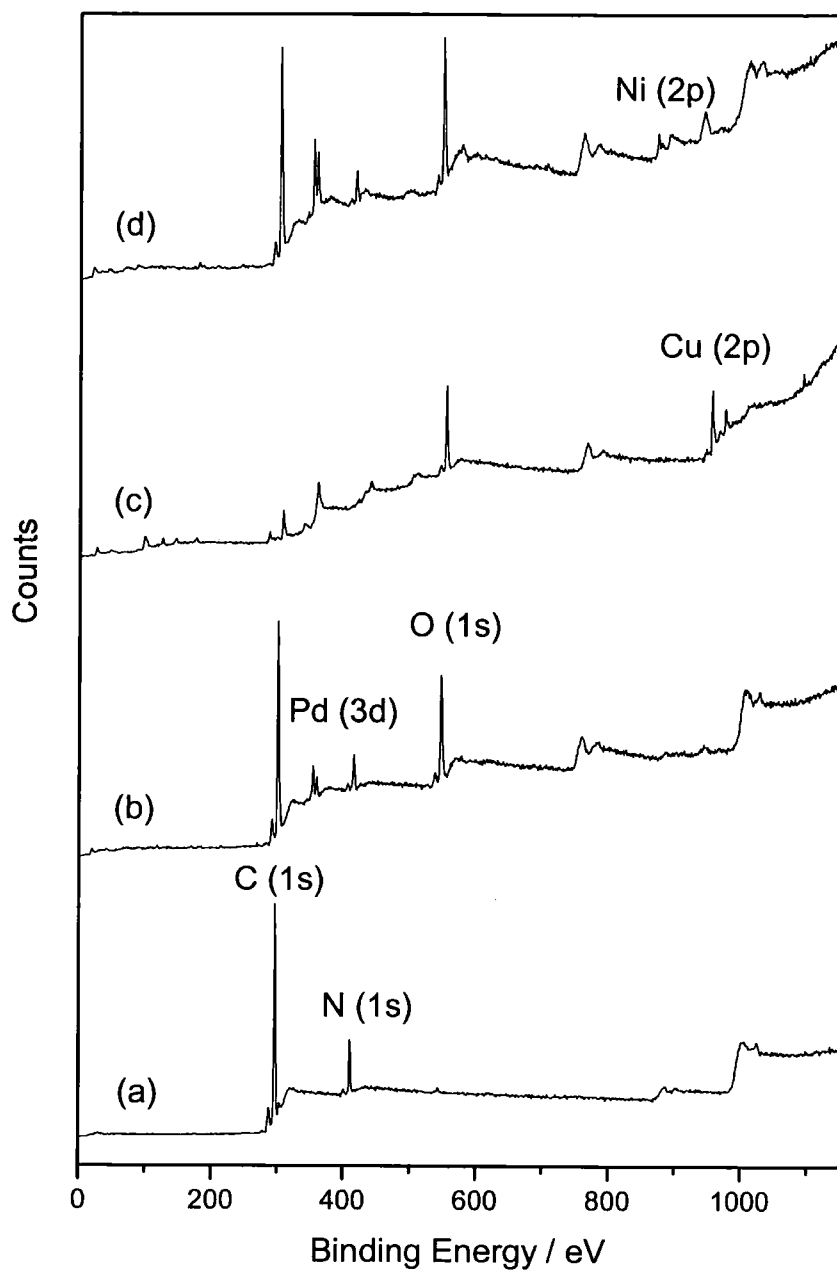


Figure 6-3 XPS wide scan of (a) 4-vinylpyridine pulsed plasma polymer; (b) 4-vinylpyridine pulsed plasma polymer reacted with Palladium chloride solution; (c) pp4VP-PdCl₂ films reacted in copper sulphate bath and (d) pp4VP-PdCl₂ films reacted in Shipley EL468 nickel bath.

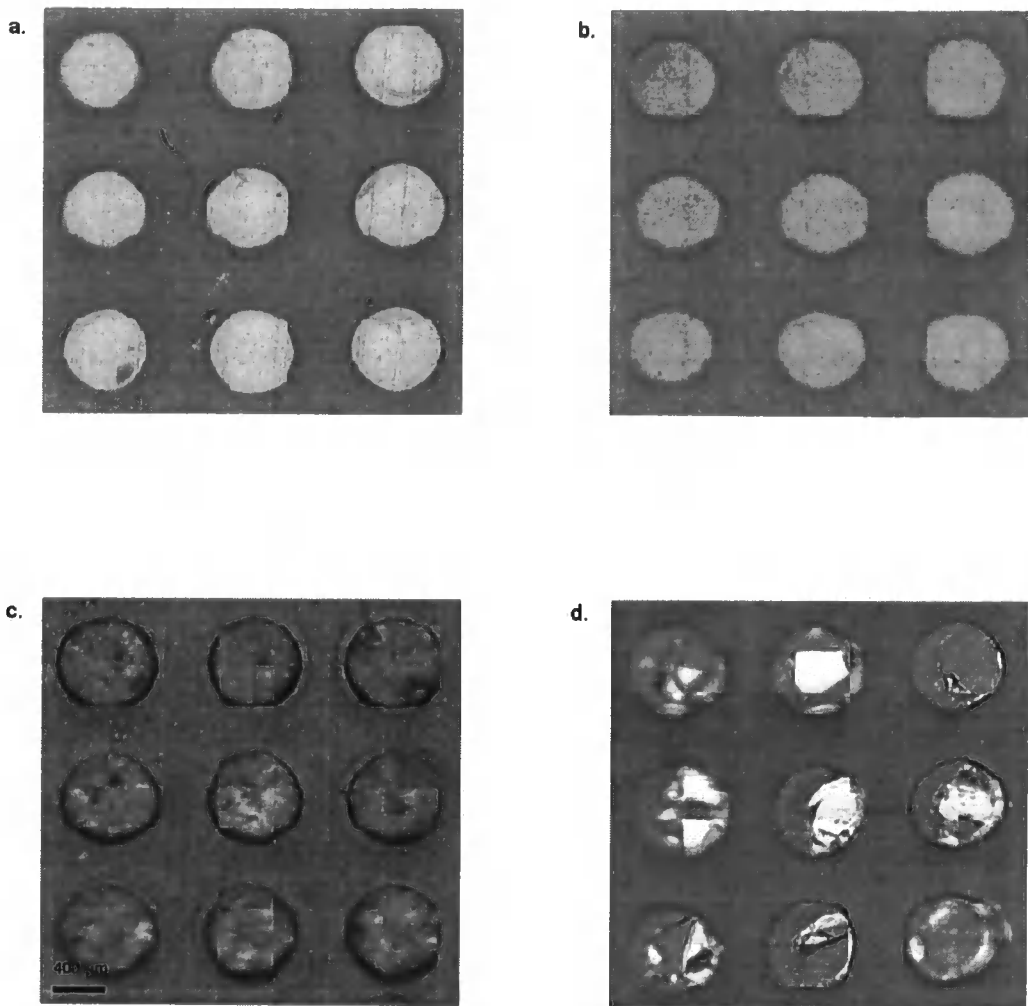


Figure 6-4 Optical images of arrays of: (a) 150 nm thick pulsed plasma deposited poly(4-vinylpyridine) onto PTFE; (b) Pd²⁺ functionalized (a); (c) electroless deposition of metallic copper onto (b); and (d) electroless deposition of metallic nickel onto (b).

6.4 Discussion

Plasma polymerization of monomers is a well-established technique for functionalizing solid surfaces. There are a number of benefits associated with this approach which include the fact that it is solventless, single-step, low cost, and substrate-independent. However, the energetic nature of continuous wave electrical discharges can cause extensive molecular fragmentation and rearrangement of the precursor, which leads to a variety of functionalities being incorporated onto the surface²². This potential drawback can be overcome by pulsing the electric discharge on a μ s-ms timescale to give rise to high levels of structural retention²³. This can be ascribed to low polymer fragmentation during the short plasma on-period (microseconds) followed by conventional polymerization reaction pathways proceeding during the extended plasma off-time (milliseconds). Examples of molecularly tailored substrates produced in this fashion include anhydride²⁴, carboxylic acid²⁵, cyano²⁶, epoxide²⁷, hydroxyl²⁸, furfuryl²⁹, perfluoroalkyl³⁰, perfluoromethylene³¹, and trifluoromethyl³² functionalized surfaces. In this study it has been shown that structurally well-defined poly(4-vinylpyridine) films can be deposited in a similar fashion.

The aromatic nitrogen functionality contained in the pulsed plasma deposited poly(4-vinylpyridine) layer is found to readily complex with Pd^{2+} ions in acidic solution.¹⁵ This stems from a Lewis-type interaction between the electron lone pairs on the pyridine nitrogen atom and the free orbitals on the Pd^{2+} ion¹⁵ (as evident by the increase in N(1s) XPS binding energy from 399.4 eV to 402.8 eV). The Pd^{2+} is then reduced by the formaldehyde (or dimethylaminoborane) contained in the deposition solution to Pd^0 . Exposure

of this Pd⁰ containing surface to metal cations in the electroless deposition solution leads to the growth of metal. After the first layer of metal is deposited, the palladium surface is no longer accessible; instead, the reaction proceeds in an autocatalytic manner using the last deposited metal surface as a catalyst. In the present study it was established that a maximum level of PdCl₂ functionalization at the surface could be achieved by using just a 2.5 μM solution. This compares favourably with the reported requirement of greater than 30 mM to initiate the electroless metallisation of poly(acrylic acid) films³³ and 1 mM needed for the conventional metallisation Pd / Sn route³⁴.

Some inherent advantages of the electroless deposition technique described in this article are that it is low-cost, non-abrasive, operates at room temperature, and is substrate-independent.

6.5 Conclusions

4-vinylpyridine has been pulsed plasma deposited with good structural retention onto a variety of substrates, including silicon wafers and PTFE. The resultant aromatic surfaces were found to readily form complexes with palladium ions in solution via lone pair electron donation from the pyridine ring nitrogen. These catalytic metal centres readily served as initiation sites for the electroless deposition of metallic copper and nickel. Micrometer sized metal patterns have been generated on PTFE substrates by the embossing of a copper grid followed by the subsequent plasma deposition into the grid holes.

6.6 Reference

- [1] Save, D.; Braud, F.; Torres, J.; Binder, F.; Muller, C.; Weidner, J. O.; Hasse, W. *Microelectro. Eng.* **1997**, *33*, 75.
- [2] *Electroless Plating: Fundamentals & Applications*, Mallory, G. O.; Hajdu, J. B. Eds.; American Electroplaters and Surface Finishers Society, Orlando, FL, 1990.
- [3] Prissanaroon, W.; Brack, N.; Pigram, P. J.; Hale, P.; Kappen, P.; Liesegang, J. *Thin Solid Films* **2005**, *477*, 131.
- [4] Marton, J. P. US Patent 3,676,213, 1972.
- [5] Meek, R. L. *J. Electrochem. Soc.* **1975**, *122*, 1478.
- [6] Zhang, M.; Lu, C.; Cong, H.; Cao, W. *Macromol. Rapid Commun.* **2004**, *25*, 1917.
- [7] Tong, H.; Zhu, L.; Li, M.; Wang, C. *Electrochimica Acta* **2003**, *48*, 2473.
- [8] Cohen, R. L.; West, K. W. *J. Electrochem. Soc.* **1973**, *120*, 502.
- [9] Osaka, T.; Nagasaka, H.; Goto, F. *J. Electrochem. Soc.* **1980**, *127*, 2343.
- [10] Osaka, T.; Takematsu, H.; Nihei, K. *J. Electrochem. Soc.* **1980**, *127*, 1021.
- [11] Cohen, R. L.; Meek, R. L. *J. Colloid Interface Sci.* **1976**, *55*, 156.
- [12] Feldstein, N.; Schlesinger, M.; Hedgecock, N. E.; Chow, S. L. *J. Electrochem. Soc.* **1974**, *121*, 738.
- [13] Horkans, J.; Kim, J.; McGrath, C.; Romankiw, L. T. *J. Electrochem. Soc.* **1984**, *134*, 301.
- [14] Charbonnier, M.; Alami, M.; Romand, M. *J. Electrochem. Soc.* **1996**, *143*, 472.

- [15] Yang, G. H.; Kang, E. T.; Neoh, K. G.; Zhang, Y.; Tan, K. L. *Langmuir* **2001**, *17*, 211.
- [16] Yu, W. H.; Kang, E. T.; Neoh, K. G. *J. Electrochem. Soc.* **2002**, *149*, C592.
- [17] Lovering, D. *NKD-6000 Technical Manual*; Aquila Instruments: Cambridge, UK, 1999.
- [18] Evans, J. F.; Gibson, J. H.; Moulder, J. F.; Hammond, J. S.; Goretzki, H. *Fresenius J. Anal. Chem.* **1984**, *319*, 841.
- [19] Beamson, G.; Briggs, D. *High-Resolution XPS of Organic Polymers: The Scienta ESCA300 Database*; John Wiley & Sons: New York, 1992.
- [20] Clark, D. T.; Dilks, A. *J. Polym. Sci., A, Polym. Chem.* **1977**, *15*, 15.
- [21] Lin-Vien, D.; Colthup, N. B.; Fateley, W. G.; Grasselli, J. G. *The Handbook of Infrared and Raman Characteristic Frequencies of Organic Molecules*; Academic Press: New York, 1991.
- [22] Lopez, G. P.; Ratner, B. D.; Rapoza, R. J.; Horbett, T. A. *Macromolecules*, **1993**, *26*, 3247.
- [23] Han, L. M.; Timmons, R. B.; Bogdale, D.; Pielichowski, J. *Chem. Mater.* **1998**, *10*, 1422.
- [24] Ryan, M. E.; Hynes, A. M.; Badyal, J. P. S. *Chem. Mater.* **1996**, *8*, 37.
- [25] Hutton, S. J.; Crowther, J. M.; Badyal, J. P. S. *Chem. Mater.* **2000**, *12*, 2282.
- [26] Tarducci, C.; Schofield, W. C. E.; Brewer, S. A.; Willis, C.; Badyal, J. P. S. *Chem. Mater.* **2001**, *13*, 1800.
- [27] Tarducci, C.; Kinmond, E. J.; Brewer, S. A.; Willis, C.; Badyal, J. P. S. *Chem. Mater.* **2000**, *12*, 1884.

- [28] Rinsch, C. L.; Chen, X. L.; Panchalingam, V.; Eberhart, R. C.; Wang, J. H.; Timmons, R. B. *Langmuir* **1996**, *12*, 2995.
- [29] Tarducci, C.; Brewer, S. A.; Willis, C.; Badyal, J. P. S. *Chem. Commun.* **2005**, *3*, 406.
- [30] Coulson, S. R.; Woodward, I. S.; Brewer, S. A.; Willis, C.; Badyal, J. P. S. *Chem. Mater.* **2000**, *12*, 2031.
- [31] Limb, S. J.; Gleason, K. K.; Edell, D. J.; Gleason, E. F. *J. Vac. Sci. Technol. A.* **1997**, *15*, 1814.
- [32] Wang, J. H.; Chen, J. J.; Timmons, R. B. *Chem. Mater.* **1996**, *8*, 2212.
- [33] Jackson, R. L. *J. Electrochem. Soc.*, **1990**, *137*, 95
- [34] Dressick, W. J.; Dulcey, C. S.; Georger, J. H.; Calabrese, G. S.; Calvert, J. M. *J. Electrochem. Soc.* **1994**, *141*, 210.

Chapter 7

Super-Repellent Anti-Reflective Surface Coatings

7.1 Introduction

7.1.1 The Fluorination of Polymer Surfaces

Many important uses of a polymer depend on the composition and structure of its surface.^{1,2,3} Polymethylmethacrylate (PMMA) has long been used as a protective coating layer due to its adhesive and film-forming properties.⁴ However, the high surface energy of PMMA ($\approx 40 \text{ mJ/m}^2$)⁵ leads to problems in applications that require a degree of water repellency.

Fluorinated polymer surfaces have many desirable properties; these include water and oil repellency, chemical inertness, low coefficient of friction and small dielectric constant values.^{6,7} Such attributes are useful in a range of products including protective clothing,⁸ stain-proof textiles,⁹ medical implants,¹⁰ marine coatings¹¹ and microelectronics. In addition, if the coating is transparent, optical protective screen technology could be a major beneficiary.¹² Highly fluorinated surfaces can be generated using a variety of techniques such as: direct exposure to F_2 gas,¹³ fluorine containing glow discharges,¹⁴ plasma polymerisation of fluoromonomers,¹⁵ VUV assisted fluorination,¹⁶ sputter deposition of fluorocarbon layers using a polytetrafluorethylene (PTFE) target¹⁷ and chemical derivitisation.¹⁸ Alternatively, small amounts of fluorine containing material can be mixed into a polymer melt,^{9,19,20,21} which upon solidification leads to preferential segregation of the additive towards the air-solid interface as a consequence of its lower surface energy.^{22,23,24,25}

The design and generation of fluorinated polymer surfaces that maintain key benefits, such as oil and water repellency, requires a consideration of a number of factors:

1. The surface should display as many CF_3 terminating groups as possible and a minimum number of CF_2 alkyl chain groups. It was established by Zisman²⁶ that the surface energy of a film depends on the constituent groups and reduces in the following order, CH_2 (36 mN/m) > CH_3 (30 mN/m) > CF_2 (23 mN/m) > CF_3 (15 mN/m). The lower the surface energy, the lower the energy of adhesion of contaminants and thus the easier the cleaning of the surface.
2. The majority of the CF_3 groups should be at the surface; if they are not at the surface their presence will not affect the surface properties.
3. The CF_3 groups should be attached to the surface with sufficient strength. A weakly bound group will be easily extracted or volatilized from the surface and will only provide a temporary beneficial effect.
4. The fluorination should cover the entire surface; partial coating will not provide the full beneficial effect.

In this chapter we describe the production of a super-repellent fluoropolymer surface. The surface produced is inexpensive, rapidly produced and adaptable to a number of different substrates. The method consists of the production of a thin PMMA coating followed by its plasma fluorination. X-ray photoelectron spectroscopy (XPS), Tapping mode Atomic Force Microscopy (AFM) and contact angle analysis techniques were used to characterise the physicochemical nature of the films.

7.1.2 Anti-Reflective Properties

The reduction of the intensity of light reflecting from a glass substrate is of importance in many applications. Reflection from a surface is the result of the difference between the refractive indices of the material and its environment. The minimum degree of reflection from a coated surface can be calculated using Fresnel's equation:

$$R_m = \left(\frac{n_c^2 - n_1 n_2}{n_c^2 + n_1 n_2} \right)^2$$

Equation 7-1

Where R_m is the reflection from the material, n_c is the refractive index of the applied coating and n_1 and n_2 are the refractive indices of air and the material respectively. For anti-reflective coatings it is desired that the value of R_m be zero or close to zero. It is possible to calculate the desired refractive index of a coating using the following equation:

$$n_c = [n_1 n_2]^{1/2}$$

Equation 7-2

The thickness of the desired coating can then be calculated, using the assumption that the light reflected from the two interfaces is required to be 180° out of phase in order for destructive interference of any reflection to occur:

$$t_c = \frac{\lambda_0}{4n_c}$$

Equation 7-3

where λ_0 is the wavelength where zero reflectivity is required. Anti-reflective coatings of these kinds are often used on devices requiring high light transmission. For a glass or transparent plastic substrate the refractive index

is typically $\sim 1.5 - 1.7$, therefore the refractive index of the coating is required to be $\sim 1.2 - 1.3$. Magnesium fluoride (MgF_2) is commonly used for the creation of anti-reflective layers as it has a refractive index of 1.38, which is higher than the ideal value. The fluorination of a polymer surface has been found to reduce its refractive index to values in the same region.²⁷

7.2 Experimental

Polymethylmethacrylate (Aldrich, $M_w = 93,000$) was dissolved in toluene (BDH, +99.5% purity) to form a 5 % (w/w) solution. Thin films were produced by spin coating onto borosilicate glass wafers (BDH 18 × 18 mm, No. 1.5) using a spin coater (Cammax Precima) operating at 2000 rpm for 30 seconds. Exposure to air at room temperature for one hour allowed any trapped solvent to evaporate.

Plasma fluorination treatments were carried out in a cylindrical glass reactor (5 cm diameter, 470 cm³ volume) with a base pressure of 4×10^{-3} mbar, and a leak rate of better than 6×10^{-9} mol s⁻¹. The system was connected to a two stage rotary pump via a liquid nitrogen cold trap and the pressure was monitored with a thermocouple pressure gauge. An L-C matching unit was used to minimize the standing wave ratio of the power transmitted from a 13.56 MHz RF generator to a copper coil wound around the reactor walls. Prior to each plasma treatment, the reactor was scrubbed with detergent, rinsed in propan-2-ol and further cleaned with a 30 minute 50 W air plasma. Next, coated glass slide samples were placed in the centre of the reactor, which was evacuated to base pressure. CF₄ gas (99.7%, Air Products) was then introduced to the system via a needle valve at a pressure of 0.2 mbar. Plasma treatment times were between 2 and 20 minutes, plasma power was varied between 20 W and 60 W. A 5 minute purge was carried out prior to and post plasma treatment. Following purging the system was re-evacuated and then vented to atmosphere.

A VG Escalab MkII spectrometer equipped with an unmonochromated Mg K_α X-Ray source (1253.6 eV) and a concentric hemispherical analyser

was used for X-ray photoelectron spectroscopy (XPS) analysis of the functionalized surfaces. Elemental compositions were calculated using sensitivity (multiplication) factors derived from standards (C:O:F = 1:0.39:0.26). All binding energies were referenced to the C (1s) hydrocarbon peak at 285.00 eV. A Marquardt minimization computer program was used to fit core level envelopes with fixed width (FWHM) Gaussian peak shapes.

AFM micrographs were acquired with a Digital Instruments Nanoscope III. Damage to the tip and sample surface was minimized by using Tapping Mode AFM.²⁸ RMS roughness values were calculated over 20 μm \times 20 μm scan areas.

Sessile drop contact angle measurements were undertaken at 20°C using a video capture apparatus (A.S.T. Products VCA2500XE). The probe liquids chosen to evaluate hydrophobicity and oleophobicity were high-purity water (B. S. 3978 Grade 1) and homogenous series of linear chain alkanes (hexadecane, tetradecane, dodecane, decane, and octane (+99% purity, Aldrich),

Film thickness measurements were carried out using a nkd-6000 spectrophotometer (Aquila Instruments Ltd.). Transmittance – reflectance curves over the 350 – 1000 nm wavelength range were fitted to a Cauchy model for dielectric materials using a modified Levenburg-Marquardt method.

7.3 Results

XPS analysis of a spin-coated polymethylmethacrylate (PMMA) film revealed stoichiometric atomic percentages of 71 % carbon and 29 % oxygen, which compares favourably to the expected theoretical values of 71.4 % carbon and 28.6 % oxygen, Figure 7-1a. Following exposure of the PMMA films to CF₄ plasmas for a fixed duration of ten minutes, the surface oxygen content of the polymer was reduced from 30 % to 5%, Figure 7-1. Additionally the reduction in oxygen content was related to power setting. A corresponding shift in the C(1s) XPS envelope toward higher binding energies was observed due to the formation of CF (287.8 eV), CF₂ (291.2 eV) and CF₃ (293.3 eV) functionalities at the expense of the C_xH_y (285.0 eV) and O-C=O (289.0 eV) carbon components.²⁹ Increasing the duration of a 50 W CF₄ plasma was also studied, Figure 7-3. XPS analysis of the surface revealed that the maximum degree of fluorination (55%) was achieved after only two minutes. Treatment of the surface for extended periods of time (> 10 minutes) resulted in a reduction in the fluorine content at the surface at the expense of increased oxygen and carbon.

AFM topographic images indicated that the PMMA surface was flat and featureless prior to plasma treatment. Following CF₄ plasma treatment an increase in the surface roughness was observed, Figure 7-1c. At low plasma powers, fine scale features appeared over the entire surface. These features grew in size as treatment power was increased. The increase in size of these features resulted in a concomitant increase in RMS roughness (a measurement of the deviation of the sample height from the mean sample height over the entire sample area), Figure 7-2.

Increasing the CF₄ plasma treatment time at a constant plasma power (W) initially resulted in little increase in surface roughness. However, once a ten minute treatment time had been reached, greater exposure to the CF₄ plasma resulted in a vast increase in the surface roughness, Figure 7-3. AFM micrographs of the surface during this transition show gradually larger height features being formed as treatment time increased, Figure 7-4.

Spin-coating PMMA onto a borosilicate glass wafer was found to increase the amount of transmitted light across the visible spectra, Table 7-1. Upon exposure to plasmas of increasing power, the transmission through the film was found to be reduced, Figure 7-5. It is interesting to note that at high wave lengths (1000 nm) the transmission was found to be greater than the untreated BDH wafer. However, at lower wavelengths following more powerful plasma treatments, the transmission was found to fall below that of the untreated cover slip.

The effect of increasing the plasma fluorination duration at a set plasma power (50 W) on the transmission through the sample was investigated. It was found that at low wavelengths (350 nm) the transmission through the sample increased as the exposure time increased. However, after a prolonged exposure (> 8 minutes) the transmission dropped severely and after a twenty minute treatment was still below that of an untreated cover slip. The same effect was observed at medium (700 nm) and high (1000 nm) wavelengths. There was also an initial drop in the transmittance below that of the untreated sample, before an increase to a maximum value after a six minute treatment.

A water contact angle of approximately 72° was observed for untreated PMMA films. CF_4 plasma treatments resulted in an increase in the measured contact angle. As the treatment power was increased the measured contact angle was found to increase until a plateau in excess of 140° was reached for electrical discharge power levels of 30 W or greater, Figure 7-1. These droplets were only loosely attached to the polymer surface and could be removed by tilting the surface or exposing it to a low nitrogen flow over the surface, indicating a low angle of hysteresis indicative of super-hydrophobic behaviour.

Increasing the treatment duration at a fixed plasma power (50 W) was found to result in an increase in sessile drop contact angle. Until at times of ten minutes and greater, the contact angle reduced, the surface finally becoming wetting after twenty minutes, Figure 7-3.

Advancing and receding contact angle values for probe liquids with different surface energies were obtained following exposure to a 50 W, 10 minute CF_4 plasma, Table 7-2. A small hysteresis value was obtained for water showing that the surface is highly hydrophobic. In contrast, alkane probe liquids gave large hysteresis values.

Table 7-1 Transmission Measurements for uncoated and PMMA coated BDH Glass Wafer at various wavelengths.

Wavelength	Transmission / %	
	BDH Wafer	PMMA Coated BDH Wafer
350 nm	89.6	89.9
700 nm	91.9	92.8
1000 nm	92.0	93.2

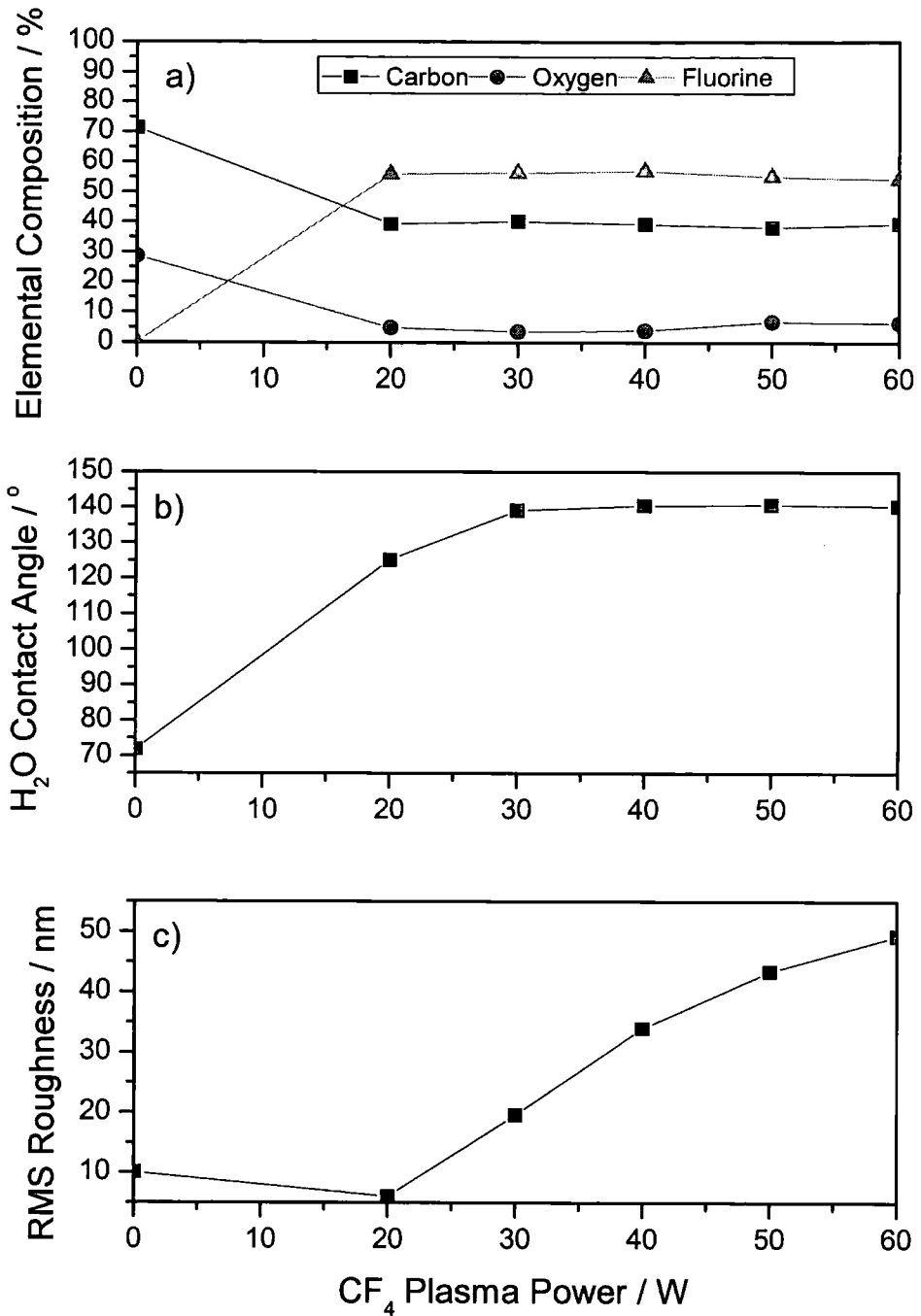


Figure 7-1 10 min CF₄ plasma modification of a 2 μm thick polymethylmethacrylate film as a function of power: (a) XPS elemental composition; (b) H₂O contact angle; (c) AFM RMS surface roughness.

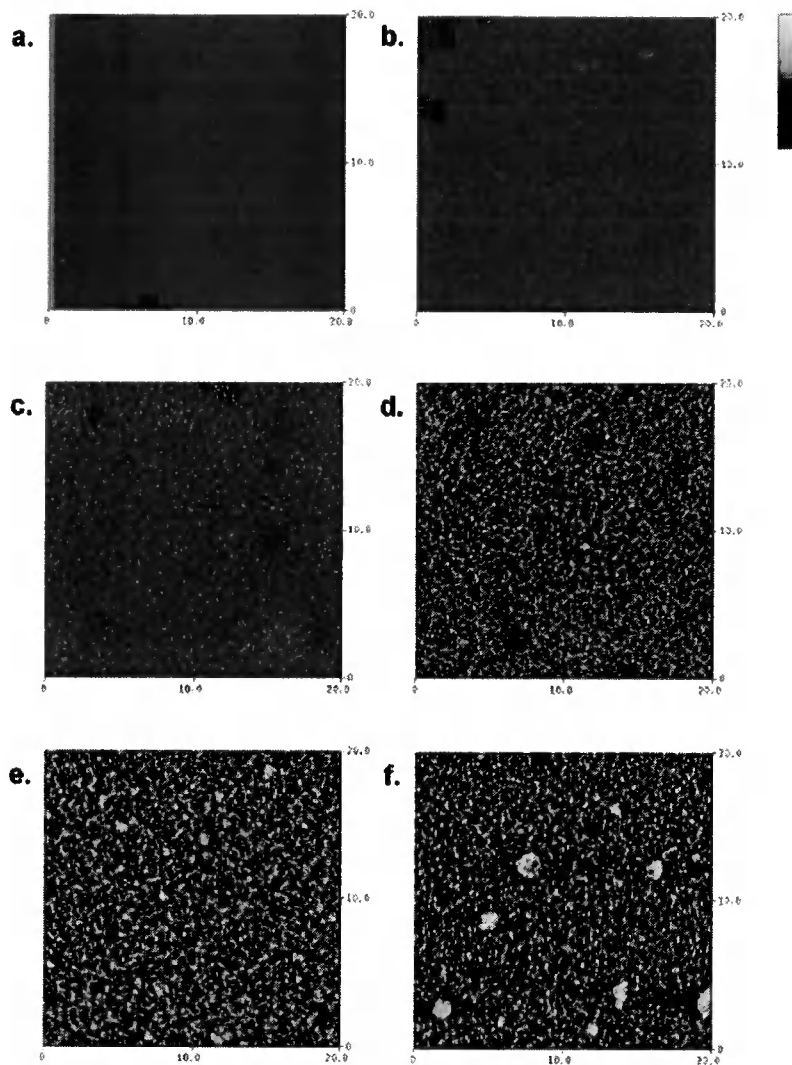


Figure 7-2 AFM height images of polymethylmethacrylate as a function of CF_4 plasma power level (time = 10 min): (a) 0 W, (b) 20 W, (c) 30 W, (d) 40W, (e) 50 W and (f) 60 W. Resolution ($x = y = 20 \mu\text{m}$, $z = 500 \text{ nm}$).

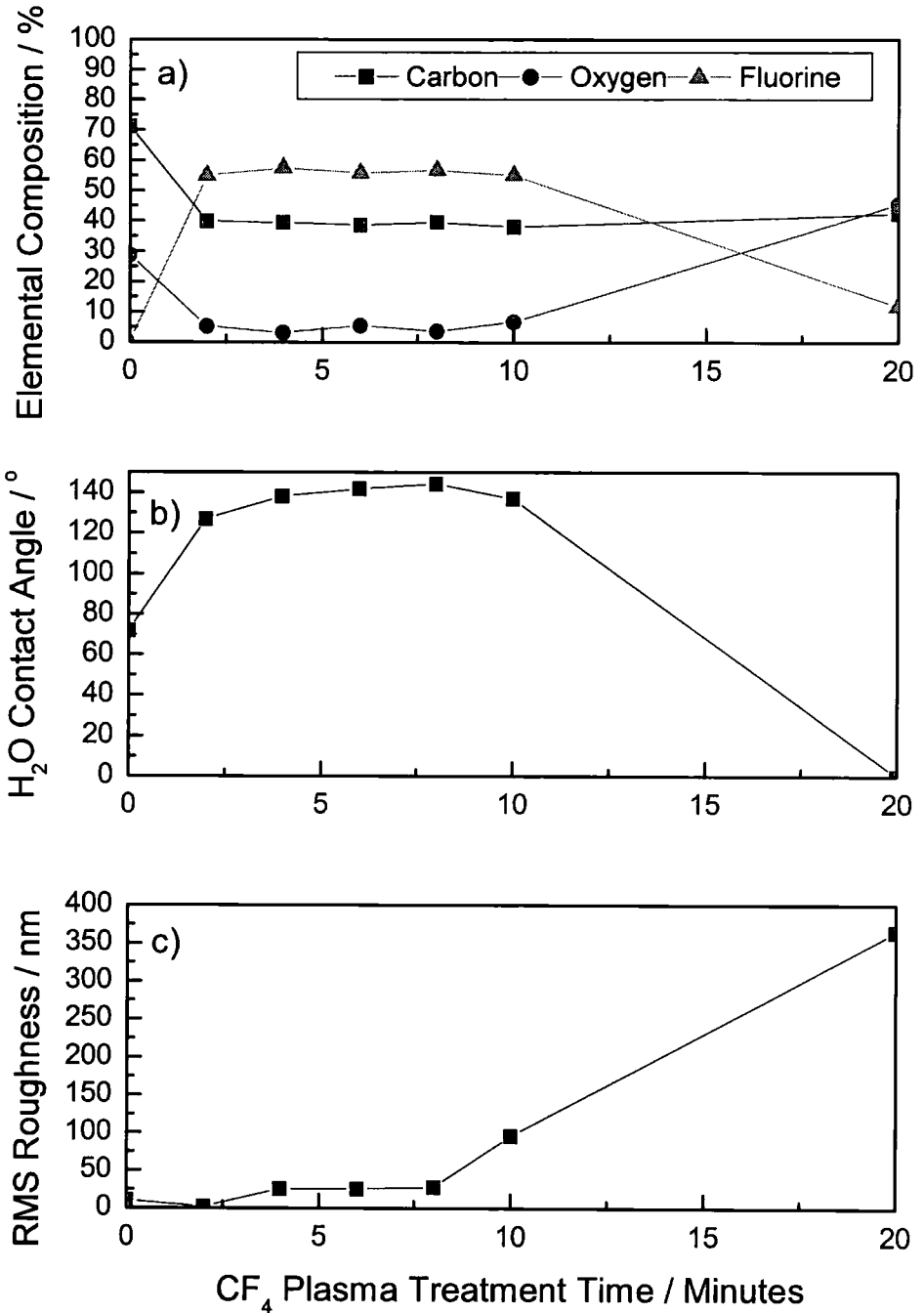


Figure 7-3 50 W CF₄ plasma modification of a 2 μm thick polymethylmethacrylate film as a function of time: (a) XPS elemental composition; (b) H₂O contact angle; (c) AFM RMS surface roughness.

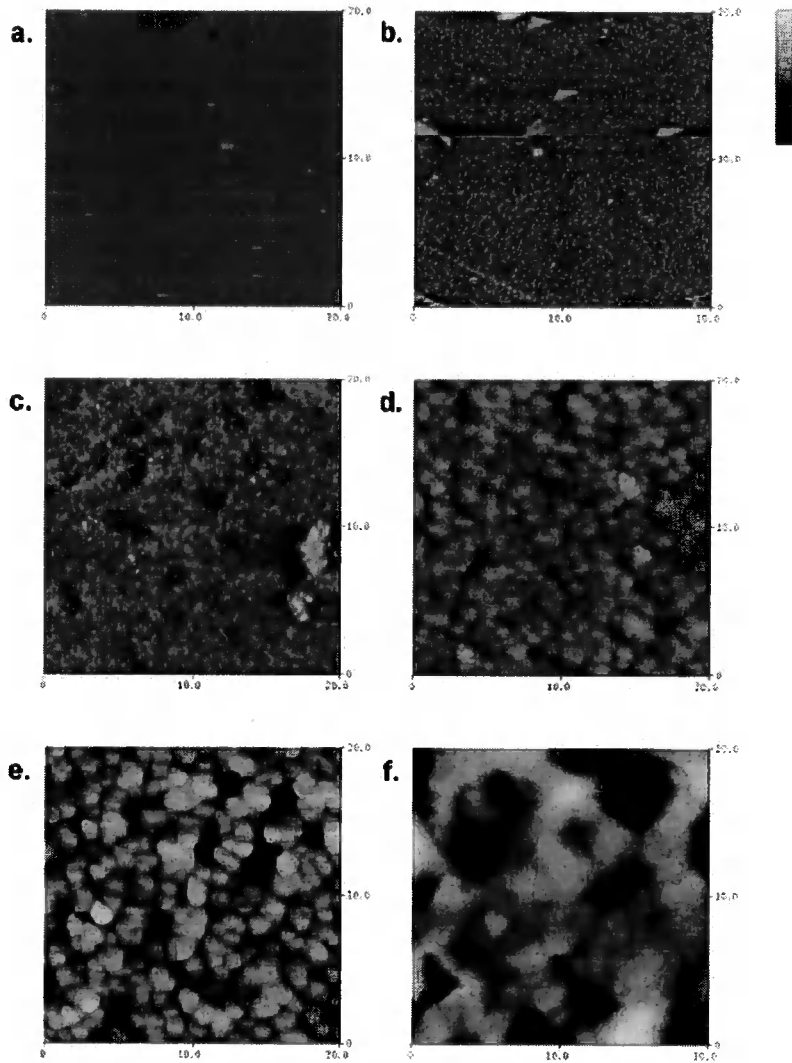


Figure 7-4 AFM height images of polymethylmethacrylate as a function of CF_4 plasma exposure time (power = 50 W): (a) 2 mins, (b) 4 mins, (c) 6 mins, (d) 8 mins, (e) 10 mins and (f) 20 mins. Resolution ($x = y = 20 \mu\text{m}$, $z = 500 \text{ nm}$ except f where $z = 2000 \text{ nm}$).

Table 7-2 Contact angle measurements for CF₄ plasma treated 2 μm thick polymethylmethacrylate (50 W, 10 min).
 Probe Liquid Surface Energy (mN m⁻¹)(at 20°C)³⁰ Contact Angle / °

Probe Liquid	Surface Energy (mN m ⁻¹)(at 20°C) ³⁰	Contact Angle / °		
		Equilibrium	Advancing	Receding Hysteresis
Water	72.8	140.7	141.6	5.4
Hexadecane	27.5	75.6	79.9	41.9
Tetradecane	26.2	70.3	76.2	44.2
Dodecane	25.4	65.5	70.6	40.8
Decane	23.8	55.7	61.2	31.5
Octane	21.6	43.0	49.2	27.0

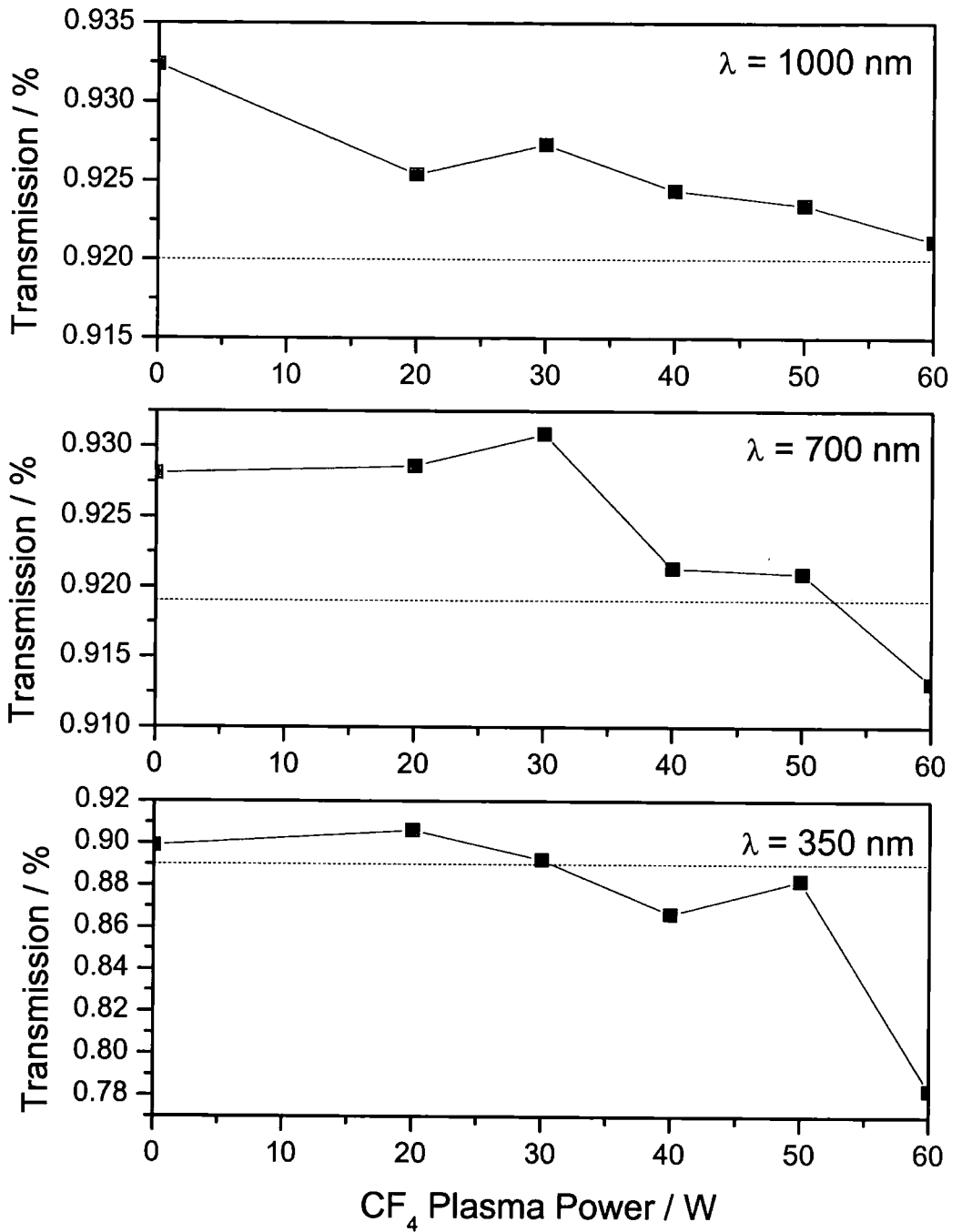


Figure 7-5 Comparison of transmittance as a function of plasma power following a 10 minute treatment at short (350 nm), medium (700 nm) and long (1000 nm) wavelengths (dotted line represents untreated sample).

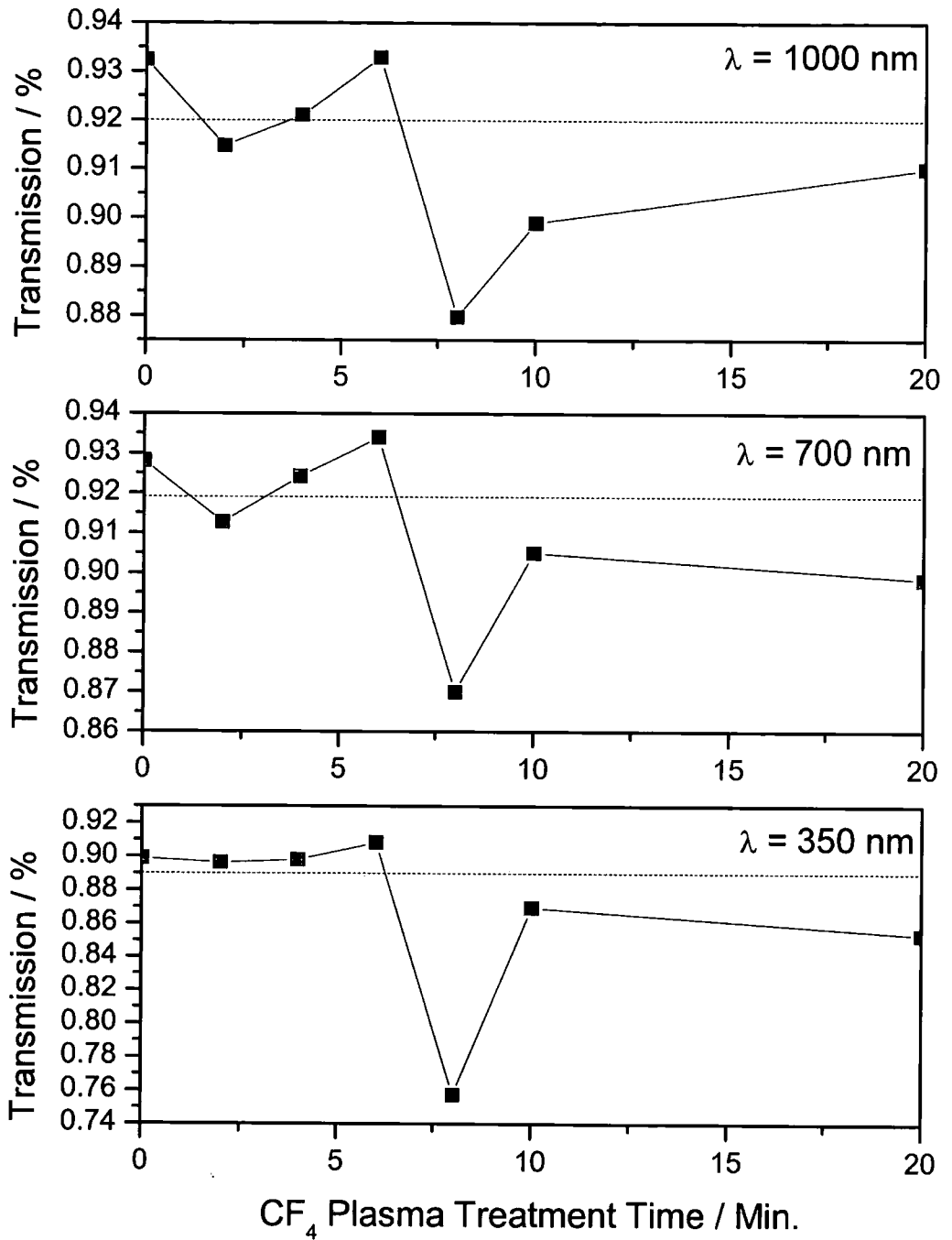


Figure 7-6 Comparison of transmittance as a function of time following a 50 W treatment at short (350 nm), medium (700 nm) and long (1000 nm) wavelengths (dotted line represents untreated sample).

7.4 Discussion

The liquid repellency of a surface is governed by a combination of two principal factors: the chemical composition (i.e. surface energy) and the topographical microstructure (surface roughness). Surfaces with a low surface energy and a flat topography have been known to exhibit a high water contact angle,³¹ although this by itself is not normally enough to produce a surface that can be classified as superhydrophobic. A classification normally reserved for surfaces upon which a water droplet is found to move spontaneously or easily across at horizontal or near horizontal surfaces.^{32,33} In order for superhydrophobicity to occur there must be a minimal difference between the advancing and receding contact angles of the surface (contact angle hysteresis). Contact angle hysteresis can be regarded as the force necessary to move a liquid droplet across a surface. Hence in cases where the contact angle hysteresis value is low, there is a small energy barrier to the droplet's movement across the surface and it travels easily.^{34,35} Theoretical studies have been carried out on rough hydrophobic surfaces and have predicted that during the initial increase in surface roughness the contact angle hysteresis will also increase, until a maximum is reached.³⁶ Beyond this maximum an increase in roughness will cause the contact angle hysteresis to fall due to the formation of a composite interface where air filled voids in the surface prevent the probe liquid from penetrating. This later behaviour can be described using the Cassie-Baxter equation.^{37,38} Therefore a low contact angle hysteresis can be obtained by roughening of the surface to produce a composite interface.

There have been a variety of methods reported in the literature for the production of super-hydrophobic surfaces via composite interface effects.

These include: the sublimation of aluminium acetylacetonate from a boehmite, titania, or silica coating,^{39,40} sol-gel deposition of alumina and silica,^{41,42} anodic oxidation of aluminum,³³ and photo-lithographically etched surfaces.⁴³ These methodologies for the production of superhydrophobic surfaces involve a roughening pre-treatment prior to an impartation of fluorine functionality at the surface in order to introduce a low surface energy. Other techniques, include embedding PTFE oligomer particles into nickel electrodes,⁴⁴ compressing sub-micrometer particles,³² fractal surfaces,⁴⁵ and plasma based etching⁴⁶ or deposition techniques.^{47,48,49}

In the present study plasma fluorination was carried out on polymer surfaces using a non-depositing fluorocarbon precursor, CF_4 ,^{50,51,52,53,54,55,56} and relies on the generation of fluorine atoms and ions.^{57,58,59} The high degree of surface fluorination (i.e. the formation of CF , CF_2 or CF_3 functionalities) on the polymethylmethacrylate is corresponds to the atomic fluorine attacking the unsaturated $\text{C}=\text{O}$ bond contained in the polymer repeat unit as well as hydrogen substitution reactions. The percentage amount of fluorination that occurs is lower than that of unsaturated hydrocarbon polymers⁴⁹ although it is higher than has previously been reported for a polymethacrylate surface.⁶⁰ The accompanying change in surface roughness can be attributed to CF_4 plasma assisted restructuring / cross-linking (by the vacuum ultraviolet component) or etching (atomic and reactive ion etching).^{61,62} The synergistic changes induced by the CF_4 plasma treatment (both the fluorination and roughening of the surface) result in the observed liquid repellency. The fluorinated groups serve to lower the surface energy due to their inert nature

and the increase in the surface roughness serves to create a composite surface.⁶³

The effect of the treatment depends on the thickness of the film. A film that is not thick enough when exposed to too high a power, or too long an exposure is completely removed from the substrate. From this we can tell that two competing procedures are occurring during the plasma treatment, namely the fluorination and etching of the surface.⁶⁴ If the surface being treated is too thin the etching effects may totally remove all the polymer layer whether fluorinated or not.

The optical properties of these films are of key interest. A PMMA layer on a glass slide was found to increase its transmittance, Table 7-1. This is due to the polymer film acting as an interface between the glass slide and the air. Fluorination of these surfaces gave an increase in the light transmitted through the sample whilst enhancing their repellent properties.

Antireflective films for use in such items as silicon photovoltaic cells have been widely reported.⁶⁵ This work concentrated upon the creation of transparent surfaces with the correct refractive index to produce antireflective behaviour on silicon. Early work relied on titanium or tantalum oxides being sputter coated⁶⁶ or chemically vapour deposited onto surfaces.⁶⁷ Although novel work involving polymerised organometallic precursors was also carried out.⁶⁸ Multilayer systems of alternating high and low refractive indices can be tailored according to layer thickness to produce anti-reflective films for a variety of substrates. Thin polymer films were also found to be suitable for production of anti-reflective layers and their properties were found to be enhanced by the inclusion of micro-voids within the films. However, the films

produced in this manner were hydrophilic with low contact angles. Hence in any outdoor application where they may be exposed to the elements fouling of the surface will quickly occur.

An attempt to produce a transparent film with a high contact angle has been carried out using the plasma enhanced chemical vapour deposition of a fluoroalkyl silane.⁶⁹ This resulted in a film with an enhanced transmission (90 % at 700 nm) and contact angle (107°), however both these properties are inferior to those of the film produced using the method described herein. A film produced by grafting tri-decafluoro-1,1,2,2 tetrahydrooctyldimethylchlorosilane to a silica gel resulted in an advancing contact angle of 165° and a maximum transmittance of 92% has also been reported. However the receding contact angle was 115° , giving a surface hysteresis value of 50° which is too high to be described as super-repellent.⁷⁰

7.5 Conclusions

Plasma surface fluorination of a PMMA film has produced a surface that exhibits both super repellent and anti-reflective properties, being both highly transparent and water repellent. The hydrophobicity of the surface can be attributed to fluorination and roughening caused by the plasma. The anti-reflective ability can be attributed to refractive index changes induced by the fluorination of the polymer surface. The materials could be potential steps forward in a wide variety of applications such as automobile glass, building materials, bathroom mirrors, and greenhouse glass.

7.6 References

- [1] Spells, S. J. *Characterization of Solid Polymers: New Techniques and Developments*; Chapman & Hall: London, 1994.
- [2] Karim, A.; Kumar, S. *Polymer Surface, Interfaces and Thin Films*; World Scientific: Singapore, 2000.
- [3] Chan, C. M. *Polymer Surface Modification and Characterization*; Hanser: New York, 1993.
- [4] Nijenhuis, K. T. *Thermoreversible Networks: Viscoelastic Properties and Structure of Gels*; Springer-Verlag: Berlin, 1997.
- [5] Brandrup, J.; Immergut, E. H.; Grulke, E. A. *Polymer Handbook*, 4th ed.; Wiley: New York, 1999; Section 6, p 526.
- [6] Kissa, E. *Handbook of Fibre Science and Technology*, Vol II, Part B, Lewin, M.; Sello, S. B. Eds.; Marcel Dekker Inc: New York, 1984.
- [7] Brady, R. F. Jr. *Encyclopaedia of Polymer Science and Technology*, Mark, H.; Bikaler, N. M.; Overberger, C. G.; Menges, G. Eds.; John Wiley & Sons: Chichester, 1984.
- [8] DeMarco, C. G.; McQuade, A. J.; Kennedy, S. J. *Modern Textiles Magazine*, **1960**, Part 2, 50.
- [9] Sargent, R. R.; Alender, J. R. U. S. Patent 5,560,992, **1996**.
- [10] Anderson, M. H.; Lyons, C. S.; Wigness, B. D. U. S. Patent 4,536,179, **1985**.
- [11] Honeychuck, R. V.; Ho, T.; Wynne, K. J.; Nissan, R. A. *Chem. Mater.* **1993**, 5, 113.

-
- [12] Haisma, J.; Pasman, J. H. T.; Pasmans, J. M. M.; Werf, P. *Appl. Opt.* **1985**, *24*, 2679.
- [13] Clark, D. T.; Feast, W. J.; Musgrove, W. K. R.; Ritchie, I. *J. Polym. Sci., Part A: Polym. Chem.* **1975**, *13*, 857.
- [14] Hopkins, J.; Badyal, J. P. S. *J. Phys. Chem.* **1995**, *99*, 4261.
- [15] Coulson, S. R.; Woodward, I. S.; Brewer, S. A.; Willis, C.; Badyal, J. P. *S. Chem. Mater.* **2000**, *12*, 2031.
- [16] Wheale, S. H. *Physicochemical Phenomena at the Plasma – Polymer Interface*. Ph.D. Thesis, Durham University, **1997**.
- [17] Ryan, M. E.; Fonseca, J. L. C.; Tasker, S.; Badyal, J. P. S. *J. Phys. Chem.* **1995**, *99*, 7060.
- [18] Popat, R. H.; Sutherland, I.; Shang, E. –S. *J. Mater. Chem.* **1995**, *5*, 713.
- [19] Fitzgerald, P. H.; Raiford, K. G.; Greenwood, E. J. U. S. Patent 5,798,402, **1998**.
- [20] Raiford, K. G.; Liss, T. A.; Greenwood, E. U. S. Patent 5,898,046, **1997**.
- [21] Smith, R. S. U. S. Patent 5,672,651, **1997**.
- [22] Kassis, C. M.; Steehler, J. K.; Betts, D. E.; Guan, Z. B.; Romack, T. J.; Desimone, J. M.; Linton, R. W. *Macromol.*, **1996**, *29*, 3247.
- [23] Schaub, T. F.; Kellogg, G. J.; Mayes, A. M. *Macromol.*, **1996**, *29*, 3982.
- [24] Champagne, F.; Li, J. F.; Schreiber, H. P.; Dipaloo-Baranyi, G. *J. Appl. Polym. Sci.* **1994**, *54*, 743.
- [25] Ebbens, S. J.; Badyal, J. P. S. *Langmuir*, **2001**, *17*, 4050.
- [26] Zisman, W. A. *Contact Angle, Wettability, and Adhesion*, *Advances in Chemistry Series 43*, Am. Chem. Soc.: Washington DC, **1964**.
- [27] Maruno, T.; Nakamura K.; Murata, N. *Macromol.*, **1996**, *29*, 2006.

-
- [28] Zhong, Q., Innis, D., Kjoller, K., Elings, V. B. *Surf. Sci.* **1993**, *14*, 3045.
- [29] Briggs, D.; Beamson, G. High Resolution XPS of Organic Polymers: The Scienta ESCA300 Database; John Wiley and Sons Ltd; 1992.
- [30] Jasper, J. J. *J. Phys. Chem. Ref. Data* **1972**, *1*, 841.
- [31] Tsibouklis, J.; Graham, P.; Eaton, P. J.; Smith, J. R.; Nevell, T. G.; Smart, J. D.; Ewen, R. J. *Macromol.* **2000**, *33*, 8460.
- [32] Chen, W.; Fadeev, A. Y.; Hsieh, M. C.; Oner, D.; Youngblood, J.; McCarthy, T. J. *Langmuir* **1999**, *15*, 3395.
- [33] Shibuichi, S.; Yamamoto, T.; Onda, T.; Tsujii, K. *J. Colloid Interface Sci.* **1998**, *208*, 287.
- [34] Furmidge, C. G. L. *J. Colloid Sci.* **1962**, *17*, 309.
- [35] Miwa, M.; Nakajima, A.; Fujishima, A.; Hashimoto, K.; Watanabe, T. *Langmuir* **2000**, *16*, 5754.
- [36] Johnson, R. E.; Dettre, R. H. *Adv. Chem. Ser.* **1964**, *43*, 112.
- [37] Cassie, A. B. D.; Baxter, S. *Trans. Faraday Soc.* **1994**, *40*, 546.
- [38] Cassie, A. B. D.; Baxter, S. *Trans. Faraday Soc.* **1944**, *3*, 16.
- [39] Nakajima, A.; Hashimoto, K.; Watanabe, T.; Takai, K.; Yamauchi, G.; Fujishima, A. *Langmuir* **2000**, *16*, 7044.
- [40] Nakajima, A.; Fujishima, A.; Hashimoto, K.; Watanabe, T. *Adv. Mater.* **1999**, *16*, 1365.
- [41] Tadanaga, K.; Morinaga, J.; Matsuda, A.; Minami, T. *Chem. Mater.* **2000**, *12*, 590.
- [42] Hong, B. S.; Han, J. H.; Kim, S. T.; Cho, Y. J.; Park, M. S.; Dolukhanyan, T.; Sung, C. *Thin Solid Films* **1999**, *351*, 274.
- [43] Oner, D.; McCarthy, T. J. *Langmuir* **2000**, *16*, 7777.

-
- [44] Kunugi, Y.; Nonaku, T.; Chong, Y. B.; Watanabe, N. *J. Electroanal. Chem.* **1993**, *353*, 209.
- [45] Shibuichi, S.; Onda, T.; Satoh, N.; Tsujii, K. *J. Phys. Chem.* **1996**, *100*, 19512.
- [46] Busscher, H. J.; Stokroos, I.; Vandermei, H. C.; Rouxhet, P. G.; Schakenraad, J. M. *J. Adhes. Sci. Technol.* **1992**, *6*, 347.
- [47] Youngblood, J. P.; McCarthy, T. J. *Macromol.* **1999**, *32*, 6800.
- [48] Teare, D. O. H.; Spanos, C. G.; Ridley, P.; Kinmond, E. J.; Roucoules, V.; Coulson, S.; Brewer, S. A.; Willis, C.; Badyal, J. P. S. *Chem. Mater.* **2002**, *14*, 4566.
- [49] Woodward, I.; Schofield, W. C. E.; Roucoules, V.; Badyal, J. P. S. *Langmuir* **2003**, *19*, 3432.
- [50] Strobel, M.; Corn, S.; Lyons, C. S.; Korba, G. A. *J. Polym. Sci, Part A: Polym. Chem.* **1987**, *25*, 1295.
- [51] Hopkins, J.; Badyal, J. P. S. *Macromol.* **1994**, *27*, 5498.
- [52] Sigurdsson, S.; Shishoo, R. *J. Appl. Polym. Sci.* **1997**, *66*, 1591.
- [53] Wang, J.; Feng, D.; Wang, H.; Rembold, M.; Thommen, F. *J. Appl. Polym. Sci.* **1993**, *50*, 585.
- [54] Egitto, F. D. *Pure Appl. Chem.* **1990**, *62*, 1699.
- [55] Truesdale, E. A.; Smolinsky, G. *J. Appl. Phys.* **1979**, *50*, 6594.
- [56] Klausner, M.; Loh, I. H.; Baddour, R. F.; Cohen, R. E. *Polym. Mater. Sci. Eng.* **1987**, *56*, 227.
- [57] d'Agostino, R.; Cramarossa, F.; DeBenedictis, S. *Plasma Chem. Plasma Process.* **1982**, *2*, 213.

-
- [58] Egitto, D. F.; Vukanovic, V.; Taylor, G. N. In *Plasma Deposition Treatment and Etching of Polymers*; d'Agostino, R., Ed.; Academic Press Inc.; San Diego, 1990; Chapter 5.
- [59] Iriyama Y.; Yasuda, H. *J. Polym. Sci., Part A: Polym. Chem.* **1992**, *30*, 1731.
- [60] Bartoli, J. R.; Costa, R. A.; Verdonck, P.; Mansano, R. D.; Carreño, M. N. *Polímeros: Ciência e Tecnologia*, **1999**, 148.
- [61] Inagaki, N.; Kobayashi, N.; Matsushima, M. *J. Membr. Sci.* **1988**, *38*, 85.
- [62] Kerle, T.; Yerushalmi-Rozen, R.; Klein, J. *Europhys. Lett.* **1997**, *38*, 207
- [63] Smart, B. E. *Chemistry of Organic Fluorine Compounds*; Hudlicky, M., Pavlath, A. E., Eds.; American Chemical Society: Washington, D.C., **1995**.
- [64] Boucher, R.; Hubner, U.; Morgenroth, W.; Roth, H.; Meyer, H.-G.; Schmidt, M.; Eich, M. *Microelec. Eng.* **2004**, *73–74*, 330.
- [65] Doshi, P.; Jellison, Jr., G. E.; Rohatgi, A. *Appl. Opt.* **1997**, *36*, 7826.
- [66] Hsu, J. C.; Lee, C. C. *Appl. Opt.* **1998**, *37*, 1171.
- [67] Battiston, G.A.; Gerbasi, R.; Porchia, M.; Marigo A. *Thin Solid Films* **1994**, *239*, 186.
- [68] Yoldas B. E.; O'Keeffe, T. W. *Appl. Opt.* **1979** *18*, 3133.
- [69] Hozumi, A.; Sekoguchi, H.; Kakinoki, N.; Takai, O. *J. Mat. Sci.* **1997**, *32*, 4253.
- [70] Shang, H. M.; Wang, Y.; Limmer, S.J.; Chou, T.P.; Takahashi, K.; Cao, G.Z. *Thin Solid Films* **2005**, *472*, 37.

Chapter 8

Conclusions

This thesis has concentrated on the functionalisation, modification and analysis of polymer surfaces using a variety of surface sensitive techniques.

Initially, the use of EFM to produce a discharge from a chromium plated AFM tip onto polymer thin films was found to behave in an analogous way to macro-scale corona discharges. Producing a characteristic charge on the substrate that was dependant on tip size, tip height, polarity of discharge and discharge area. The trends observed were interpreted with reference to the fundamental physical properties of the individual polymers.

In addition, a polymer blend system exhibiting nano-scale polybutadiene islets within a polystyrene matrix was subjected to EFM discharge. The charge pattern created on this substrate illustrated the possibility of creating selectively charged, patterned substrates with polymers of divergent electrical properties were utilised.

The charged patches generated on these thin polymer films were utilised in the electrostatic attraction of charged particles. This yielded a simple methodology for the production of micro-scale metal surface patterns through xerography.

An alternative methodology for the production of patterned surfaces was demonstrated by depositing a pulsed plasma polymer and the subsequent employment of electroless deposition. Embossed grids were used to yield a functionalised, patterned surface. Subsequent activation by a catalyst initiated an electroless deposition process creating patterned metal surfaces for potential use in integrated circuit boards. Micro-scale copper and nickel patterns were prepared on PTFE substrates by following a simple and adaptable scheme.



A further use of plasma technology for the modification of surface properties was then demonstrated with the fluorination of thin PMMA films on transparent substrates. The resulting films showed both super-repellent and anti-reflective properties and therefore have potential use in applications requiring a clear screen that is anti-fouling, such as car windscreens.